A STUDY ON THE MULTIPLE FRICTION JOINT TENSION PILES SUBJECTED TO LARGE HORIZONTAL DISPLACEMENTS

by

Mohammad Fahim Saidy

B.S., Civil Engineering, Boğaziçi University, 2019

M.S., Civil Engineerig, Boğaziçi University, 2021

Submitted to the Institute for Graduate Studies in
Science and Engineering in partial fulfillment of
the requirements for the degree of
Master of Science

Graduate Program in Civil Engineering

Boğaziçi University

2021

ACKNOWLEDGEMENTS

I would like to express my sincere thanks and utmost gratitude to Prof. Gökhan Baykal for his support, encouragement, and constant guidance throughout this research work. I would also like to present my utmost thanks to the members of my thesis committee, Prof. Ayşe Edinçliler, and Assist. Prof. Tanay Karademir, for their kind attitude and their valuable suggestions.

Thanks to Mr. Uğurcan Erginağ, research assistant, for his fruitful discussions, help, and unconditional support throughout this thesis work. I am indebted for his kind assistance in the preparation and performance of the tests. I would like to thank the research assistant, Mr. Onur Öztürk, for his assistance and advice on conducting the three-point bending moment tests on monolithic model piles.

To the research assistants, technicians, and staff of the geotechnical laboratory of Boğaziçi University, thank you all for extending the helping hand in case of need, and thank you all for your kind attitude.

Finally, I would like to express my deepest thanks to my family, especially my Mom and Dad, for their love, support, and priceless encouragement throughout my life and this study. Without their love and support, this thesis work would have been way difficult.

ABSTRACT

A STUDY ON THE MULTIPLE FRICTION JOINT TENSION PILES SUBJECTED TO LARGE HORIZONTAL DISPLACEMENTS

Tension piles supporting some vital structures such as transmission towers, offshore wind turbines, jetties, chimneys, submerged floating tunnels, and tension leg platforms, are, often, subjected to large horizontal displacements. Experimental studies have been conducted on a type of pile, known as multiple friction joint piles developed at Boğaziçi University, to investigate the response and capacity of piles under combined large horizontal displacement and tensile forces, and to observe the effect of some parameters such as tensile forces, pile rigidity, and soil stiffness on the capacity and behavior of tension piles. The tests were conducted by placing multiple friction joint pile, or MFJP, having 34 cm length and five centimeters width, in a special large size large displacement direct shear apparatus and applying lateral or combined lateral and tensile loadings at the head of them. The head displacements of the piles and the lateral load on the piles were measured during the experiments to draw the load-displacement curves at the head of the piles. The model piles' inclination was also measured about the model piles longitudinal axis with the help of inertial measurement unit sensors. It was observed that as the pile's rigidity increases, the load-pile head displacement gets steeper and the pile head displacement at which the ultimate lateral load reaches decreases. The lateral capacity of the piles increases when the soil stiffness increases. The post-tension force on the wire, keeping the mortar blocks together in the multiple friction joint model pile, increases up to a displacement equal to the ultimate lateral displacement or the displacement at which soil failure occurs. The multiple friction joint piles subjected to large horizontal displacements have the capacity to undergo large deformations in the order of one pile's width without breakage. When the piles are subjected to both lateral displacement and tensile force, they experience a decrease in their lateral capacity compared to that of the piles subjected to lateral displacement alone.

TABLE OF CONTENTS

LIST OF FIGURES

LIST OF TABLES

LIST OF SYMBOLS

a_{max}	Maximum ground acceleration
C_u	Undrained shear strength of soil
d	Pile diameter or width
D_r	Relative density
e	Eccentricity
e_{min}	Soil minimum void ratio
e_{max}	Soil maximum void ratio
E	Pile's modulus of elasticity
E_d	Pressure meter modulus
E_s	Soil modulus of elasticity
E_{sr}	A reference value for soil modulus
E_pI_p	Pile's flexural rigidity
G_s	Soil Specific gravity
I	Pile's moment of inertia
k	Bearing capacity factor
k_s	Soil subgrade modulus
k_1	Sliding layer subgrade modulus
k_2	Stable layer subgrade modulus
K_P	Passive earth pressure coefficient
K_r	Modular ratio
K_R	Pile flexibility factor
L	Pile's length
L_s	Pile length's portion in the sliding soil layer
L_r	Length ratio
L_m	Embedded length of the pile in the stable soil layer
M	Moment at pile head
M_{max}	Maximum bending moment
M_{cap}	Pile cap mass
N_C	Stability number in cohesive soils
n_h	Soil modulus of subgrade

P	Pressure per unit length along the pile depth
P_u	Limiting soil pressure
Q	Lateral load acting on pile head
Q_{ult}	Ultimate lateral resistance of the pile
S_u	Soil undrained shear strength
T_{max}	Maximum shear force
u_x	Lateral free field soil movement
u_p	Lateral displacement of the pile
Y_t	Dimensionless pile head displacement
Y_0	Pile head displacement
Z_{max}	Dimensionless pile length
Z_r	Depth of rotation
γ	Soil unit weight
δ_0	Soil displacement at pile head
$\delta_{(Z)}$	Horizontal soil displacement profile
ε	Strain
ε_g	Ground loss ratio
ν	Poisson's ratio
ν_s	Soil Poisson's ratio
ρ	Pile displacement along its length
ρ_e	External soil displacement
σ'_v	Effective overburden soil pressure
σ_h	Horizontal soil pressure
φ_m	Mobilized friction angle in front of the pile
φ_s	Mobilized interface friction angle at the sides of the pile

LIST OF ACRONYMS/ABBREVIATIONS

1D	One Dimensional
2D	Two Dimensional
3D	Three Dimensional
ADC	Analog to Digital Converter
AHRS	Attitude Heading Reference System
ASTM	American Society for Testing and Materials
BEF	Beam on Elastic Foundation
BS-EN	British Standards European Norm
DAQ	Data Acquisition System
DMP	Digital Motion Processor
FEM	Finite Element Method
FEA	Finite Element Analysis
FDM	Finite Difference Method
IMU	Inertial Measurement Unit
IDE	Integrated Development Environment
KGF	Kilo Gram Force
LVDT	Linear Variable Differential Transformer
MEMS	Micro Electrical Mechanical Systems
MPU	Micro Processor Unit
NED	North East Down
PTF	Post Tension Force
PWP	Pore Water Pressure
SL	Stress Level
MFJP	Multiple Friction Joint Pile
SWM	Strain Wedge Method

1. INTRODUCTION

Tension Piles are used to support jetty structures, transmission towers, offshore wind turbines, submerged floating tunnels, and tension leg platforms. These piles, in addition to tensile forces, have to withstand large horizontal displacements and lateral loads due to ground movements, high wind loads, hydrostatic pressures, excavations, and tunneling operations as well. Therefore, they need to be studied under combined lateral displacement and tensile forces.

There have been numerous studies, in recent decades, tackling the issue of a pile subjected to Lateral displacements, and lateral loadings, both in active and passive cases. Similarly, piles resisting tensile forces alone have been researched thoroughly also. In contrast, there are few studies investigating piles carrying combined tensile and lateral loads. Even if there are some numerical and analytical postulations related to piles under combined lateral and tensile forces, they have not been backed thoroughly by experimental data. Therefore, tensile piles under lateral loadings need to be studied furthermore. In addition, the effect of some important parameters including pile rigidity, soil stiffness, tensile forces needs to be evaluated on these types of piles as well.

To investigate the capacity, and behavior of tensile piles subjected to large soil displacements and to study the effect of soil stiffness, pile rigidity, and tensile forces on them, an experimental study was conducted on a type of pile developed at Boğaziçi University, Known as multiple friction joint pile or MFJP. The MFJP piles are made of a series of mortar blocks, between which rubber sheets are placed to enhance the ability of the piles to absorb more deformation energy, and are fixed with each other with a tensile steel rod in the middle. An advantage of The MFJP piles is that their flexibility is adjustable by posting tensioning techniques. The experimental studies were performed on monolithic piles, having the same length and width as that of MFJP piles, as well to control and compare the results with that of MFJP piles.

All the tests were conducted in a large shear large displacement apparatus, developed at Boğaziçi University. The device is a multitasked versatile machine that is capable of conducting lateral, tensile, and cyclic loading tests on model piles. Therefore, the implementability of this device in conducting combined lateral and tensile forces on model piles was also among the main objective of this research study.

To study the effect of rigidity and how the MFJP pile is behaving in comparison to that of the monolithic pile, the lateral active tests, in which the lateral load is applied at the head of the pile, lateral passive tests, in which the upper sliding part of the model piles was subjected to a rectangular lateral soil movement, and combined lateral and tensile tests were performed on three different model piles with different flexibility. These three model piles were a MFJP pile which has been post-tensioned to a force of 750N, which represents a relatively flexible pile in this study, a MFJP pile post-tensioned to 1500N force, which is a relatively moderate rigid model pile, and a monolithic square concrete model pile, which is a relatively rigid pile.

The influence of soil stiffness has been considered by conducting all the required tests in loose sand, having a relative density of 20%, and in medium sand, having a relative density of 50%. The tensile force effect has been taken into account by applying a tensile force, equal to 75% of its related uplift capacity in loose and medium sand, on the model piles while the model piles were subjected to lateral displacement.

The behavior of the MFJP and monolithic piles along their length has been analyzed by measuring the inclination of them along their length with the help of the MPU9250 sensors, Arduino board, and the Arduino software.

To summarize, MFJP tensile piles have been studied under large horizontal displacements, and the effect of some parameters such as pile flexibility, soil stiffness, tensile forces, and type of loadings have been investigated on tensile piles. In addition, the implementability of the large shear large displacement device in conducting separate and combined lateral and tensile forces on model piles has been evaluated as well.

2. LITERATURE REVIEW

2.1. Introduction

In this chapter, some of the studies regarding laterally loaded piles in academic literature have been summarized and discussed. Practically laterally loaded piles can be divided into two broad categories of active piles and passive piles which are explained in the following two subsections thoroughly.

2.2. Piles under Active Lateral Loading

When the pile is laterally loaded in a way that the lateral load is principally applied at the top of the pile, the pile is considered to be an active pile. In other words, if the lateral load is transmitted by an external source through the structure that the pile supports, it is said that the pile is under active loading. The main sources of the lateral loads on pile foundations according to Poulos and Davis [1] can be listed as:

(i) Wind loads.

(ii) Seismic loads.

(iii) Wave forces when the pile is supporting offshore structures.

(iv) Earth pressure due to retaining walls.

(v) Cable forces from suspension bridges and transmission towers.

(vi) Vehicle forces on bridges.

(vii) Berthing loads.

Piles are resisting the lateral loads through the their side friction and lateral bearing which is quite different than the skin friction and toe bearing associated with piles under axial loads. Therefore, there should be a separate analysis for piles under active loading. To design pile foundations, generally, two requirements must be insured: first, there should

be a sufficient factor of safety against ultimate lateral resistance of pile; and second, the deflections under the designed lateral load must not exceed the tolerable pile head deflection [1].

The lateral capacity of the piles under active loads spin around the ultimate lateral resistance of piles and the allowable pile head deflection as mentioned above. Therefore, the methods developed to evaluate pile capacities under lateral loading are based on one of these two criteria.

Generally, two types of methods are used for calculating the lateral resistance of piles under active loading which are theoretical methods and experimental methods.

2.2.1. Theoretical Methods

Theoretical methods are the simplest methods for estimating the ultimate lateral resistance of piles subjected to active lateral loadings. In these methods, the lateral resistance of piles are estimated based on the statics of the pile or force and moment equilibrium of the pile and earth pressure theory [1, 2].

Based on force and moment equilibrium and taken that the earth pressure (soil resistance) mobilized at the back and in front of the pile is P_u due to a lateral load of Q acting at some eccentricity of e on the pile as in Figure 2.1, the lateral resistance of the pile can be related to the lateral force Q and the generated moment M by considering statics of the pile as

$$Q_{ult} - \int_0^{Z_r} P_u . d . dz + \int_{Z_r}^{L} P_u . d . dz = 0 \tag{2.1}$$

$$Q_{ult} . e + \int_0^{Z_r} P_u . d . z . dz - \int_{Z_r}^{L} P_u . d . z . dz = 0 \tag{2.2}$$

where P_u is limiting soil resistance or pressure along the pile, Q_{ult} is the ultimate lateral resistance of the pile, Z_r is the depth of the point around which the pile will rotate from

ground surface, e is the lateral load eccentricity from ground surface, d is the pile width or diameter, and L is the pile total length [1].

As it is seen from equations (2.1) and (2.2), if the soil resistance distribution (P_u) is known along the pile length, then the depth of rotation and the ultimate lateral resistance can be determined. This limiting soil resistance has been assessed and estimated by many researchers. Some of the existing relationships in literature are listed in the Table 2.1.

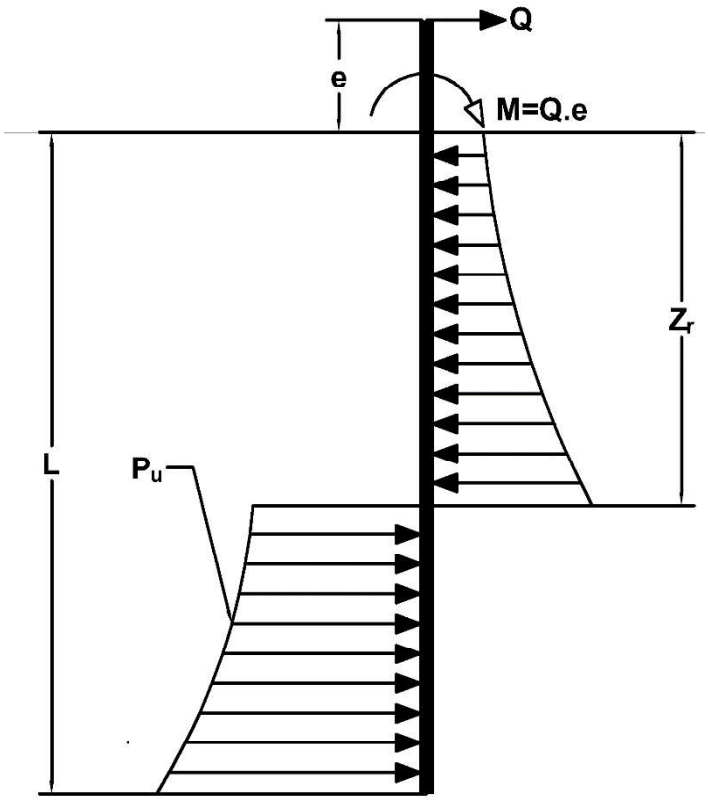

Figure 2.1. The schematic of a pile under active lateral loadings. Modified from Poulos and Davis [1].

The general equations (2.1) and (2.2) have been simplified furthermore by Broms [3] by proposing some simplifications such as dividing soil into pure cohesive or cohesion-less soils and the pile into rigid and flexible piles. In the case of rigid piles, the pile is assumed sufficiently rigid in which failure of the soil will occur before the failure of the pile, i.e. the maximum bending moment on the pile does not exceed the plastic moment

yield moment of the pile. While, in the flexible piles, the pile fails first due to bending moment. Broms set the $\frac{L}{T} \leq 2$ *and* $\frac{L}{T} \geq 4$ criteria for rigid and flexible piles respectively. where:

$$T = \left(\frac{EI}{n_h}\right)^{\frac{1}{5}}$$

E is the modulus of elasticity of pile.

I is the moment of inertia of the pile.

n_h is the subgrade modulus of the soil.

Table 2.1. Summary of limiting or ultimate pressure on a laterally loaded piles in literature.

Source	Relationship	Soil Type
Broms [3]	$P_u = 3K_P.\sigma'_v.d$	Non-cohesive
Reese et al [4]	Initial Depths: $P_u = K_P.\sigma'_v.d$ Greater Depths: $P_u = {K_P}^3.\sigma'_v.d$	Non-cohesive
Barton [5]	$P_u = {K_P}^2.\sigma'_v.d$	Non-cohesive
Reese [6]	$\frac{P_u}{d} = 2C_u + \sigma'_v + \alpha C_u \frac{z}{d}$	Cohesive
Broms [7]	Up to a depth=3d: $P_u = 2C_u d$ Depth>3d: $P_u = 9C_u d$	Cohesive
Matlock [8]	$\frac{P_u}{d} = 2C_u + \sigma'_v + \alpha C_u \frac{z}{d}$	Cohesive
Marsland&Randolph [9]	$\frac{P_u}{d} = \sigma_h + 6C_u$	Cohesive
Murff&Hamilton [10]	$\frac{P_u}{d} = N_p C_u + \sigma'_v$ $N_p = N_{pl} - (N_{pl} - 2).e^{-\xi z/d}$ $\xi = 0.25 + 0.05\frac{C_{u0}}{kd} \leq 0.55$	Cohesive
Brinch Hansen [11]	$\frac{P_u}{d} = a.K_a + c.K_c$	Cohesive & Non-cohesive
Mei [12]	$P_s = \left[\frac{k_\varphi}{1+e^{-bs}} - \frac{k_\varphi - 4}{2}\right]\frac{P_0}{2}$	Cohesive & Non-cohesive

In Table 2.1:

P_u & P_s : Limiting soil resistance distribution along the pile length.

P_0 : Lateral earth pressure at rest.

k_{φ} : A parameter which is a function of friction angle.

K_P : Passive earth pressure coefficient.

d and z: Pile diameter or width, and depth of soil from ground surface.

C_u : Undrained shear strength of cohesive soil.

σ'_v and σ_h : Effective overburden soil pressure and horizontal soil pressure respectively.

a and c: Vertical overburden pressure and cohesion respectively.

b: A parameter dependent on friction angle and soil displacement.

s: Soil displacement.

K_a and K_c: Factors which are dependent on friction angle and depth of soil.

C_{u0} and N_{pl} : The value of C_u and N_p at z=0 or ground line respectively.

2.2.2. Experimental Methods

Experimental methods generally provide an accurate and more reliable estimation of the lateral capacity of piles under active loading. Full-scale lateral load tests and Model lateral load tests are two main types of the methods which are used to determine the lateral capacity of active piles.

2.2.3. Load-Deflection Methods

In the majority of cases, the maximum deflection of the pile foundation is governing the design of the pile under active lateral loadings rather than the ultimate lateral load resistance. There are mainly two dominant approaches for load-deflection prediction of piles under lateral load which are the subgrade reaction approach and elastic approach [1].

These two approaches are explained and discussed in detail in the piles under the passive loading subsection of this chapter as the mechanism behind these two approaches are the same in both cases of passive loading and active loading.

2.3. Piles under Passive Loadings

When piles are placed through soils experiencing horizontal soil movements, they are considered as passive piles or piles subjected to passive loadings.

These kind of piles are considered to have a preventive effect against the lateral soil movement, as a result of which additional lateral forces, bending moments and deflections are induced into the pile foundation which may cause structural distress and failure of the pile [13, 14].

As it is stated, externally induced soil movements are what triggering passive loadings over the pile lengths. These soil movements may develop due to embankment construction over soft clays, unstable or marginally stable slopes, soil creep, liquefaction induced ground movements, cavity formation, and deep excavation, pile driving operations, and tunneling operations [14, 15].

Although passive piles are subjected to lateral loads as the active piles are, the case of passive piles is more complex since the induced lateral forces are on the pile now depend on the soil movement, and these soil movements, in turn, are affected by the pile presence [16, 17]. In other words, the earth pressure applied to the piles is highly dependent upon the relative movement of the soil and the pile.

The analysis methods utilized to investigate the lateral response of piles subjected to horizontal soil movements can be categorized into the following three methods.

(i) Analytical methods.
(ii) Experimental methods.
(iii) Finite element method (FEM).

A flow chart outlining the above methods and their subcategories is presented in Figure 2.2.

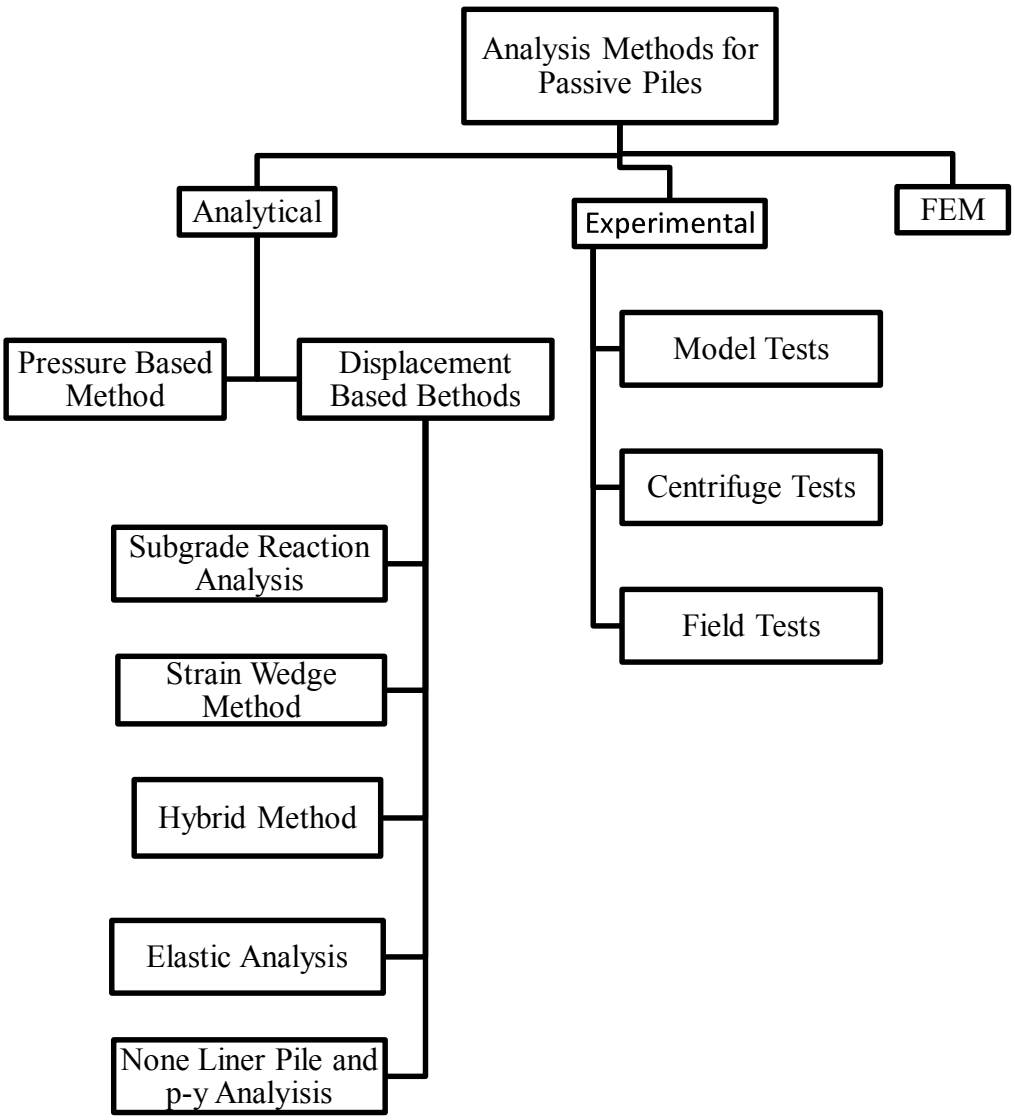

Figure 2.2. Summary of analysis methods for passive piles.

2.3.1. Analytical Methods

2.3.1.1. Pressure Based Methods. This approach attempts to find the induced shearing stresses and max bending moment on a pile subjected to lateral soil movement based on the limiting pressure generated on the pile-soil interface while assuming a proper limiting pressure distribution based on soil properties and geometry of the problem.

As it is evident, this method is spinning around the idea of limiting or ultimate contact pressure at the pile-soil surface. Therefore, the first step in this approach would be the determination of limiting pressure values.

The following four methods are usually used for determining limiting pressure along a pile subjected to lateral loads [18].

(i) Force equilibrium on a passive soil wedge.
(ii) Upper bound method of plasticity on a conical soil wedge.
(iii) A strain wedge mode of soil failure.
(iv) FEM method.

A summary of limiting pressure values, in case of laterally loaded piles, are given in the literature, are presented in Table 2.1.

Viggiani's [19] method is a pressure based method which attempts to find the shear force at the sliding surface and maximum bending moment on a pile subjected to an upper sliding soil and penetrating a stable underlying soil in cohesive soils. The model in question studied by Viggiani [19] is shown in Figure 2.3 in which C_{u1}, C_{u2}, $l_{movable}$, and l_{stable} are shear strengths and pile lengths for sliding and stable part of the soil respectively, and d is pile diameter.

In this method, it is assumed that the relative pile-soil displacement is enough to fully mobilize the limiting pressure on the pile, and its value can be expressed by $P_{ult} = kC_u d$ where d is pile diameter, C_u is soil undrained shear strength and k is a bearing capacity factor for which values of 4 and 8 have been suggested by Viggiani [19] for sliding part and stable part of the soil.

Viggiani (1981) [19] proposed six modes of failure for the pile in question based on the geometry of the problem, yield moment of the pile section and strength of the stable and sliding soil for the cohesive case, and then evaluate the shearing force at the sliding surface and max bending moment based on limit equilibrium method.

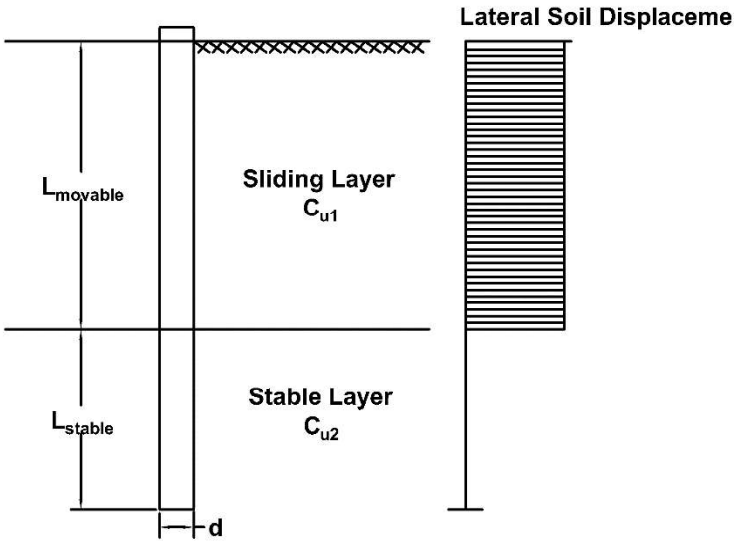

Figure 2.3. Scheme of the problem. Modified from Viggiani [19].

Another pressure based method is Ito and Matsui's [13] method. This method is a theoretical analysis of the lateral forces acting on a row of piles placed through a plastically deforming soil. It states that in order to find a theoretical solution for the lateral forces induced on the piles, it is sufficient to deal with the behavior of the soil between and just adjacent to the piles.

This method assumes that either plastic state satisfying Mohr-Coulomb's yield criterion, called the theory of plastic deformation, or state considering the ground as visco-plastic solid, named as theory plastic follow, occur in the surrounding soil just around the piles based on whether hard soil layer or a creep deformation in a soft soil layer is encountered respectively [13].

The model proposed for the case of plastic deformation state by Ito and Matsui [20] for a soil with an internal friction angle of φ and cohesion c is shown in Figure 2.4 (a) in which d is pile diameter, D_1 is pile to pile spacing, and D_2 is pile center to center spacing.

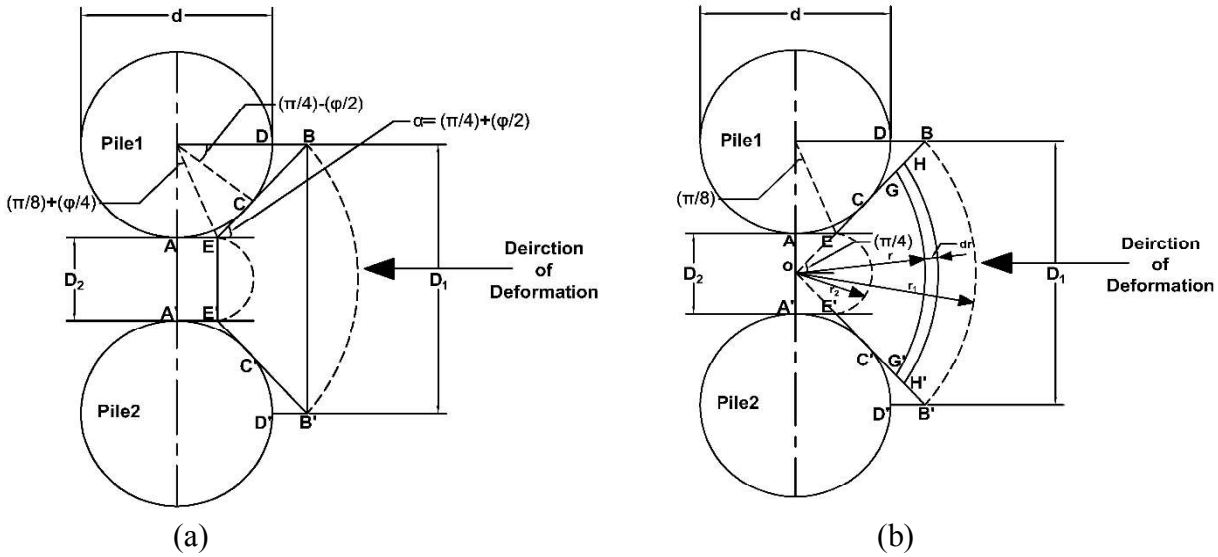

Figure 2.4. (a) Plastic deformation state (b) Plastic flow state just around the piles. Modified from Ito and Matsui [13].

The lateral load force acting on a pile per unit of thickness of a layer in the horizontal direction is then found by limit equilibrium of forces on a soil portion adjacent to the piles as it is indicated with ‚EBE′B′.

If the plastic flow state is predicted to be encountered, then the method propose a model as shown in Figure 2.4 (b) in which the lateral forces are calculated as the sum of resistive forces due to flow of a visco-plastic, i.e., Bingham solid with yield stress τ_y and a plastic viscosity of η_p along the sides OEGB and OE′G′B′ and the active earth pressure on the sides EB and E′B′ [20].

Begemann and De Leeuw's method estimate the maximum pile bending subjected to a surface surcharge by compatibility solution of the free field soil displacement due to surface surcharge and a pile displacement due to an assumed uniform load as it is represented in Figure 2.5**.** The horizontal soil stress in the soil, lateral soil movement in the soil and pile deformation are found from elastic theory.

This method takes into account the rigidity of the pile by applying a horizontal stress equals to two times of that calculated form elastic theory for a completely rigid pile at point

A and zero stress for fully flexible pile at point B in Figure 2.5, But it does not allow for relative movement between the pile and the soil which is a clear shortcoming of this method.

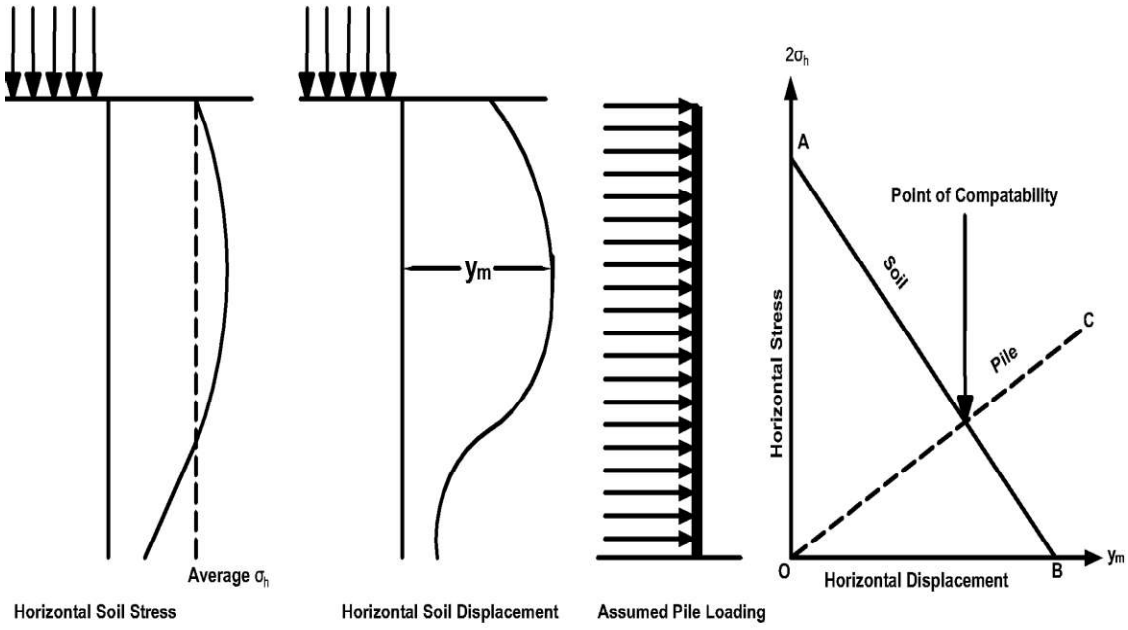

Figure 2.5. Design method from modified Begemann and Leeuw [20].

Although pressure-based methods are simple, fast, and easy to deal with, because of the following disadvantages associated with them, they do not represent the behavior of an actual pile to a valid degree and, therefore, are used only for preliminary designs [21].

(i) Soil pile interaction is not considered.
(ii) The pile is assumed rigid and infinitely long generally.
(iii) The soil is assumed enough soft to flow plastically around the pile.
(iv) The soil is modeled as rigid perfectly plastic often.
(v) Needs simplified soil properties and geometry.

2.3.1.2. Displacement Based Methods. As the name indicates, the response of a pile subjected to lateral soil movement in these methods are studied based on the load-

displacement mechanism of the pile. Therefore, it can be claimed that the pile-soil reaction and how to model this reaction is the main subject of the displacement methods.

In the case of the passive piles, the lateral soil movement is what triggering this pile-soil interaction. Consequently, if the profile of the lateral ground movement is assessed, the effects on the pile-soil interaction can be estimated via a pile-soil interaction analysis [22].

The accuracy of the displacement-based methods depends upon the characterization of the interaction between the pile and the surrounding soil. A particularly good representation of soil-pile interaction gives a more realistic solution [23].

The main advantage of displacement-based methods over pressure-based methods is that load-deflection, slope, bending moment, and shear force curves along the depth can be obtained readily. As it is shown in the Figure 2.2, the displacement-based methods can be divided into the following three methods.

(i) Subgrade reaction analysis.
(ii) Elastic analysis.
(iii) Non-linear pile and p-y analysis.

In subgrade reaction approach, which was originally proposed by Winkler in 1867, the pile-soil interaction is modeled as an elastic beam connected with the soil through a series of unconnected linear or nonlinear springs along the pile length [1-24].

The pressure and the deflection at a point along the pile are related by a coefficient known as modulus of subgrade and the pile is assumed to act as a thin strip whose behavior is governed by the beam equation [1].

In the case of a pile subjected to lateral soil displacement, the deflection arises from the following two sources:

(i) The stresses developed at the pile-soil interface by the loading of the pile.
(ii) The external (or free field) soil movement which are induced from the passive loadings.

Therefore, from the flexural relations of an elastic beam on a soil foundation, the governing equations for a pile acting against lateral soil displacement along its length for the sliding and stable layers, the model of which is shown in Figure 2.6, can be written as

$$EI\frac{d^4y}{dz^4} + k_1 y = k_1\delta_{(Z)} \text{ for } 0 \leq Z \geq L_1 \tag{2.3}$$

$$EI\frac{d^4y}{dz^4} + k_2 y = 0 \text{ for } Z \geq L_2 \tag{2.4}$$

where in above equations, y is the pile displacement, δ_z is the soil displacement profile of the sliding layer, k_1 and k_2 are the sliding and stable parts subgrade modulus respectively and can be expressed in the forms $k_1 = k_a.Z^n$, and $k_2 = k_b.Z^n$, E is the modulus of elasticity of the pile, L_1 and L_2 are sliding and stable layers depths respectively, and I is the pile sectional moment of inertial [15.

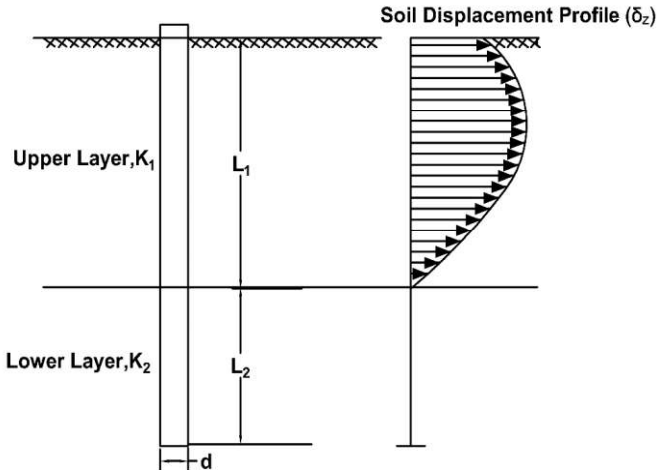

Figure 2.6. Schematic view of a pile undergoing lateral soil movement. Modified from Chaudhuri [15].

In order to solve the governing equations (2.3), and (2.4), the following two parameters need to be determined firstly.

(i) Modulus of subgrade k.

(ii) Free field soil displacement δ_z.

The modulus of subgrade k, which is relating pressure along the pile length to the deflection by relationship $P = ky$ (where P is pressure per unit length along the pile depth), is found generally through one of the following methods [1].

(i) Full-scale lateral loading test.
(ii) In-situ tests (plate loading test, pressure-meter test, and flat dilatometer test).
(iii) Empirical correlations with other soil properties.

All the above three methods can be used to estimate the modulus of subgrade since the bending moment, shear and deflection are not very sensitive to small changes to modulus values [25]. However, the use of the pressure-meter is preferable since it eliminates the approximation required to interpret plate load test data and empirical correlations. In addition, the pressure-meter provides modulus values in the horizontal direction which are desirable in the case of piles subjected to lateral loads [16]. Table 2.2 summarizes some of the suggested relationships for the subgrade modulus (k) in case of cohesive and non-cohesive soils.

As for the lateral soil movement, the data shows that the theoretical solutions of the governing equations for the piles subjected to lateral soil movement are only in good agreement with the experimental measurements if accurate soil movements are predicted [26].

The most reliable means of estimating lateral soil movements is from in-situ measurements, however, since in-situ measurements are not always possible, the lateral soil movements may need to be assessed using other methods. Such methods may include an appropriate elastic theory, the finite-element method, empirical correlations, or approaches based on similar case histories [14].

Although closed-form solutions can be obtained for equations (2.3) and (2.4), they are only useful under limited conditions and they utilize assumptions for oversimplification of the problem that may not be true in practice such as making constant subgrade modulus and constant soil displacement profile assumptions [15, 25].

As a result, numerical methods such as the finite difference method (FDM) which allow us to deal with more complex geometries and better representation of soil-pile interaction are commonly used to solve the governing equations (2.3) and (2.4).

Table 2.2. Summary of some of proposed relationships for modulus of subgrade in literature.

Source	Relationship	Soil Type	Pile Type
Vesics [27]	$k_s = \frac{0.65}{d}.\sqrt[12]{\frac{E_s d^4}{E_p I_p}}\left(\frac{E_s}{1-\upsilon_s{}^2}\right)$	Cohesive	Active
Brinch Hansen [28]	$k_s = 8.14\frac{C_u}{d}$	Cohesive	Active
Wenz [29]	$k_s = (8.28\sim11.42)\frac{C_u}{d}$	Cohesive	Active
Francis [30]	$k_s = \frac{1.30}{d}.\sqrt[12]{\frac{E_s d^4}{E_p I_p}}\left(\frac{E_s}{1-\upsilon_s{}^2}\right)$	Cohesive	Active
Broms [7]	$k_s = (8.28\sim12.56)\frac{C_u}{d}$	Cohesive	Active
Davisson [31]	$k_s = 67\frac{C_u}{d}$	Cohesive	Active
Yoshida & Yoshinaka [32]	$k_s = \frac{2.31}{d}E_d(d)^{\frac{1}{4}}$	Non-Cohesive& Cohesive	Active
Smoltczyk [33]	$k_s = 4.0\frac{C_u}{d}$	Cohesive	Passive
Ito&Matsui [13]	$k_s = 3.33\frac{C_u}{d}$	Cohesive	Passive
DE Beer et al [34]	$k_s = 2.80\frac{C_u}{d}$	Cohesive	Passive
Chen [35]	$k_s = \frac{1.6E_d}{d}$	Cohesive	Active
Chen [35]	$k_s = \frac{3.3E_d}{d}$	Non-Cohesive	Active

A solution in a dimensionless form which can be utilized for different geometric conditions and soil properties for equations (2.3) and (2.4), which are derived based on the model shown in Figure 2.6, using FDM is given by Debanik Chaudhuri [15].

The pile, in this solution, has been divided into N number of cells based on the FDM method along its length plus four additional imaginary cells, two at each end of the pile, to implement boundary conditions, and the equations have been turned into dimensionless relationships by using a variable R which is dependent on pile stiffness (EI), and k_b which is related to stable layer modulus of subgrade. The dimensional forms of depth (z), pile length (L), sliding layer depth (L_1), and stable layer depth (L_2) using R value are as

$$R = \sqrt[n+4]{\frac{EI}{k_b}} \tag{2.5}$$

$$Z = \frac{z}{R} \tag{2.6}$$

$$Z_1 = \frac{L_1}{R};\ Z_2 = \frac{L_2}{R} \tag{2.7}$$

$$Z_{max} = \frac{L}{R}\ . \tag{2.8}$$

The dimensionless forms of the governing equations (2.3) and (2.4), and their dimensionless finite difference formulations taking that the soil displacement can be expressed in a series form as in equation (2.9), in this way different soil displacement can be generated by choosing different values for the coefficients a_i, proposed by Debanik Chaudhuri [15], are given in equations (2.10), (2.11), (2.12), and (2.13) respectively as

$$\delta_z = \delta_0 \left[1 + a_1.\frac{z}{L_1} + a_2\left(\frac{z}{L_1}\right)^2 + a_3\left(\frac{z}{L_1}\right)^3 + a_4\left(\frac{z}{L_1}\right)^4 \ldots\right] \tag{2.9}$$

$$\frac{d^4Y}{dZ^4} + K_r Z^n Y = K_r Z^n \delta_0 \left[1 + a_1.\frac{Z}{Z_1} + a_2\left(\frac{Z}{Z_1}\right)^2 + \cdots\right] \ for\ \ 0 \le Z \ge Z_1 \tag{2.10}$$

$$\frac{d^4Y}{dZ^4} + Z^n Y = 0 \ \ for\ \ Z_1 \le Z \ge Z_{max} \tag{2.11}$$

$$Y_{i-2} - 4Y_{i-1} + (6 + \Delta Z^4 K_r {Z_i}^n)Y_i - 4Y_{i+1} + Y_{i+2} = \Delta Z^4 K_r \left[1 + a_1.\frac{Z}{Z_1} + \cdots\right] \tag{2.12}$$

$$Y_{i-2} - 4Y_{i-1} + (6 + \Delta Z^4 {Z_i}^n)Y_i - 4Y_{i+1} + Y_{i+2} = 0 \tag{2.13}$$

where in above equations, $Y = \frac{y}{\delta_0}$ is the dimensionless displacement and $K_r = \frac{k_a}{k_b}$ is the modular ratio, in which k_a and k_b are related to sliding and stable modulus ratio respectively.

The above two finite difference equation (2.12), for sliding layer, and (2.13), for stable layer, yield N equations with N+4 unknowns. The remaining four equations comes from the boundary equations at two end of the pile which will enable us to solve for the deflection along the pile length. The complete problem can be defined by three parameters: modular ratio, $K_r = \frac{k_a}{k_b}$, length ratio $L_r = \frac{L_1}{L}$, and a dimensionless pile length $Z_{max} = \frac{L}{R}$.

Based on the studies of Debanik Chaudhuri [15] using finite difference method to solve the governing equitions (2.3) and (2.4), both pile head displacement and maximum bending moment increase with increase in modular ratio K_r, as it is shown by the histograms in Figure 2.7. In addition, pile head displacement increases with increasing L_r as well which indicates that a decrease in embedment depth or stable layer depth results in higher head pile displacements. As for Maximum bending moment, it increases firstly and reach a peak value then decreases subsequently as L_r increases, as it is shown by the histograms in Figure 2.8. The results of the studies by Debanik Chaudhuri [15] indicates also that the main factors affecting pile response to lateral soil movement are:

(i) Pile length.
(ii) Modulus of subgrade.
(iii) Boundary conditions.
(iv) Axial load.
(v) Linearity and yielding of soil.
(vi) Soil displacement profile.
(vii) Pile flexibility.

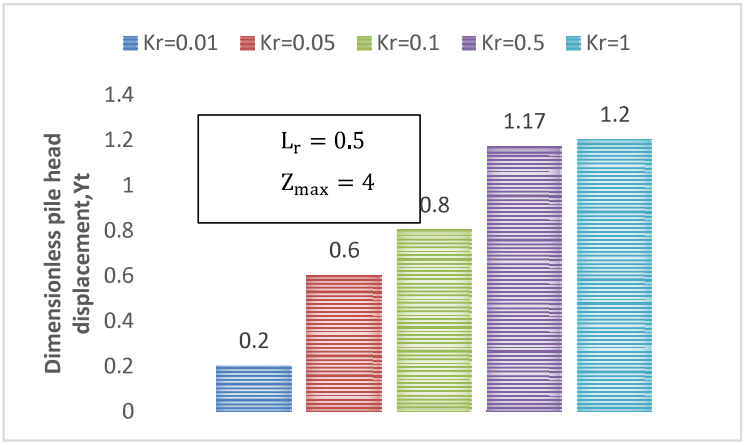

(a)

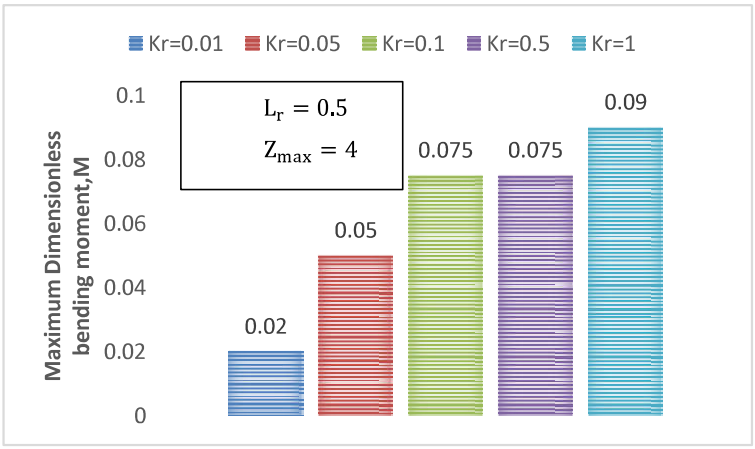

(b)

Figure 2. 7. Effect of modular ratio (K_r), i.e. relative stiffness of soil layers, on (a) pile head displacement and (b) maximum bending moment. Modified from Chaudhuri [15].

Another displacement method is strain wedge approach. In this method, the mobilized soil behavior in front of a passive pile is evaluated based on the stress-strain strength behavior of the soil from the tri-axial test along with the effective stress condition. It is based on analysis of a passive wedge developed in front of the pile upon lateral loading of the pile as it is represented in Figure 2.9 [23].

(a)

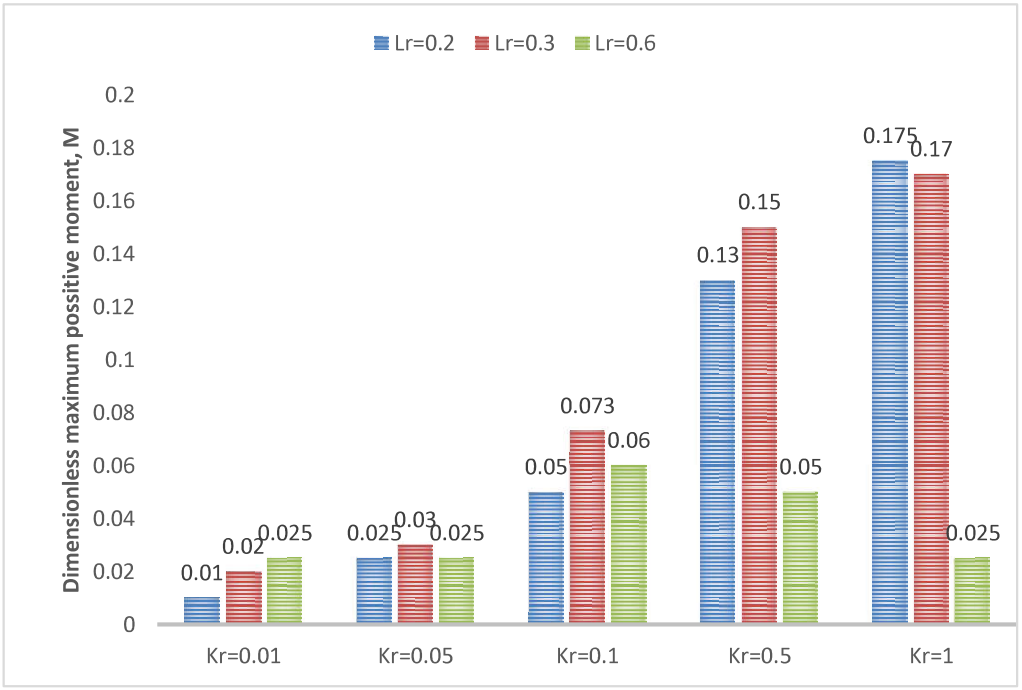

(b)

Figure 2.8. Effect of length ratio (L_r), i.e. pile embedment effect, on (a) pile head displacement and (b) on maximum bending moment. Modified from Chaudhuri [15].

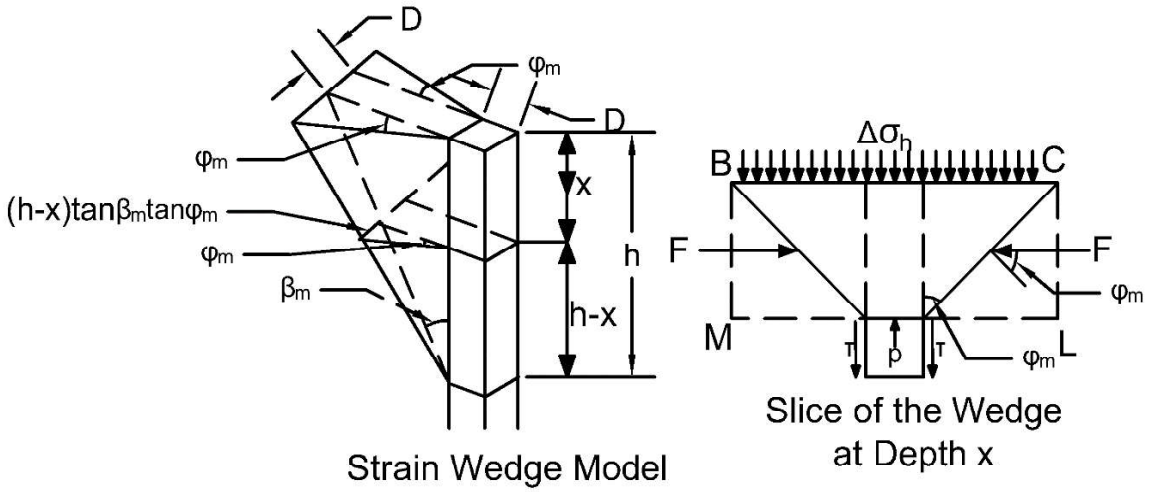

Figure 2.9. Schematics of a passive wedge developed in front of a pile subjected to lateral soil movement. Modified from Ashour [23].

The strain wedge model, as it is shown in Figure 2.9, is developed to solve the beam on elastic foundation (BEF) problem of a laterally loaded pile. In other words, the BEF problem based on the envisioned soil-pile interaction which allows us to find proper values of reaction modulus, E_s, by taking into account both pile and soil properties effect on this parameter. In a nutshell, it can be said that it is an enhancement over the BEF method [23]. The governing equation for a BEF problem can be given as

$$EI\left(\frac{d^4y}{dx^4}\right) + E_s(x) = 0. \tag{2.14}$$

The configuration of the passive wedge at any instant of the load is given by the mobilized friction angle, which is a function of mobilized strain, and as the strain changes along the developing passive wedge length, the shape and depth of passive wedge, pile deflection and state of loading are changed by it constantly [23].

One of the main advantages of the strain wedge method is that it can take into account different sublayers with different soil properties along the pile length and the influence of one layer on another layers displacement and induced stresses are considered since the passive wedges in sublayers are interdependent on each other through the depth of the compound wedge, the geometry of which depends on properties, number of soil types, and the global equilibrium between the soil layer and the loaded pile [17, 23].

The method requires an iterative process to be performed to satisfy the equilibrium between the mobilized geometry of the passive wedge and the deflected pattern of the pile for any level of loading. The following steps are done to find the load developed in the passive wedge at an assumed level of strain [17, 23].

(i) Assuming a strain ε and depth h for the passive wedge developed below which no deflection supposed to happen on the pile.

(ii) Finding the horizontal failure stress at the passive wedge at sublayer i from the relationship

$$(\Delta\sigma_{hf})_i = (\bar{\sigma}_{v0})_i \left[tan^2\left(45 + \frac{\varphi_i}{2}\right) - 1\right]. \quad (2.15)$$

(iii) Calculating the horizontal stress level (SL) using following hyperbolic stress-strain relationships as

$$SL_i = \frac{\lambda_i.\varepsilon}{\varepsilon_{50}}.\exp(-3.707SL_i) \quad (2.16)$$

$$SL_i = \frac{\lambda_i.\varepsilon}{\varepsilon_{50}}.\exp(-3.707SL_i) \quad (2.17)$$

$$SL_i = \exp[\ln(0.2) + \frac{100\varepsilon}{(m\varepsilon+q_i)} \quad (2.18)$$

where

$\varepsilon \leq \varepsilon_{50\%}$ and $\lambda_i = 3.19$ in equation (2.16)

$\varepsilon_{50\%} \leq \varepsilon \leq \varepsilon_{80\%}$ and $2.14 \leq \lambda_i \leq 3.19$ in equation (2.17)

$\varepsilon_{80\%} \leq \varepsilon$, $m = 59$ and $q = 95.4\varepsilon_{50}$ in equation (2.18).

(iv) The horizontal stress developed in front of the wall, and mobilized friction angle can then be calculated by the following relationships as

$$(\Delta\sigma_h)_i = SL_i.(\Delta\sigma_{hf})_i \quad (2.19)$$

$$SL_i = \frac{(\Delta\sigma_h)_i}{(\Delta\sigma_{hf})_i} = \frac{\tan^2(45+\varphi_{mi})-1}{\tan^2(45+\varphi_i)-1}. \quad (2.20)$$

(v) The shear stresses generated at the sides of the pile as

$$\tau_{i,sand} = (\overline{\sigma}_{v0})_i . \tan\varphi_{si} = 2(\overline{\sigma}_{v0})_i . \tan\varphi_{mi} \quad (2.21)$$

$$\tau_{i,clay} = SL_i . \tau_{ult,i} . \quad (2.22)$$

(vi) The induced load at the passive wedge at the face of the pile can written as

$$p_i = (\Delta\sigma_h)_i \overline{BC_i} S_1 + 2\tau_i D S_2 . \quad (2.23)$$

where

$\overline{BC_i} = D + 2(h - x)\tan\beta_{mi} . \tan\varphi_{mi}$

$\beta_{mi} = 45 + \frac{\varphi_{mi}}{2}$

S_1 and S_2 are 0.75 and 0.5 for a circular pile, 1 for a square pile respectively

φ_{mi}: is moblized frictiona anlge at each sublayer

D: is pile diameter or width

h: is developed passive wedge depth

$\overline{\sigma}_{v0}$: is normal stresses ate the midle of each sublayer

φ_{si}: is moblized interface friction anlge at the sides of the pile.

The deflection pattern of the pile in strain wedge model is taken linear over the controlling depth of the soil near the pile top [17, 23]. This allows us to have a linearized deflection angle as it is shown in Figure 2.10(a). Based on this assumption the deflection at the pile head can be found by summing the deflection values at each sublayer starting with the base of the mobilized passive wedge and moving upward as shown in Figure 2.10(b) using the following expressions given as

$$y_0 = \sum y_i \quad (2.24)$$

$$y_i = H_i . \delta_i = H_i \frac{\varepsilon}{\psi_s} \quad (2.25)$$

$$\psi_s = \frac{2}{(1+\nu)\sin 2\Theta_{mi}} \quad (2.26)$$

$$\Theta_{mi} = 45 - \frac{\varphi_{mi}}{2} \quad (2.27)$$

$$\delta_i = \frac{\gamma_i}{2} \quad (2.28)$$

where

y_0: is the pile head deflection

H_i: is the thickness of sublayer i

δ_i: is the deflection angle at sublayer i

γ_i: is the developed shear angle at the passive wedge related to sublayer i [17, 23].

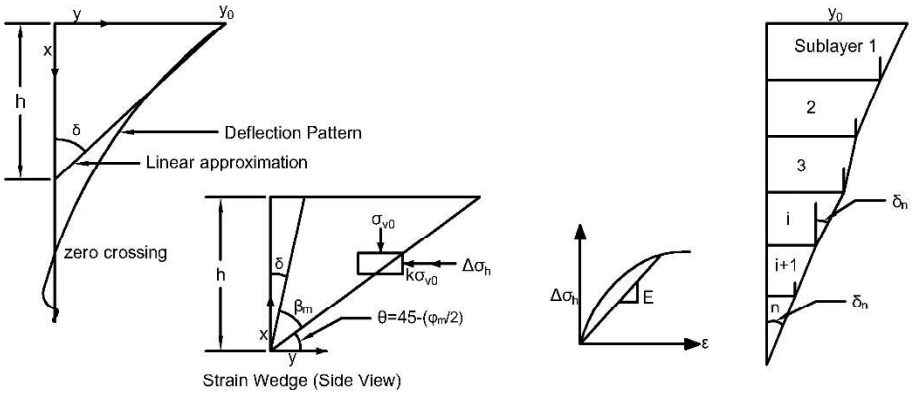

Figure 2.10. (a) Deflection pattern (b) Pile head deflection assembling of a laterally loaded pile. Modified from Ashour [23].

The strain wedge model can be used to enhance beam on elastic foundation (BEF) prediction of pile deflection by suggesting some realistic values for the modulus of subgrade reaction to start with [23]. That is the subgrade reaction modulus to be used in the BEF governing equation can be calculated by using the load (p_i) and pile deflection (y_i) at each sublayer through the relationship $(E_s)_i = \frac{p_i}{y_i}$. Then compatible values of $(E_s)_i$ can be find by comparing the head deflection (y_0) computed from strain wedge method and the BEF method by iteration. If $(y_0)_{SWM}$ turns out to be greater than $(y_0)_{BEF}$ the assumed strain (ε) is decreased until comparable values are encountered and vice versa [23].

The hybrid method is a novel displacement based approach proposed by Kourkoulis et al recently in 2012 for estimating the lateral capacity of passive piles used in slope stabilization. It aims at reducing the amount of computational effort associated with rigorous 3D analysis by modeling pile and the soil at its immediate vicinity instead of

modeling the whole slope-soil pile system [36]. This method consists of the following two simple steps [36].

(i) Estimating the lateral resistance required to increase the factor of safety of the precarious slope to the desired level.
(ii) Calculating the ultimate pile resistance by imposing a uniform displacement profile onto the model boundary.

Although the actual soil displacement imposed in the second step depends on slope geometry, the ultimate resistance of the pile is achieved if the applied displacement at the boundaries is large enough to mobilize the capacity of piles [36].

The displacement profile is applied at a distance of 5D, where D is denoting pile diameter, away from pile center. The selection of the boundaries in the direction of slope as 5D away from the center of piles upward and downward in a homogenous soil has been confirmed by an adequate number of finite element analysis by R. Kourkoulis (2012), showing that soil displacement may be considered as uniform, i.e., unaffected by pile presence beyond a distance of 5D from pile center in a slope stabilization problem [36].

One the the main and most popular displacement based approach is elastic analysis approach. The elastic approach is analyzing the response of a pile subjected to lateral soil movements by modeling the pile as a simple elastic beam and the soil an elastic continuum. Assuming the soil to be an elastic continuum grants this method the power to consider the influence of stresses and forces at other points along the pile length on the displacement of a particular point. This is a major advantage over the subgrade reaction analysis which ignore the continuity of the soil medium [1, 37].

The main advantages of this approach over the subgrade reaction approach is that this approach [1]:

(i) Considers the continuous nature of the soil.
(ii) Enables the analysis of group action of piles under lateral loads.
(iii) Enables consistent analysis of both immediate movements and total final movements.

In the elastic analysis, the solution to the problem of a passive pile is obtained by imposing the compatibility of displacements between the pile and the adjacent soil. The

pile displacement is obtained from the bending equations assuming pile as a thin strip and is affected by the pile bending stiffness and horizontal pile-soil interaction stresses. While the displacement at the soil is evaluated from the Mindlin [38] equation for horizontal displacement caused by horizontal loads within a semi-infinite mass and is related to the soil stiffness, pile-soil interaction stresses and free field soil horizontal movement [16, 37].

Based on this concept, Poulos [37] proposed the model, which is presented in Figure 2.11, in which the pile is assumed to be a thin vertical strip of width d, length L, and constant flexibility of E_pI_p. By dividing the pile into small elements with equal lengths except those at the top and tip of the pile, in order to get deflection exactly at pile head and using finite difference technique, three expressions for pile displacement, soil displacement, and governing equation by considering the model in Figure 2.11 and compatibility of displacement as long as the conditions at the pile soil interface remain elastic have been proposed by Poulos [37]. These equations are given as

$$[D]\{\rho\} = -\frac{dL^4}{E_pI_p}\{p\} \tag{2.29}$$

$$\{\rho\} = \frac{d}{E_{sr}}\left\{\frac{E_{sr}}{E_s}\right\}[I]\{p\} + \{\rho_e\} \tag{2.30}$$

$$\left[D + \frac{II}{K_R n^4}\right]\{\rho\} = \frac{[II]}{K_R n^4}\{\rho_e\} \tag{2.31}$$

where

$\{\rho\}$ is pile displacement vector.

$\{p\}$ is horizontal pressure vector.

[D] is matrix of finite difference coefficients.

E_{sr} is a reference value of soil modulus.

E_s is soil modulus at an element.

[I] is matrix of soil displacement factors.

$\{\rho_e\}$ is vector of external soil displacements.

$[II] = [I]^{-1}$ is the inverted soil displacement factor matrix.

$K_R = \frac{E_pI_p}{E_sL^4}$ is pile flexibility factor.

The expressions in (2.29), (2.30), and (2.31) along with an appropriate boundary condition application at the head and tip of the pile make a system of equations from which

displacement and horizontal pressure at each node or element can be determined. These determined pressures are compared with the yield pressure of soil along the pile length, in case, the computed pressure is greater than the yield pressure of soil at an element, the displacement for that particular element is obtained from the beam equation using the yield pressure. This process is iterated until the pressure is not exceeding the yield pressure of soil at any element along the pile length.

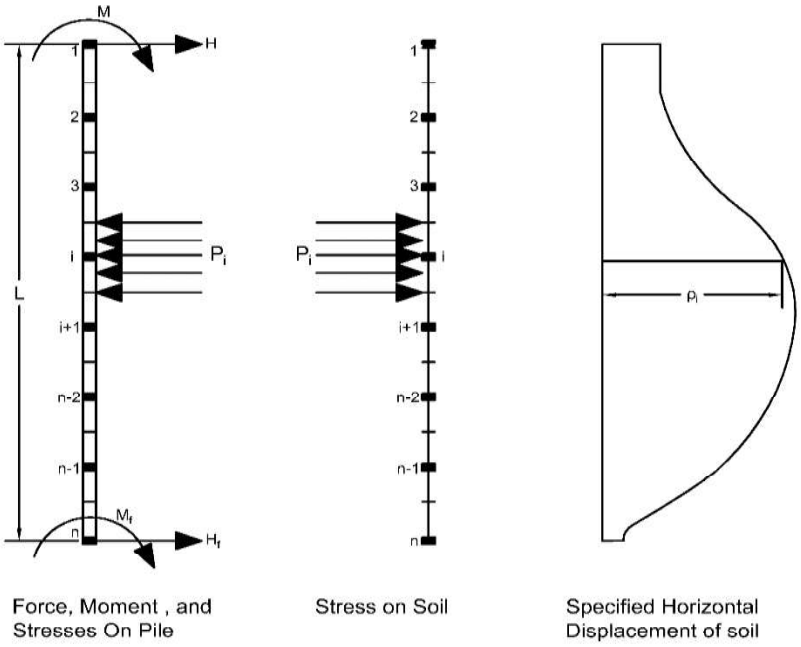

Figure 2.11. Pile model used by Poulos (1995) in elastic analysis in soil undergoing lateral movement. Modified from Poulos [37].

As it is seen in the governing equation (2.10), one of the dominant factors affecting the response of piles subjected to lateral loads is the magnitude and profile of the external or free-field soil movement (ρ_e). This external lateral soil movement can be generated due to unstable slopes, deep excavation, tunneling operations, seismic activities and embankment construction. The response of piles subjected to lateral soil movement due to the mentioned causes by elastic analysis has been briefly discussed here.

The use of piles in the stabilization of slopes and potential landslide has become a noticeable technique in recent decades. The lateral soil movement due to landslides and unstable soil induces lateral loading and bending moment in these types of soils and hence

they are considered passive piles [17-39]. The design of piles for slope stabilization generally consists of three steps [24].

(i) Evaluating the shear force needed to increase the safety factor to the desired level.
(ii) Evaluating the maximum shear force that each pile can provide to resist sliding of the slope.
(iii) Estimation of the optimum pile configuration providing the required resistance.

Among the above three steps, the second step which is related to the response of pile due to lateral soil movement is usually evaluated using elastic analysis by modeling the pile as an elastic beam and the soil as an elastic continuum. One of such an analysis is presented by Poulos [37] by using a simple boundary element and using the governing equation (2.13), and by considering a soil movement distribution for the unstable part of the slope above the critical slip surface as shown in Figure 2.12.

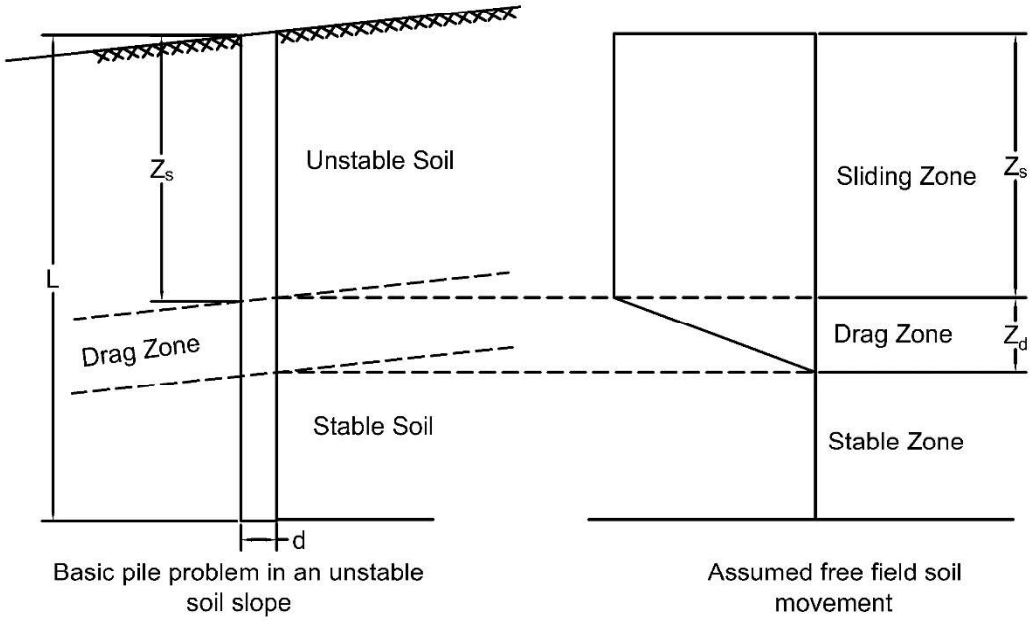

Figure 2.12. A basic pile problem, and free field soil movement in an unstable slop. Modified from Poulos [37].

The factors affecting the bending moment and pile deflection of piles used in the slope stabilizations can be listed as [37]:

(i) Length, diameter and section of the pile.
(ii) Strength and deformation properties of the pile.
(iii) Strength and deformation properties of the soil in stable and unstable part.
(iv) Relative lengths of the pile in stable and unstable part.
(v) Spacing between adjacent piles.

There are many academic studies pointing that pile foundations can be affected or damaged by excavation-induced lateral soil movements. Deep excavation near existing piles generates vertical and horizontal soil movements as a result of which bending moments and deflections are induced in the pile [26].

Due to simultaneous vertical and horizontal induced soil movements, which is indicating the 3D nature of the problem of a pile near the deep excavations, a full 3D finite element analysis (FEA) of the problem, in which pile and soil are modeled together, seems to provide a better prediction of pile response if a detailed site or geotechnical information is available [14]. However, detailed geotechnical data lack in the case of many existing piles near deep excavation and the 3D FEA are time-consuming and complex. Therefore, an elastic analysis is often used to evaluate the lateral response of piles by determining the free field soil movement induced by excavation and imposing this on the pile by a boundary element method [14].

The main factors influencing the lateral response of an existing pile near a deep excavation are [14]:
(i) Excavation dimensions.
(ii) Excavation support conditions.
(iii) Construction procedure.
(iv) Soil properties.
(v) Pile properties.

Figure 2.13 shows a typical response of a reinforced concrete pile with a 22m length, 0.5m diameter which is located 1m away from a 10 m deep braced excavation in terms of pile deflection and bending moment in clay soil for three different stability numbers or strength.

Pile foundations are very common in the stabilization of high-rise buildings in the urban area where they can be greatly affected by underground construction such as tunneling. Tunneling causes ground movements which in turn induces lateral forces and bending moment on adjacent existing piles. Therefore, their effect needs to be considered in the design and execution of underground works [22-41].

Although the problem of a pile subjected to lateral soil movements due to tunneling, essentially, is a 3D problem and hence can be handled conveniently by a 3D finite element analysis, the cost and complexity of such analysis, especially when the non-linear behavior of the soil surrounding the tunnel is to be considered, has always encouraged the researchers to seek alternative options [22].

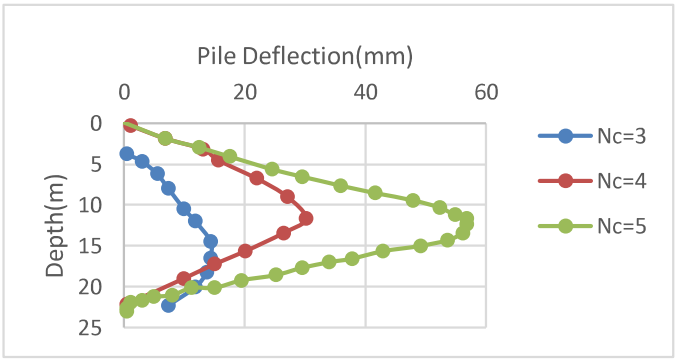

(a)

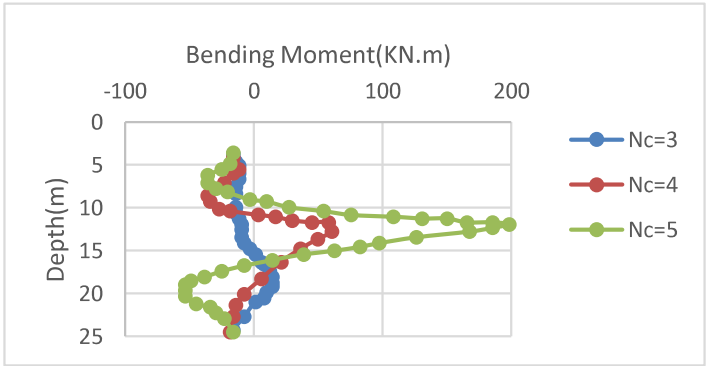

(b)

Figure 2.13. Pile response due to deep excavation (a) deflection (b) bending moment. Modified from Poulos [26].

A more efficient way for assessing of lateral pile response to tunneling has been proved to be a two staged elastic analysis. The first stage include the evaluation of free field lateral soil movement without the presence of pile due to tunnel excavation by either a finite element method as has been demonstrated by Poulos [26], and Surjadinat [22] or an analytical method as has been used by Chen [40], which is given as

$$u_x = -\varepsilon_g R^2 x \left\{ \frac{1}{x^2+(h-z)^2} + \frac{(3-4v)}{x^2+(h+z)^2} - \frac{4z(z+h)}{[x^2+(h+z)^2]^2} \right\} e^{\left[\frac{1.38x^2}{(h+R)^2}+\frac{0.69z^2}{h^2}\right]} \quad (2.32)$$

where

u_x: is lateral soil movement.

R: is tunnel radius.

z: is depth below ground surface.

x: is lateral distance from tunnel centerline.

h: is depth of tunnel horizontal axis level.

ν: is Poisson's ratio.

ε_g: is ground loss ratio.

The second stage involves predicting the pile response to lateral soil movement due to tunneling by imposing the free field soil movement determined in the first stage on the pile by a boundary element method using the finite difference technique. The typical used in the second stage is shown in Figure 2.14 [41]. The soil equilibrium equation used in the second stage can be expressed as

$$\{u_p\} - \{u_x\} = [I_s]\{p\} \quad (2.33)$$

where

$\{u_p\}$= lateral displacement vector of the pile.

$\{u_x\}$= lateral free field soil movement.

$[I_s]$= soil flexibility matrix.

{p}= pile-soil contact pressure vector.

The main advantage of this two-staged analysis is that a single lateral soil movement evaluation for each tunnel configuration is sufficient which can be used with multiple pile configurations [22].

The two-staged elastic analysis indicates that lateral response of the pile to tunneling depends on factors such as tunneling geometry, ground loss ratio, soil strength, pile diameter, and ratio of pile depth to tunnel cover depth, and the maximum deflection and bending moment occur near the spring line of the tunnel [40, 41].

Soil liquefaction has been proved to be one of the main sources leading to the damage of deep foundations during major earthquakes. The loss of soil strength and stiffness due to excess pore water pressure (PWP) in liquefiable soils may bring about lateral ground movement and inertial loads on the pile which in turn may induce large bending moments and shear forces in piles. [42, 43].

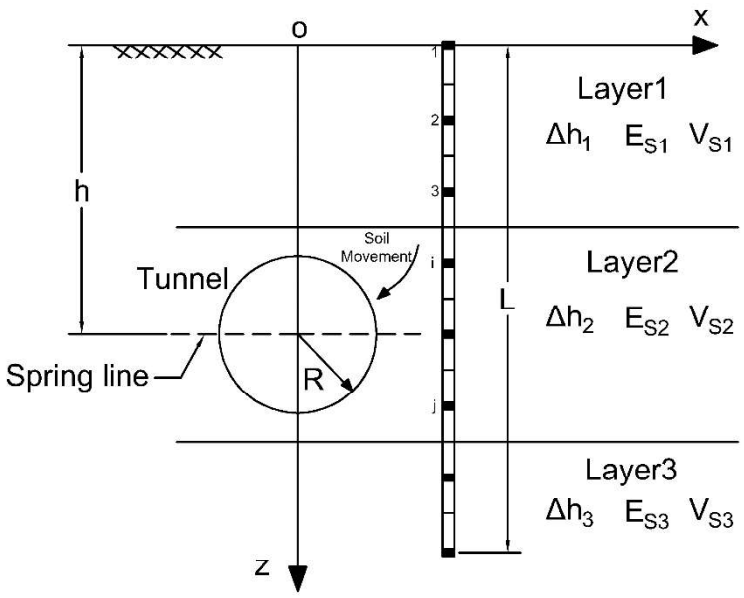

Figure 2.14. Single pile model subjected to lateral soil movement due to tunneling. Modified from [41].

The investigation of the lateral response of piles subjected to liquefaction is more complex than the cases previously mentioned in this section since the dynamic loads are involved in this particular case. Piles are affected by both kinematic loads from lateral ground movement and inertial loads from the vibration of the structure.

Assessment of the lateral response of piles due to liquefaction usually involves the following two steps [42]:

(i) A free field ground response analysis is performed, using a 3D finite element technique usually, from which time history of ground surface acceleration, and maximum ground displacement along the length of the pile is obtained. The former is used to find maximum acceleration of superstructure and hence inertial forces on pile due to the structure.

(ii) Pile response evaluation, bending moment and shear stress calculations along the pile length, utilizing a 1D Winkler model as shown in Figure 2.15 or any other appropriate elastic model by using maximum soil displacement profile and inertial loads determined in the first step.

Parametric studies indicates that factors such as cap mass, pore pressure generation, nature of the earth quake, non-homogeneity of the soil, length of non-liquefiable layer, pile head restriction and presence of slope have significant effect on lateral response of piles exposed to liquefaction [42].

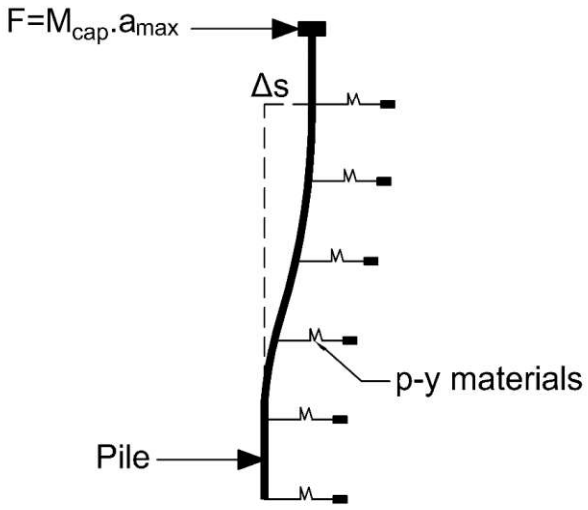

Figure 2.15. Beam on nonlinear Winkler foundation model for analysis of pile subjected to lateral soil movement due to liquefaction. Modified from [42].

In the traditional subgrade reaction approach the pressure developed in front of a laterally loaded pile is related to the pile deflection through linear relationship ($p = k.y$)

often, but the experimental data obtained indicates that the relationship between pressure and deflection at any point along a pile is non-linear as its shown in Figure 2.16 [25, 37]. Therefore, the traditional subgrade approach cannot be used to obtain larger deformation or collapse of the pile in non-linear soils [25, 37].

The non-linear and p-y approach takes this nonlinearity into consideration by applying explicit non-linear relationships between pressure and pile deflection known as p-y curves along the pile length as in Figure 2.17 where p denotes the pressure and y shows the pile deflection. This method is widely known as the p-y method. Although the p-y method was proposed by Reese and Matlock [25] as early as the 1950s, the recent development of high-speed computers and remote strain-gauge reading technique has made the method very volatile and useful.

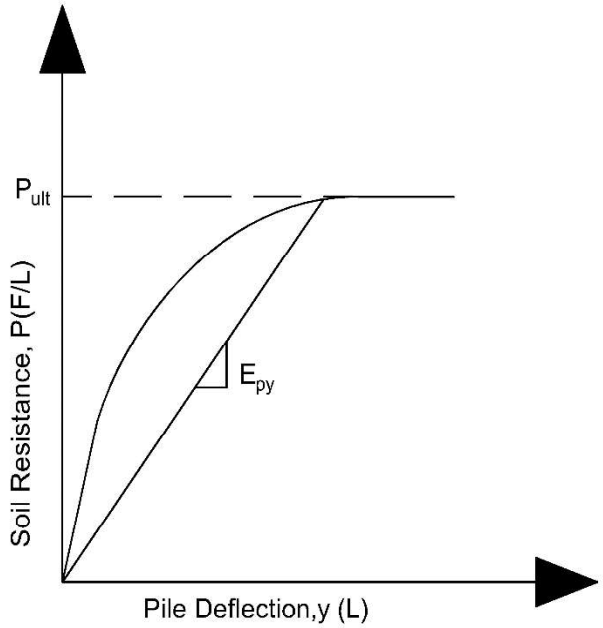

Figure 2.16. A typical p-y curve. Modified from Reese and Matlock [25].

In this method, the solution requires the input of a series of p-y curves in the governing equation (2.12) of a laterally loaded pile along the pile length. Then an iterative solution of the governing equation (2.13) is done using the finite difference technique until compatible p and y values are obtained at all points along the pile length [1].

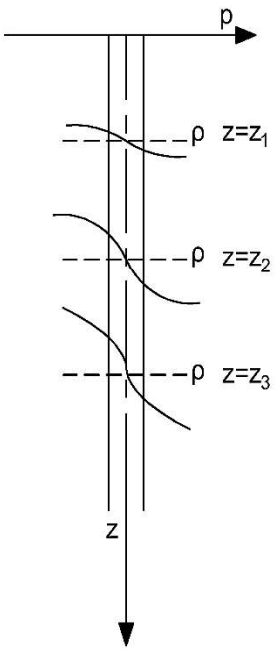

Figure 2.17. p-y curves concept along the pile length. Modified from Poulos [1].

The p-y curves can be constructed using one of the following approaches [1]:

1. Full scale load tests on piles.
2. Empirical relationships.
3. Theoretical relationships.

2.3.2. Experimental Methods for the Analysis of Piles Subjected to Lateral Soil Movement

The existing experimental methods for the investigation of pile response due to lateral soil movement can be divided broadly into the following three categories.

(i) Model tests
(ii) Centrifuge tests
(iii) Full-scale tests

The following subsections present a review of some of the relevant published academic papers related to the above three categories respectively. In each case, a brief description of the test, the design of the apparatus used to perform the test, and the results of the test have been discussed briefly. In addition, the recently reported tests related to model

tests, centrifuge tests, and full-scale tests have been summarized in Table 2.5, Table 2.6, and Table 2.7 chronologically.

2.3.2.1. Model Tests. One of the most popular model tests evaluating the response of passive piles to lateral soil movement was conducted by Matsui et al [44]. He carried out a series of model tests for various conditions of pile and soil to check the validity of the theoretical formulas for lateral force prediction as a result of horizontal soil movement on a row of piles based on the theory of plastic deformation presented by Ito and Matsui [44].

Matsui et al [44] conducted a series of tests in both clay and sand with the aid of an apparatus consists of mainly an air pressure device for applying lateral force, a recording system, and a container box, which is 60 cm long, 30 cm wide, and 30 cm deep, in the center of which a row of model piles have been placed. The experimental results of these tests show that the plastic deformation assumption made for the derivation of theoretical equations is valid and there is a good agreement between the theoretical and measured values for lateral force on pile rows for both clay and sand cases. Moreover, it was shown that, although, the analytical equations proposed by De Beer and Carpentier [45] slightly underestimate the lateral force on piles for clayey soil, it significantly underestimates the lateral force in the case of sand and for a larger pile to pile distance.

Later on, in 1995 Poulos and Chen [46] conducted some tests on single instrumented aluminum circular model piles in calcareous sands undergoing lateral soil movement to assess the influence of some key parameters such as pile head fixity, pile embedded length, and pile diameter on the maximum bending moment developed in the pile. The equipment used for conducting the tests consisted of a steel vessel having internal dimensions of 450mm wide by 565mm long and by 700mm deep. The lateral movement was imposed on the soil inside the vessel by a manually controlled loading system and with the aid of two vertical steel plates inside the vessel each of which hinged at the mid-height.

The experiment results indicate that the maximum bending moment occurs at the vicinity of the interface between the moving and stable soil layers and it increases as the soil surface displacement(y) increases. The results also seem to suggest that when the stable layer thickness is very small compared to unstable layer thickness, the pile is carried by the

unstable layer without casing substantial bending moment in the pile, hence demonstrating a short pile mode. In the opposite case, the soil tends to pass the pile and does not produce substantial bending moment as well which represents a long pile behavior. But in the case when stable layer and unstable layer thicknesses are similar, the bending moment is higher than in the first two cases.

As for the head fixity and pile diameter, the result of the current model test suggests that if the pile head is fixed then the maximum bending moment value drops and it tends to happen at a depth slightly above the sliding depth, and the maximum bending moment increases with increase in diameter.

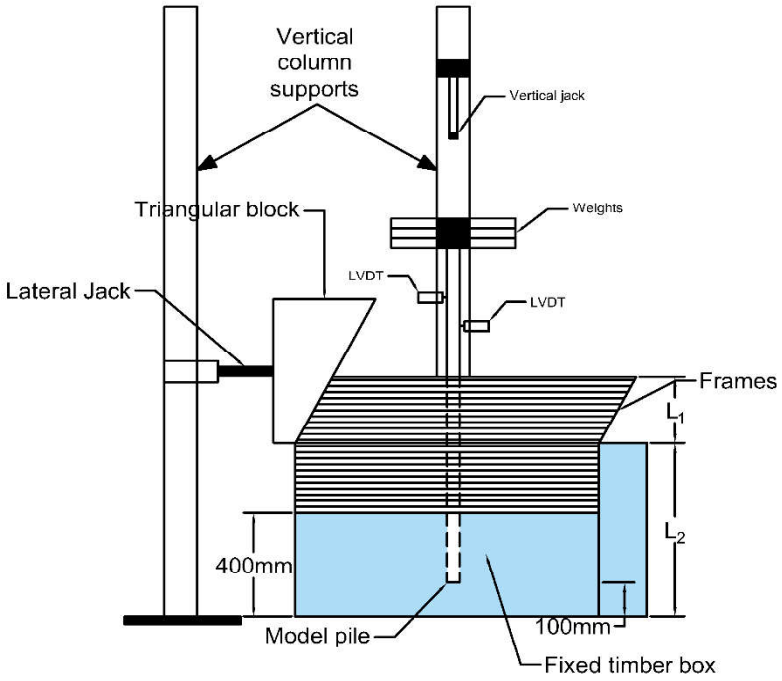

Figure 2.18. Schematic of the test setup used by Qin and Guo. Modified from Qin and Gue [47].

In 2002 J. L. Pan [48], conducted some model tests on coupled piles subjected to passive loadings in soft clay the focus of which was to investigate the ultimate soil pressure acting on a pile shaft. The result of his experiments suggest that the ultimate soil pressure P_u for coupled piles in a row was $7.1S_u$ for a pile spacing of 3B, and $8.6S_u$ for pile spacing of 5B. Where, S_u is the undrained shear strength of clay and B is the width of the model piles. These ultimate soil pressure values are close to the values, $9\text{-}12S_u$, suggested by

Randolph and Houlsby [49] and Chen [50], and was shown that the magnitude of soil pressure required to mobilize them were 0.2B to 0.7B for spacing of 3B and 5B respectively.

Qin and Guo [47] examined the effect of lateral movement profile and axial load presence on the response of a passive 1200mm long aluminum model pile with a diameter of 25mm embedded in the sand. They used an apparatus consists of a loading system and a shear box, having 1m length, 1m width, and 0.8m height, the schematic view of which is shown in Figure 2.18. The upper part of the equipment they used in their experiment was made of a series of 25mm thick square laminar steel frames on which a triangular or rectangular lateral movement could be imposed with the help of a triangular or rectangular block.

Their test results indicate that the maximum bending moment along the model pile increases up to 95~160% for a triangular profile than a rectangular soil movement. It was also shown that maximum bending moment (M_{max}), maximum shear force (T_{max}) and deflection at ground surface (y) of the piles subjected to a rectangular soil profile increases linearly with frame movement immediately while the M_{max}, T_{max}, and y of the piles subject to triangular lateral movement are nearly zero up to a 40mm frame movement and then increases linearly.

Recently, in 2014 Ersoy and Yıldırım [51] studied the response of piles used to increase slope stability under lateral soil movement by conducting large scale model tests on 800mm long pipe piles having 32mm diameter and 5mm thickness in sands with different relative densities (50%, 60%, and 70%). Their test involved the lateral movement of four instrumented pile in a row with a center to center spacing of 2.7 times the pile diameter in a shear box consists of a moveable upper box, 77 cm wide, 70 cm long, and 45 cm high, and a fixed lower box, 77 cm wide, 85 cm long, and 45 cm height.

Their measurements of maximum bending moment, pile deformation, and pile head deflection with the aid of installed strain gauges along the pile show that both maximum bending moment along the pile section below the sliding surface and lateral pile displacement increase as the relative density decreases.

2.3.2.2. Centrifuge Model Tests. In geotechnical engineering, centrifuge model tests on piles are done in order to simulate and mimic the conditions of a prototype pile for better investigation of pile response to different loadings by spinning the model on a centrifuge. The purpose of spinning is to increase the g-forces on the model so that the load on the model is equal to loads on the prototype.

Stewart et al [52] reported the result of a series of centrifuge model tests examining the response of piled bridge abutment on soft clay in which he assessed the effect of some important factors on the behavior of the model piles such as group effect, embankment geometry, embankment height, raking piles effect, and time.

His model tests were conducted with an Acutronic mode 661 centrifuge having a platform radius of 1.8m, and a maximum capacity of 40 g-tone on a single pile and two rows of seven piles, having a center to center spacing of 4.9 pile diameters, with 3.18mm width fabricated from brass.

The experimental results from these tests indicate that although the bending moment distributions of single pile and pile group show generally similar shapes, the pile group bending moments are higher in the upper part of the pile as it is shown in Figure 2.19. In addition, Maximum bending moment and pile head deflection values increase as embankment load increases, and if raking piles are used there will be a 20 to 30% reduction in these values. İn addition, the pile response is time-dependent with 70% of the moment and pile deflection due to undrained deformation and the remaining 30% as a result of ongoing consolidation.

In the 2000s the results of several centrifuge model tests on piles were reported by C. F. Leung in which the response of a single pile subjected to excavation induced soil movements in the sand in 2000 by Leung [53], the response of pile groups subjected to lateral soil movements due to deep excavation in the sand by Leung [54], pile behavior due to excavation induced soil movements behind a collapsed wall in clay by Leung [55], 2006), and pile behavior due to excavation induced soil movements behind a stable wall in clay by Ong, and Leung [56] were evaluated.

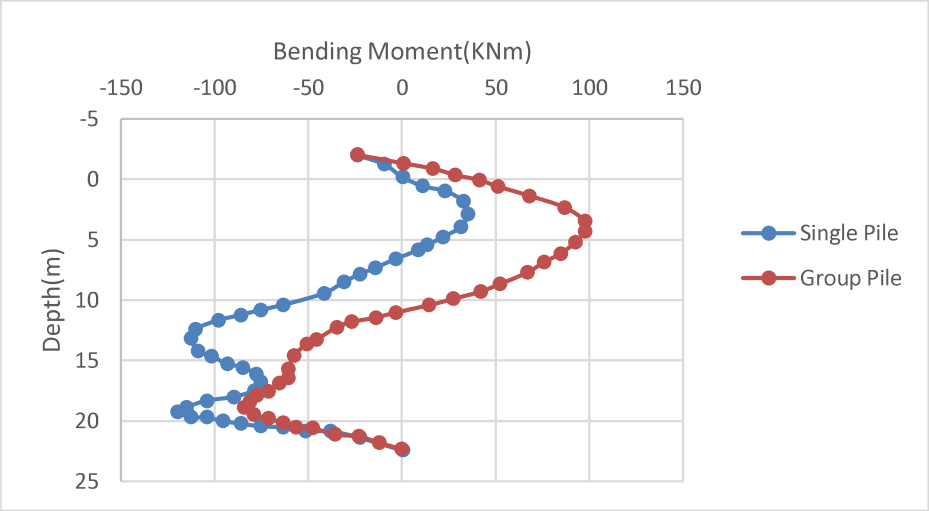

Figure 2.19. Bending moment distribution along the pile length for single and group piles from a centrifuge model test. Modified from Stewart et all [52]

The model tests in these studies were conducted at 50g on a 2m radius centrifuge machine in the National University of Singapore. The centrifuge model container utilized had internal dimensions of 540mm length, 200mm width, and 470mm height (the schematic setup of which is shown in Figure 2.20). Alluminum tube piles and aluminum alloy plate at 50g were used to simulate the retaining wall of the excavation and prototype concrete piles respectively, and the excavation process was simulated by gradually draining a latex bag containing zinc chloride ($ZnCl_2$), having the same density and height as the removed soil in front of the wall.

The general results from these centrifuge model tests done by C.F. Leung in the 2000s can be summarized as follows:

(i) The induced maximum bending moment and pile head deflection increase as excavation depth is increased and decrease exponentially as the pile is located further away from the retaining wall both in clay and sand.

(ii) Maximum bending momenta and pile head deflection in case of clay continue to increase with time even after the excavation completion owing to PWP dissipation.

(iii) Piles located within the failure zone behind the retaining wall experience higher bending moment and pile head deflection compare to piles located outside the failure zone.

(iv) The soil movement around the pile behind a collapsed wall is far more severe which indicates that the 3D nature of the pile response, in this case is, more significant.

(v) İndividual piles are not affected significantly by the group interaction when the piles are located in a row parallel to the retaining wall. In contrast, if the piles are arranged in line perpendicular to the wall, the front piles reduce the influence of induced soil movements due to excavation significanlty on rear piles.

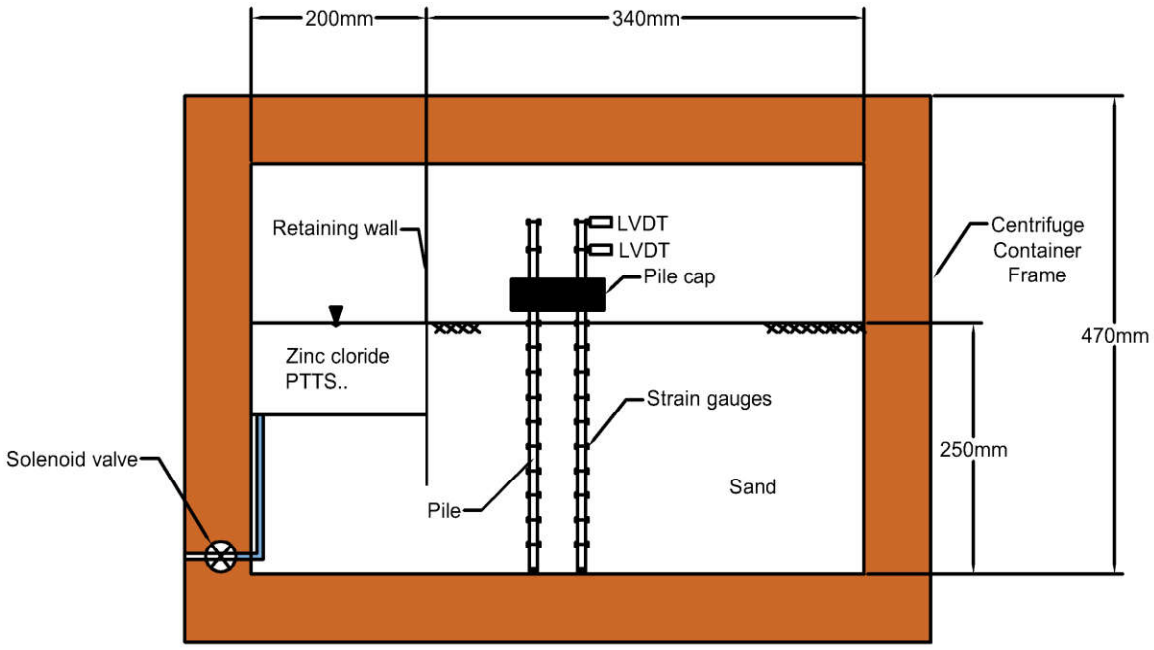

Figure 2.20. Schematic set up of centrifuge model test used by C.F. Leung. Modified from Leung [53].

2.3.2.3. Full Scale Field Tests. Field tests are the most reliable techniques for lateral pile response due to soil movements which are done on actual instrument piles. The only problem with these types of tests is the difficulty of instrument existing piles practically.

Goh and Wong [57] conducted an actual full-scale instrument test to evaluate the response of a row of 1m diameter and, 46m long concrete bored piles located 3m behind a

0.8m thick concrete diaphragm wall supporting a 16m deep cut and cover tunnel. The pile deflection and soil movement were monitored during the excavation by two inclinometers: one in a pile and another one 6m away from the edge pile in soil (the plan layout of piles and inclinometers are shown in Figure 2.21). The test results suggest good conformity between the measured pile movement and bending moment values along the pile length with predicted values by a numerical procedure based on a finite element method as is shown in Figure 2.22.

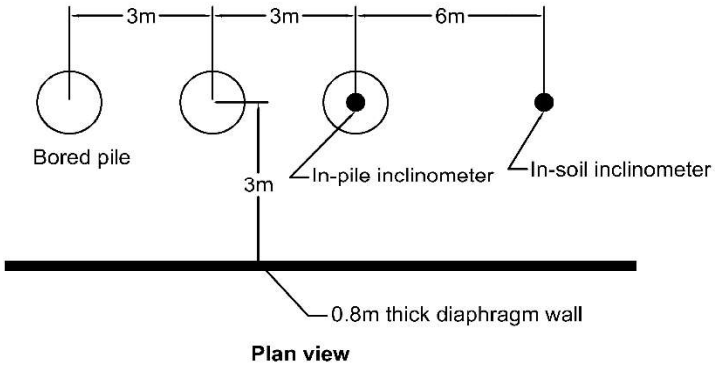

Figure 2.21. Piles and inclinometers plan view used in the field. Modified from [57].

In 2012, S. Lirer [58] reported his observation of a field test on five piles in a row installed in an active mudslide in the Basento Valley, Southern Italy. The piles used in this test were 10m long, 6mm thick, and 0.4m in diameter steel tubes installed in the middle of the mudslide having a 5m sliding body thickness. Soil movements, pile displacement, and bending moment were monitored for 3 years using three inclinometers (one uphill, one downhill, and one inside the pile in the direction of mudslide), and 12 pairs of strain gauges. The results show that even a single row of piles have not been able to stop the mudslides in this case, it has affected the displacement field around it as the displacements of the downhill inclinometer are smaller than the uphill one, indicating the preventive capacity of piles against mudslides and slope instabilities.

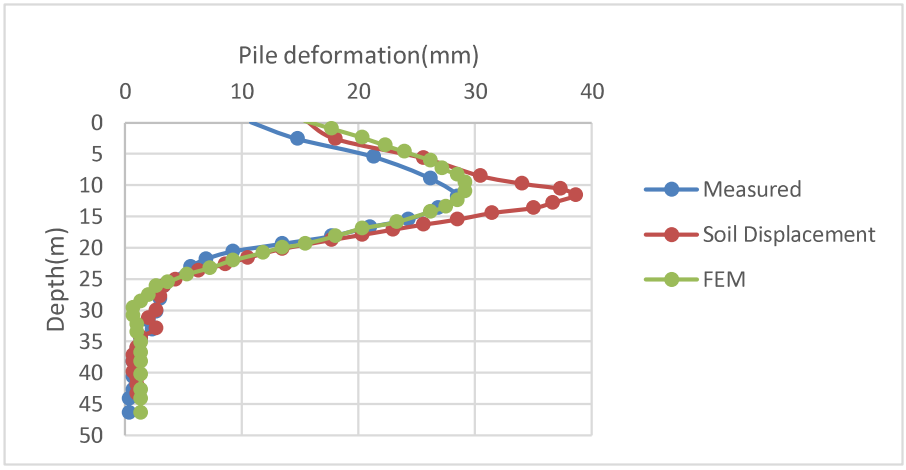

(a)

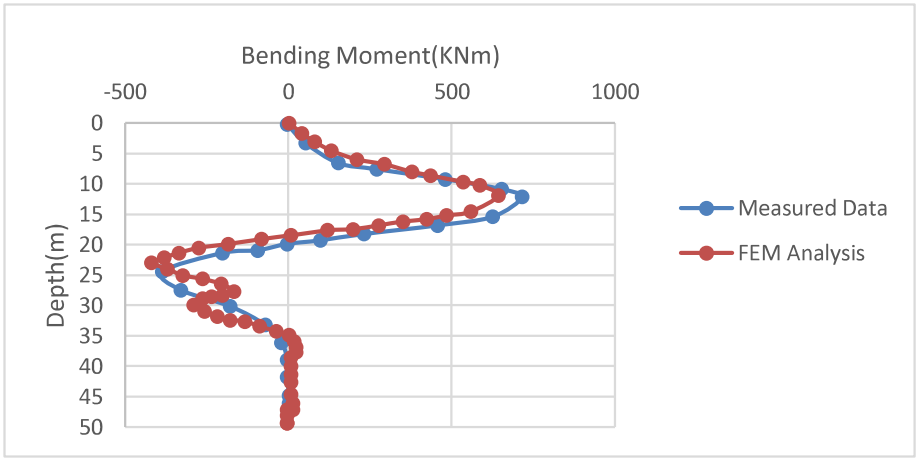

(b)

Figure 2.22. Measured and predicted (a) pile displacement and (b) pile bending moment. Modified from [57].

Recently Xiang [59] performed a field test in which the behavior of a group of pipe piles used in the slope-stabilization of a highway, hence simulating the performance of slope-stabilization pile groups subjected to lateral soil movement, was evaluated. Three test pile groups, M1, M2, and M3, each having different configuration, consists of steel pipes with 6m length, and 140mm in diameter were installed in the slope and loaded by filling soils behind the pile group in four stages, the heights of the fill were 3,5,7, and 10m respectively.

The main purpose of this field test was to investigate the influence of the number of pile rows, row spacing, and pile spacing on the overall behavior of the pile groups. It was

observed that the maximum displacement of M3 group of piles, having less row spacing and pile spacing than M2 and more number of piles than M1, was 55% of that of M1 and 62-71% of that of M2 demonstrating pile center to center distance and the number of piles importance. In addition, it was observed that the maximum bending moments in the front, middle, and rear rows all occur near the sliding surface, and the earth pressure above the sliding surface has a triangular distribution. The earth pressure and bending moment distribution along the depth of the pile for a pile in M2 group are shown in Figure 2.23.

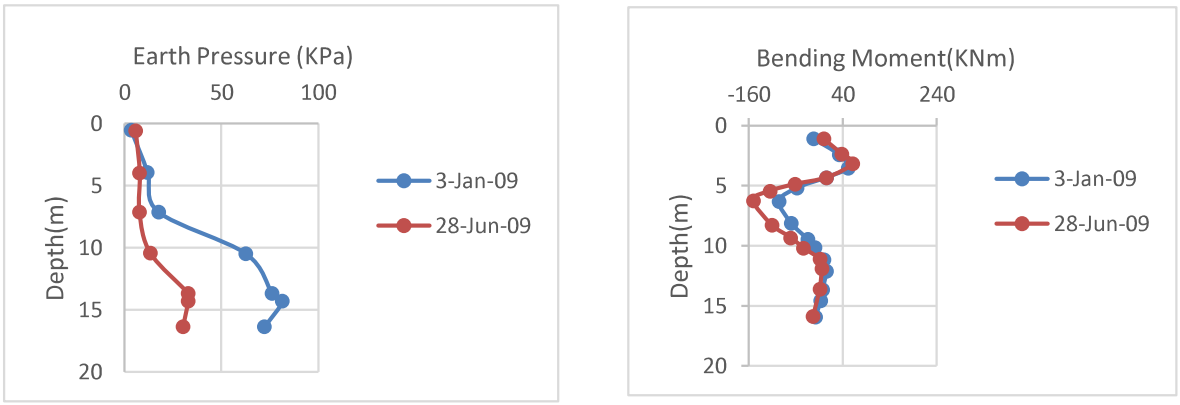

(a) (b)

Figure 2.23. (a) Earth pressure distribution and (b) bending moment distribution for a pile in the center of group M2 piles. Modified from Xiang [59].

2.3.3. FEM Analysis

One of the most rigorous and reliable methods in the analysis of piles response subjected to lateral soil movement is the finite element method (FEM). The method is capable of considering both pile and soil with a complex geometry simultaneously and hence can present a better, accurate, and non-linear soil-pile interaction. Despite the fact that the FEM is rigorous and accurate method in passive pile analysis, a full 3D FEM analysis is not preferred in small projects due to higher computer execution time and higher costs in terms of data preparation.

The recently reported tests in the literature on FEM analysis, model tests, centrifuge model tests, and full-scale field tests are summarized in the following tables chronologically.

Table 2.3. Summary of some of the recent FEM studies on passive piles.

Main Authors	Spring-man	Stewart	Bransby	Chen	Chen	Miao et al
Year of Publication	1989	1992	1995	2001	2001	2006
2Dimensional /3Dimensional	3D	2D	3D	3D	2D	3D
Program Used	CRISP SINPILE	AFENA	CRISP94	FLAC	FLAC	ABAQUS
Analysis Type	Finite Element	Plain-Strain	Finite Element	Finite Element	Axi-symmetric	Finite Element
Soil Type	Clay and Sand	Cohesive Soil	Cohesive Soil	Cohesive and Cohesion-less	Cohesive and Cohesion-less	Cohesive
Soil Model	Linear Elastic	Linear Elastic	Linear Elastic	Mohr-Coulomb	Mohr-Coulomb	Mohr-Coulomb
Pile Model	Solid Element	Beam-Column Element	Solid Element	Beam Element	Beam Element	Beam Element
Reference	60	61	62	63	63	64

2.3. Piles under Combined Uplift and Lateral Loading

Pile foundations designed to support structures like transmission towers, mooring systems, tall chimneys, and jetty structures are often subjected to a series of combined loading. These types of piles are supposed to carry both tensile forces and lateral passive loadings in case they are placed near the excavation, tunneling operations, and embankments due to lateral soil movement and overturning moments.

Although, the response of pile and pile groups subjected to lateral soil movement and tensile forces independently have been thoroughly studied by many researchers, however,

very limited studies on the behavior of piles subjected to both lateral soil movement and tensile forces simultaneously are reported.

The results of model tests on a single pile subjected to both lateral loading (active load) and tensile forces simultaneously in dense sand by Madhusudan [67] indicate that the behavior of the pile under combined lateral and tensile loading is substantially different compared to pile response under lateral and tensile forces independently. The observation from the same test shows that, although, the ultimate lateral/uplift capacity of the pile increases relatively under combined lateral and tensile loading, the pile head deflection increases as well at the safe lateral/uplift force which means that the increased capacity may not be possible in practical design. Even though the pile was subjected to combined tensile and active loading in Madhusudan [67] test, not passive loading, it seems that the response of the pile under combined tensile and passive loading would show somehow similar behavior. The model piles properties, tank dimensions used in Madhusudan [67] are given in Table 2.4. Meanwhile, Table 2.8 gives the lateral capacity of the model piles subjected to 40%, 60%, and 80% of their correspondent uplift capacity.

Table 2.4. Model piles and tank properties used in Madhusudan. Modified from Madhusudan [67].

Model Piles Properties	
Pile Material	Aluminum
Outer Diameter	25.4mm
Inner Diameter	19mm
Model Test Tank	
Tank Material	Steel
Length	1m
Width	1m
Depth	1.2m

Table 2.5. Summary of reported model tests, centrifuge tests, and field tests on passive pile from 1982 to 2002.

Main Authors	Matsui et al	Stewart	Poulos and Chen	Leung et al	Pant et al
Year of publication	1982	1994	1995	2000	2002
Type of test	Model test	Centrifuge test	Model test	Centrifuge test	Model test
Group/Single test	Group	Group	Single	Single	Coupled piles
Loading type	Static	Static	Static	Static	Static
Soil profile	Sand and Clay	Soft Clay	Sand	Sand	Soft Clay
Pile cross-section	Circular	Square tube	Circular	Square	Square
Pile material	N/A	Brass	Aluminum	Aluminum	Steel
Pile dimensions	Diameter: 2,3,and 4cm	Width: 3.18mm	Diameter: 25,35, and 50mm Length: 100cm	Width: 12.6mm Length: 350mm	Width:20mm Length: 295mm Thickness:6mm
Center to center pile spacing	5cm, 6cm, 7.5cm, 15cm, or 30cm	4.9d	N/A	N/A	3xpile width & 4xpile width
Container box material	Steel	Aluminum	Steel sheets	Stainless steel	N/A
Container box dimensions	Length:600mm Width: 300mm Height:300mm	39x65x32.5cm	Length:565mm Width: 450mm Height:700mm	Length:540mm Width: 200mm Height:470mm	Length:570mm Width: 321mm Height:215mm
Lateral movement Profile	Rectangular	N/A	Triangular	N/A	Rectangular
Reference	22	25	23	34	35

Table 2.6. Summary of reported model tests, centrifuge tests, and field tests on passive pile from 2003 to 2010.

Main Authors	Leung et al	Goh et al	Ong et al	Leung et al	Qin and Gue
Year of publication	2003	2003	2006	2006	2010
Type of test	Centrifuge test	Field test	Centrifuge test	Centrifuge test	Model test
Group/Single test	Group	Group	Single	Single	Single
Loading type	Static	Static	Static	Static	Static
Soil profile	Sand	Sand and Clay	Clay	Clay	Sand
Pile cross-section	square	Circular	Square	Square	Circular
Pile material	Aluminum	Reinforced Concrete	Aluminum	Aluminum	Aluminum
Pile dimensions	External width:9.53mm Internal Width: 6.35mm	Diameter:1m Length:46m	Width:12.6mm Length:350mm	Width: 12.6mm Length: 350mm	Diameter:25mm Length: 1200mm Thickness:1.6mm
Center to center pile spacing	3.2xwidth	3m	N/A	N/A	N/A
Container box material	Stainless steel	N/A	Stainless steel	Stainless steel	Sliding part: Steel Fixed part: Timber
Container box dimensions	Length:540mm Width: 200mm Height:470mm	N/A	Length:540mm Width: 200mm Height:470mm	Length:540mm Width: 200mm Height:470mm	Length:1000mm Width: 1000mm Height:800mm
Lateral movement Profile	N/A	N/A	N/A	N/A	Uniform and Triangular
Reference	26	27	36	37	24

Table 2.7. Summary of reported model tests, centrifuge tests, and field tests on passive pile from 2011 to 2015.

Main Authors	Zhang and White	Lirer	Ersoy and Yildirim	Xiang and Zhang
Year of publication	2011	2012	2014	2015
Type of test	Centrifuge test	Field test	Model test	Field Test
Group/Single test	Single	Group	Group	Group
Loading type	Cyclic	Static	Static	Static
Soil profile	Soft Clay	Clay	Sand	Sand Overlain by Clay
Pile cross-section	Circular	Circular	Circular	Circular
Pile material	Aluminum	Steel	Aluminum	Steel
Pile dimensions	Diameter:12mm Thickness:1mm Embedment Depth:60mm	Diameter:0.4m Length:10m Wall thickness:6mm	Diameter:35mm Length:80mm Wall thickness:5mm	Diameter:140mm Length:6m Wall thickness:4.5mm
Center to center pile spacing	N/A	2.25d and 3d	2.7d	1.5 and 1.7m
Container box material	N/A	N/A	N/A	N/A
Container box dimensions	Length:650mm Width: 350mm Height:390mm	N/A	Length:155cm Width: 154cm Height:90cm	N/A
Lateral movement Profile	N/A	N/A	Triangular	N/A
Reference	38	39	40	28

Table 2.8. Ultimate lateral load on model pile head. Modified from Madhusudan [67].

Length to Depth Ration	**Ultimate Lateral Load(N)**			
	Without Pullout Load	40% of Pullout Capacity	60% of Pullout Capacity	80% of Pullout Capacity
18	429	590	665	714
26	540.6	635	712	820
38	545	658	726	865

2.4. Past Studies on Multiple Friction Joint Piles (or MFJP piles)

Multiple Friction Joint Pile or MFJP is a type of pile designed at Boğaziçi University [68]. The MFJP piles consist of a series of mortar blocks, and rubber sheets in between them. The rubber sheets increase the ability of the piles to absorb more energy while deforming. The mortar blocks and the rubbers have holes in their center which facilitate the assembling and fixing of them together with a high tensile strength rod. This configuration provides the ability to control the flexibility of the pile to the desired level by the post-tensioning technique [68].

The MFJP pile has been studied in detail at Boğaziçi University by many researchers in the past years to investigate flexural rigidity of this type of pile, as well as stress distribution between the mortar blocks in MFJP. In addition, the response and capacity of the MJFP pile subjected to lateral loading, and cyclic loading have been analyzed and evaluated also.

Yahia [69] studied multiple friction joint piles (known as segmental piles with variable flexural rigidity in his studies) under static and cyclic loadings using Winkler's beam on elastic foundation theory. The MFJP piles used were either post-tensioned to 750N force or 2250N force. The flexural rigidities of the MFJP pile post-tensioned to 750N and the MFJP pile post-tensioned to 2250N were determined through a series of bending moment tests and it was shown that the MFJP pile with 2250N have a flexural rigidity four times greater than that of the MFJP post-tensioned with 750N force.

The MFJP piles were supported on manufactured springs with 1K, 2K, and 3K (K=4N/mm) spring constants, and they were deformed under lateral loads to reach a maximum displacement of 4mm. During the application of the lateral and cyclic load, the deformation of spring was recorded from which the load-deflection curve, and shear and bending moment distributions along the model pile were obtained. The materials used in the preparation of MFJP piles along with their properties and the results of the cyclic and static loads on the MFJP piles by Yahia [69] are shown in Table 2.8 and Table 2.9.

Table 2.9. Materials used to produce MFJP piles by Yahia [69].

Mortar Blocks	
Cement Type	Portland Cement
Mix Proportions	1:0.5:3 (C:W:S)
Dimensions	50mmx50mmx20mm
Compressive Strength	20MPa
Number of Mortar Block Used	15
Rubber shore 60	
Rubber Type	Neoprene Rubber 1
General Description	Soft Rubber
Style	7797
Colour	Black
Tensile Strength $\left(\frac{KN}{m^2}\right)$	$10x10^3$
Elongation ar Failure(%)	125
Elastic Modulus(Mpa)	3
Thickness(mm)	3
Rubber Shore(A)	60
Aluminum Profile Plates	
Dimensions	50mmx50mmx20mm
Functionality	As Bearing Plate

The MFJP piles under cyclic load were also studied by Sengez [70] . The tests were conducted in loose and medium dense sand and on three MFJP model piles. The First MFJP pile was post-tensioned to 750N force while the second and third model piles were post-tensioned to 1500N and 2250N force. The cyclic loading was applied by the agonistic and antagonistic pneumatic muscles. The cyclic load was applied at the head of the model piles

while the deflection along the model pile length was measured by a series of LVDTs along the model piles length.

In addition, the load-displacement, shear force, and bending moment curves along the model piles length were also constructed with the help of the stress mapping technique. Sengez [70] demonstrated that as the MFJP pile rigidity increases, the pile head displacement experiences a decrease under lateral cyclic loading. Moreover, increasing the number of cycles in cyclic loading causes a small increase in the displacement. The MFJP piles were subjected to a cyclic loading of 300N with 100 cycles and then loaded up to a static load of 600N. The pile head displacements, and maximum shear forces along the MFJP pile length (which had a length of 34 cm and a width of 5 cm) under this loadings are given in Table 2.10.

Table 2.10. Lateral load tests' results on MFJP piles from Yahia [69].

Load Type	Spring Coeficient (N/mm)	Max Pile Head Displacement(mm)	Pile Head Force(N)	Slope at the Pile Head (Degree)	Max Bending Moment (KNm)	Max Bending Moment Position from Pile Head	Max Shear Force (KN)
Static	4	4	80	0.00395	0.0061	2D	0.088
static	8	4	200	0.00961	0.014	2.5D	0.177
static	12	4	200	0.0133	0.0173	2.7D	0.206
cyclic	4	4	100	NA	NA	NA	NA
cyclic	8	4	200	NA	NA	NA	NA
cyclic	12	4	150	NA	NA	NA	NA

Keklik [71] conducted a series of tests on MFJP piles under static lateral loading. The tests were carried out on an MFJP pile (post-tensioned to 750N force), and on an MFJP pile (post-tensioned to 2250N force). Both model piles were subjected to 50mm lateral displacement at their head in loose and medium-dense sand. The load at the pile head was measured with a load cell and the load-displacement curves were constructed to evaluate the capacities of the MFJP Piles. The inclination and displacement of the mortar blocks along the MFJP piles length were also measured by installing magnetometers sensors on each block.

Keklik[71] results indicate that although the MFJP piles used in the experiments are classified as short piles base on their length, the MFJP pile with a post-tension of 750N force behaves like a flexible pile both in loose and medium-dense cases. The MFJP with 2250N post-tensioned force acts like a rigid pile in loose sand while its response in medium-dense sand is similar to that of flexible piles. It was also observed that both MFJP piles didn't show any sign of breakage during the experiments even they were subjected to a large displacement of 50mm. The lateral capacities of the MFJP piles are summarized in Figure 2.24.

Burak [72] also conducted tests on MFJP pile post-tensioned to 750N by applying a lateral displacement of 50mm at the pile head with a rate of 1mm/min and measuring the pile head load with a load cell in loose sand (with Dr=33%). The MFJP model pile used was 32.5 cm long and 5 cm wide, and it was shown that the MFJP pile reaches an active lateral capacity of 325N in loose sand at a pile head displacement of 50mm. Meanwhile, the post-tension force in the cable increases from 750N force to 1400N force after 50mm displacement happens at the pile head.

Table 2.11. Summary of the tests results from Sengez [70].

	Pile Head Displacement(mm)			Max Shear Force(N)		
Pile Type	Loose	Medium	Dense	Loose	Medium	Dense
MFJP with 750N PTF	2.5	2.4	2.3	300	300	300
MFJP with 1500N PTF	2.2	2.35	2.2	300	300	300
MFJP with 2250N PTF	2.5	2.2	2.2	300	300	300
Monolithic Pile	2.2	2.2	2.2	320	320	320

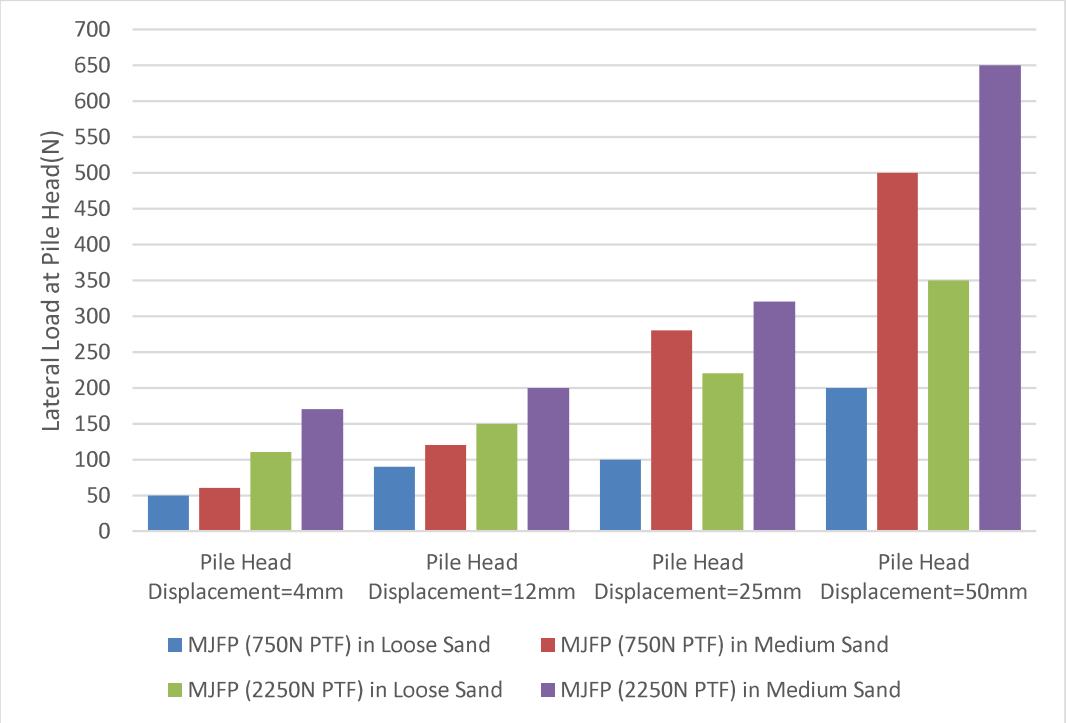

Figure 2. 24. Lateral load capacities for different head displacements from Keklik [71].

2.5. Conclusion

In many cases, piles exposed to active lateral loadings, lateral soil movements due to deep excavation, unstable slope, embankments, and tunneling operations have to withstand additional induced bending moments, shear stresses, and deflections. Therefore, the structural integrity, beaver, and response of piles subjected to lateral loadings need to be checked separately against the additional induced bending moments, shear stresses, and deflections if proven critical.

When the lateral loads are applied at the head of the pile foundations, the pile is considered to be under active lateral loadings. The lateral capacity of the piles under active loads spin around the ultimate lateral resistance of piles and the allowable pile head deflection. Generally, two types of methods are used for calculating the lateral resistance of piles under active loading which are theoretical methods and experimental methods.

In the theoretical methods, the lateral resistance of piles subjected to active lateral loading is estimated based on the statics of the pile or force and moment equilibrium of the

pile and earth pressure theory. Another group of methods used widely to find the lateral capacity and behavior of pile under active lateral loading is experimental methods. Experimental methods generally provide accurate and more reliable estimation of lateral capacity of piles under active loading.

When the piles are experiencing lateral loading due to lateral soil movement, they are called piles under passive loading. There are mainly three methods for the analysis of the response of piles subjected to horizontal soil movement: (1) analytical methods (which can be divided into pressure-based methods and displacement-based methods), (2) experimental methods, and (3) finite element methods, FEM.

Pressure based approach is the traditional and simplest method of pile response assessment subjected to lateral soil movement. This method is an attempt to find induced shear stresses and maximum bending moment on the passive pile by assuming a proper limiting pressure distribution over the pile based on the soil properties and geometry of the problem. Although pressure-based methods are fast and simple, they are preferred in actual designs, since they do not estimate pile displacement, and do not take into account pile-soil interaction.

Displacement-based methods are studying the response of piles subjected to lateral soil movement based on the load-displacement mechanism of the pile. The method is spinning around the pile-soil interaction modeling. Therefore, the accuracy of this method depends highly upon the characterization of the interaction between the pile and the surrounding soil. The most popular displacement methods are the modulus of subgrade approach and elastic approach, and their main advantage over pressure-based methods is that load-deflection, slope, bending moment, and shear force curves along the depth can be obtained readily.

Model tests, centrifuge model tests, and full-scale field tests are the most common existing experimental tests used in the study of passive piles. Model tests and centrifuge tests can be carried for various conditions of pile and soil to check the validity of the theoretical formulas for lateral force prediction as a result of horizontal soil movement, and try to simulate the field conditions as much as possible. Although full-scale field tests are the most reliable techniques for lateral pile response due to soil movements which are done

on actual instrumented piles, they are difficult to be carried due to the difficulty to instrument existing piles practically.

The finite element method (FEM) can present a better, accurate, and non-linear soil-pile interaction of passive piles, and is capable of considering both pile and soil with a complex geometry simultaneously, but a full 3D FEM analysis is only preferred in large projects due to higher computer execution time and higher costs in terms of data preparation.

As for the piles subjected to both passive and tensile loads simultaneously, it has not been addressed in the literature thoroughly. There are a few studies investigating pile behaviors under combined lateral and tensile loading, but the lateral loading in these studies are active and not passive loadings (loading due to lateral earth pressure). Therefore, there is a need for investigation of pile behavior, and their lateral capacity under combined lateral active loading, and tensile forces and under combined lateral soil movement and tensile force.

3. METHODOLOGY

3.1. Introduction

In this chapter, the apparatus setup used in the investigation of the behavior and lateral capacity of multiple friction joint pile (MFJP), referred as MFJP pile in its short form hereafter, and continuous plane concrete model piles, referred as monolithic pile thereafter, subjected to active lateral loadings, passive loadings and both tensile and lateral loads simultaneously, as well as experimental procedure, materials used in the experiments, loading systems, data acquisition system, model piles preparation and their instrumentation have been thoroughly explained.

3.2. Testing Apparatus

The apparatus, known as large size-large displacement direct shear device, used in the current study has been developed at Boğaziçi University and is shown in Figure 3.1 [73, 74]. Although it has been only used, in this study, to perform active lateral capacity tests, Passive lateral loadings, and combined lateral and tensile loading tests on MFJP and monolithic concrete model piles, it is very versatile and multi-tasked equipment by which many experiments such as, large displacement direct shear tests, interface tests, and separate and combined axial, lateral and cyclic load tests on model piles and model pile groups can be conducted as well.

This apparatus consists of four main parts which are explained separately in the subsequent subsections.

(i) Shear Box.
(ii) Tension frame.
(iii) Loading application system.
(iv) Measurements and data acquisition system.

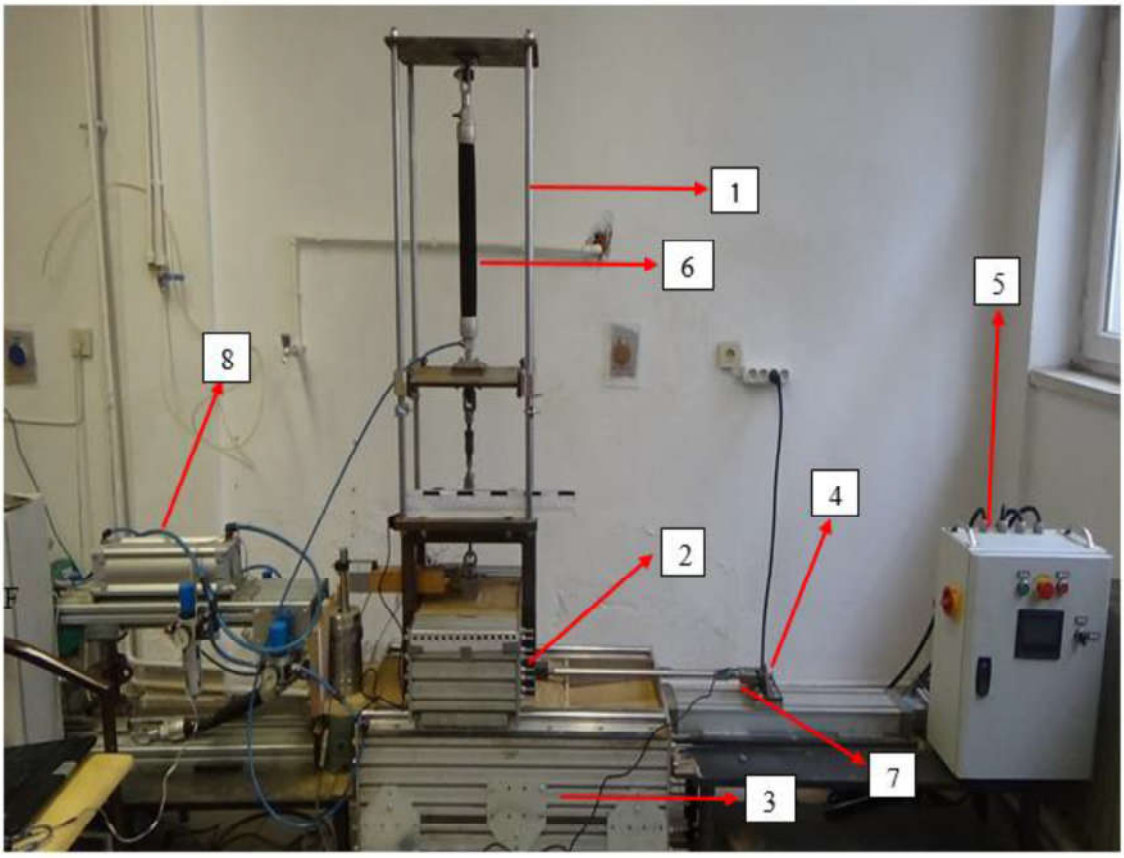

Figure 3.1. Experimental Apparatus Setup.

The designated numbers in the Figure 3.1 shows the following compartments of the apparatus.

(i) Tension frame.
(ii) Upper box (sliding box).
(iii) Lower box (fixed box).
(iv) Linear actuator for application of the lateral forces or horizontal displacements.
(v) Horizontal displacement controlling system toolbox.
(vi) Pneumatic muscle.
(vii) Load cell (for measuring lateral loads).
(viii) Compressed Air Pressure tank.

3.2.1. Shear Box

The shear box constitutes the main body of the device and consists of a moving and fixed part which are made of steel plates. The moving part or upper box has an internal length, width, and depth of 30 cm, 30 cm, and 20 cm respectively. The upper box can freely move over the lower fixed box with the help of a frictionless railing mechanism and is used to apply lateral loads on the pile head in case of active tests and lateral rectangular soil movements while passive tests are performed on the model piles.

The fixed part or lower box has the dimension of 90 cm length, 30 cm width, and 60cm depth and can be adjusted to have either a depth of 20 cm or 40 cm based on the requirement of the tests. In the current study, only 59 cm length of the lower box has been used and filled with sand while the depth of the lower box has been adjusted to 40 cm, as the length of the model piles is 34 cm, to conduct tests on model piles considering boundary conditions.

3.2.2. Tension Frame

The tension frame is made of a bottom chair with four legs, with the help of which the tension frame can be fixed at the sides of the upper shear box, and an upper frame attached to the bottom chair in which a movable plate is connected to a pneumatic rubber muscle (Figure 3.1). The pneumatic rubber muscle, the loading mechanism of which is explained in the following loading application system subsection, is used to apply tensile forces at the top of the model piles while investigating the pile tensile capacity and when both lateral and tensile loading tests are conducted.

3.2.3. Loading Application System

The device has the capability of applying tensile forces, cyclic loads, and horizontal loads separately and simultaneously. Therefore, it is a very useful and versatile apparatus for the investigation of model pile capacities under different types of loadings.

The horizontal strain-controlled static and cyclic load is applied by a step motor connected to a linear actuator on the side of the shear box. The step motor, produced by Festo, has a 1 mm/min strain rate and has a displacement range of 170 cm. the axial forces and load-controlled cyclic loads can be applied through Pneumatic muscles produced by Festo with the help of an air pressure system.

In the tests conducted in this study, only strain-controlled horizontal loading and tensile loads are applied on model piles. The horizontal load applied by the step motor is carried to the upper shear box by a steel bar connected to a linear actuator of the step motor on one side and attached to the upper sliding shear box on the other side in case of application of passive loading on model piles (Figure 3.1). While active loading is concerned, the upper shear box is then connected to the pile head by a nearly nonflexible wire (Figure 3.2).

The tensile load is applied at the top of the pile head by Pneumatic muscles, DMSP-40-250N- RMRM model, which has a diameter of 40 mm and a length of 250 mm and applies a load of 6500N upon 25% contraction [75]. The muscle is connected to the pile head through a steel bar. The setup for the application of tensile loads by the pneumatic muscle is demonstrated in Figure 3.3.

3.2.4. Measurements and Data Acquisition System

To measure the horizontal load applied on the pile head and on the shear box, and the tensile load applied on the pile head two S-type load cells each having a capacity of 10000 N are used during the experiments.

The load cell for lateral load measurement is assembled between the linear actuator of the step motor and the shear box as it is shown in Figure 3.1, and the load cell for tensile load is placed between the pile head and movable plate attached to Pneumatic muscle (Figure 3.3).

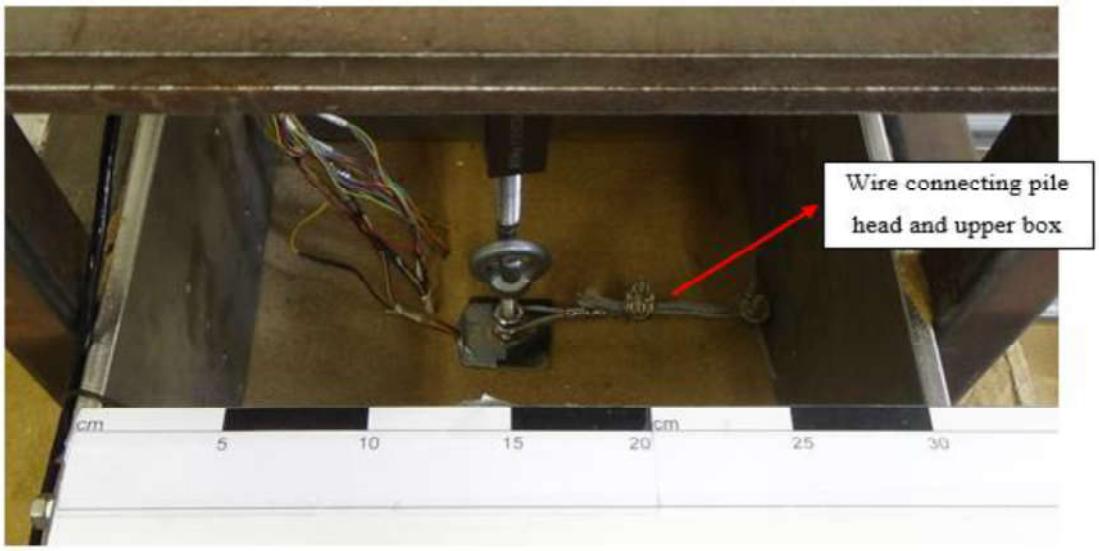

Figure 3.2. Pile head connection in active lateral tests.

The data from these two load cells are collected through a DAQ (data acquisition system) test box which is converting Analog signals to Digital data. The test box has 8 channels which are able to collect data from 8 measuring devices, load cells, and LVDTs. The data from the test box is then exported and stored to a software, known as TestLab Basic programmed and coded by Teknik Destek Gurubu, TestLab Basic has to panels. One for activating the required channels, and introducing the calibrations of the load cells, configuration panel, and another for recording the data, data acquisition control panel.

Before conducting the tests, both load cells were first calibrated manually by applying known loads on the load cells (Figure 3.4). Since the test box is measuring the loads in voltage difference and then convert it to loads in KGF, the load cells were calibrated by assigning the known applied loads to the measured voltage difference by the test box.

The pile head deflection in passive and tensile tests is measured by a Linear Variable Differential Transformer (LVDT) as shown in Figure 3.5. The LVDT is read in MATLAB program with the help of a National Instrument Data Acquisition System (NI cDAQ-9174). In the case of active tests, the pile head deformation is calculated from the amount of linear step motor displacement as it is equal to linear step motor displacement.

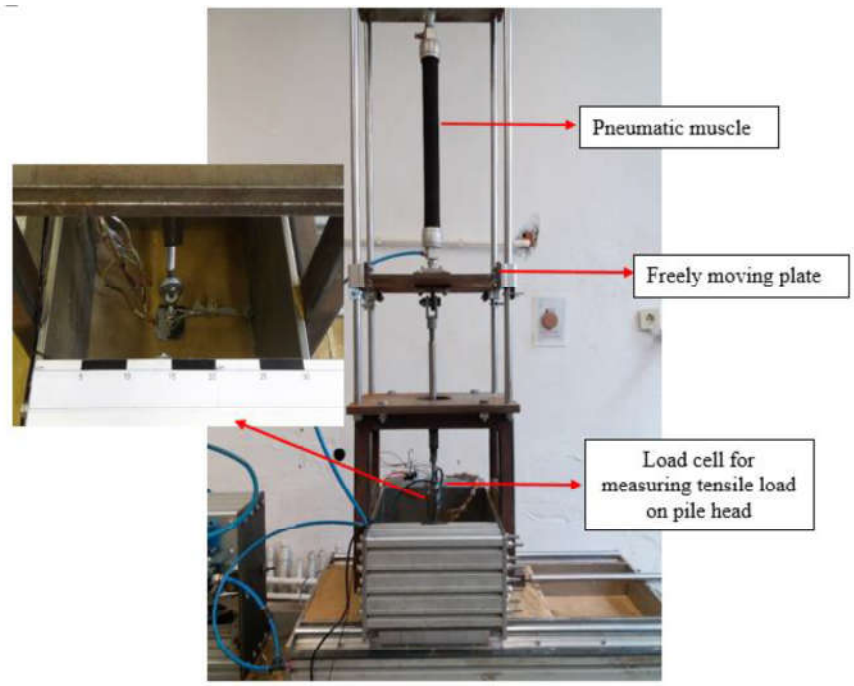

(a)

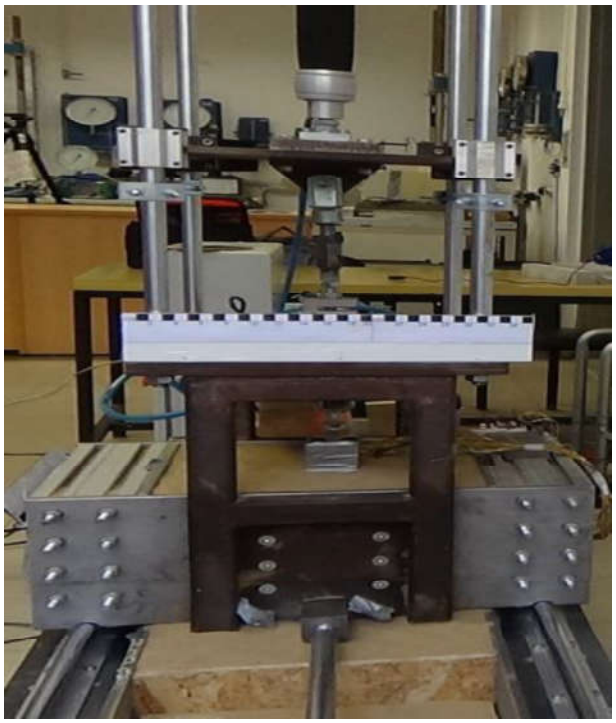

(b)

Figure 3.3. Set up for application of tensile loading; (a) front view (b) side view.

Figure 3.4. Load cells calibrations.

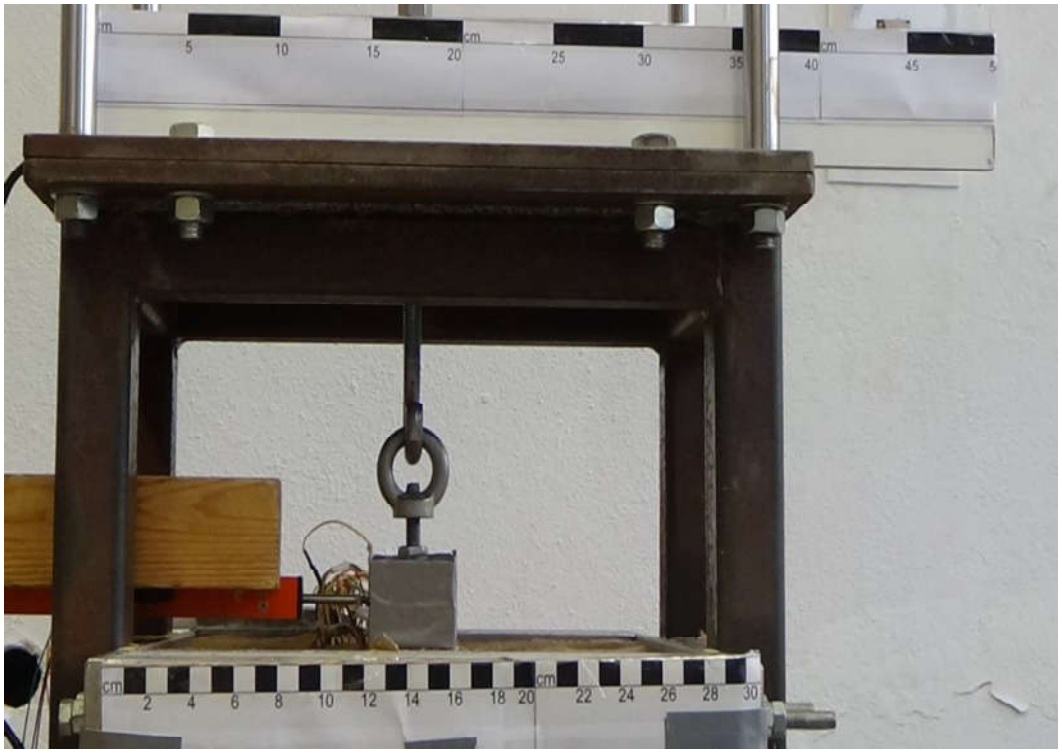

Figure 3.5. Pile head deflection measurement by LVDT.

3.3. Sand Properties and Preparation

The model piles were placed and tested in the shear box filled with natural dry Akpınar sand. The particle size distribution of the sand and its properties are shown in Figure 3.6 and Table 3.1 respectively.

To observe the effect of relative density of sand on the capacity and behavior of model piles subjected to both lateral and tensile forces combined, the tests were conducted in two different relative densities. Therefore, the tests were performed in loose sand with $D_r = 20\%$ and medium sand with $D_r = 50\%$. To produce uniform sand beds, the compaction placement method was used and the sand was placed in the shear box in layers of 10 cm thickness, with a total thickness of 40 cm, from the bottom of the box and compacted with a wooden tamper with the required energy to attain either loose or medium state sand. The calculated relative densities for all tests were ensured to have an error of less than 1 percent.

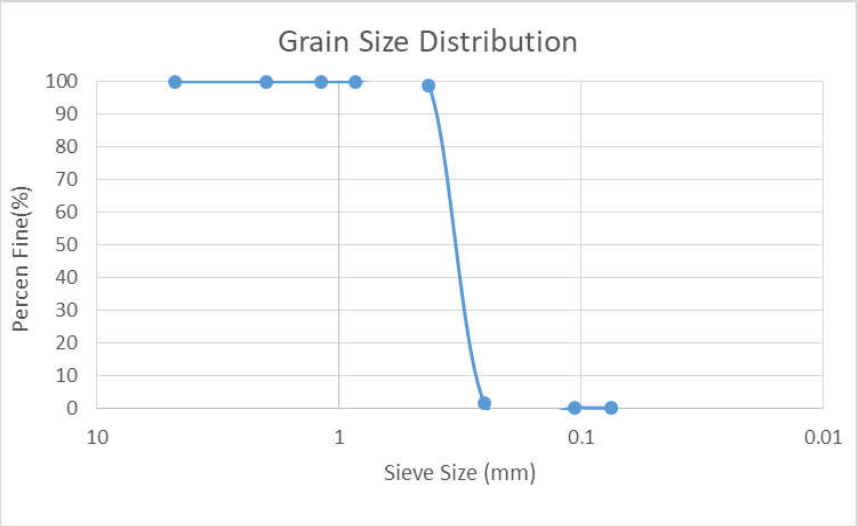

Figure 3.6. Grain size distribution of the Akpınar sand.

Table 3.1. Akpınar sand properties.

$\gamma\left(\frac{KN}{m3}\right)$	G_S	e_{Max}	e_{Min}	C_u	C_c
15.6	2.63	0.68	0.47	1.22	1.15

3.4. Model Piles and Their Instrumentation

Two types of model piles, multiple friction joint pile or MFJP, and monolithic or straight concrete model piles, were studied under lateral active loads, lateral passive loads, combined lateral active loads, and tensile loads, and combined lateral passive loads and tensile forces in this study. The materials, assembling, and manufacturing of the model piles are explained in the following subsections while the results of the tests on these two types of piles and the comparisons between them are presented in chapter 4.

3.4.1. Multiple Friction Joint Pile (MFJP)

MFJP is a type of pile proposed and designed by professor Baykal at Boğaziçi University. In this type of pile, a series of mortar blocks, between which rubber sheets are placed in order to improve the energy absorption of the piles, are fixed together with the help of a rod, with high tensile strength. This configuration provides the ability to control the rigidity of the pile to the desired level. In the current study, a model MFJP pile has been used with the same materials and configuration as mentioned above but on a small scale.

The model MFJP piles, shown in Figure 3.7, used in the tests here have a length of 34 cm and are made of square concrete mortar blocks, which have an average width of 5 cm, and a thickness of 2 cm with a small hole of 10 mm diameter in the center of each block, steel rod having 3000N tensile strength to keep the blocks together, and rubber shore 60 sheets in between the mortar blocks.

The same square concrete mortar blocks, shown in Figure 3.8, produced to construct model MFJP piles for the study of lateral capacity of MFJP piles subjected to cyclic loading by Sengez [70] have been used to form MFJP piles here as well. The blocks are produced according to ASTM C270 from a mortar having cement, water, and sand mixing ratio of 1:0.5:3 respectively, and have an average compressive strength of 49.6KN [76]. The length, width, and thickness of the mortar blocks are 5 cm, 5 cm, and 2 cm respectively.

The rubber shore 60 has the same width and length as the mortar concrete blocks with a thickness of 3 mm. The properties of the rubber shore 60 are presented in Table 3.2 and a unit rubber shore 60 is shown in Figure 3.9.

The steel bar used to keep the blocks and the rubber shore has a diameter of 10 mm with a steel block at the bottom and a threaded rod at the top which provide the fixing of mortar blocks and rubber sheets together and allow us to obtain the desired level of flexibility of the pile by fixing the nut used in the threaded rod as it is shown in Figure 3.7.

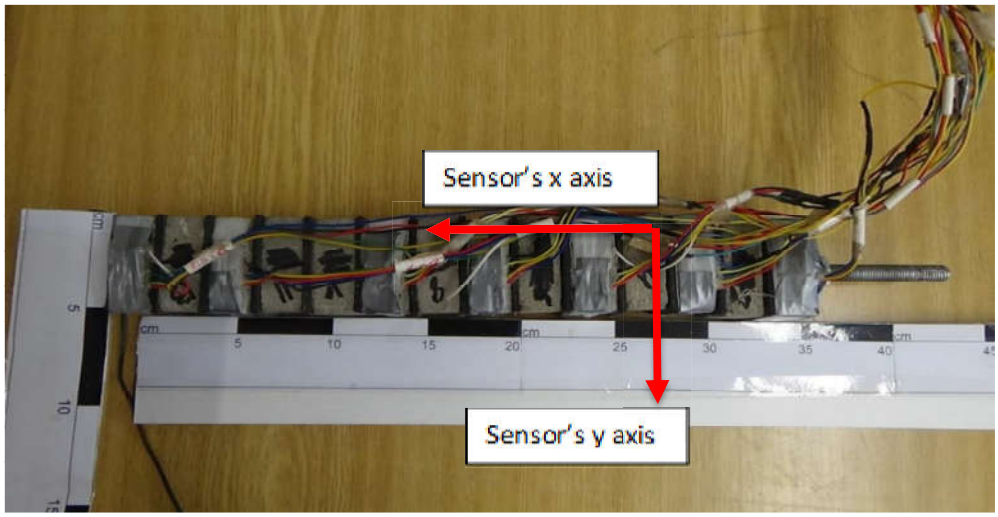

Figure 3.7. MFJP (multiple friction joint pile) model pile.

Figure 3.8. Mortar Block.

Table 3.2. Properties of rubber used between the mortar blocks [69].

Rubber Type	Neoprene Rubber 1
General Description	Soft Rubber
Style	7797
Color	Black
Tensile Strength $\frac{KN}{m^2}$	$10x10^3$
Elongation at Failure (%)	125
Elastic Modulus (MPa)	3
Thickness (mm)	3
Rubber Shore (A)	60

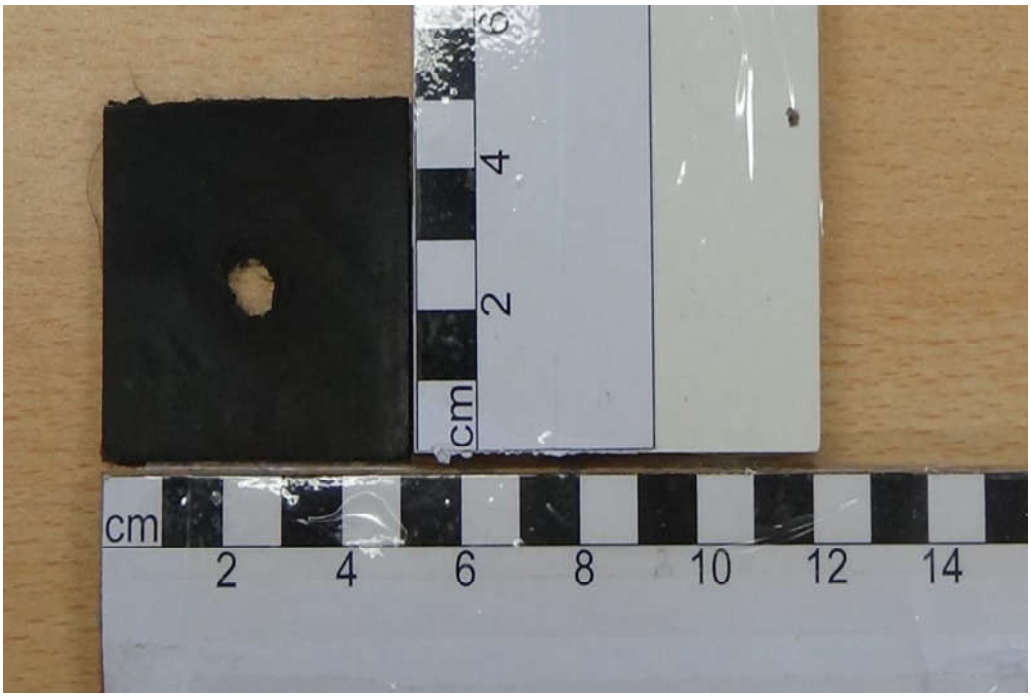

Figure 3.9. A unit of rubber shore 60 used in the model piles.

3.4.2. MFJP Assembling Procedure

The procedure of assembling multiple friction joint pile (MFJP) model piles are as follows:

(i) A small load cell that has a hole in the center is passed through the rod and placed at the bottom of the model pile. This load cell has a capacity of 10KN and is used to measure the amount of post-tension on the pile.

(ii) The bottom block which is used as a support to hold concrete blocks are fixed at the bottom.

(iii) 12 concrete mortar blocks and 2 plastic blocks and 13 rubber shore 60 in between them is then inserted one upon each other in the steel rod. It is noteworthy to mention that one of the plastic blocks is used between the lowest mortar block and load cell to prevent mortar blocks damage upon tensioning the rod, and the other is used between the nut and the first, or highest block at the top, for the same reason.

(iv) After the load cell and the concrete mortar blocks are inserted through the steel rod. The rod is post-tensioned by fixing and turning a nut on the threaded bar at the top of the steel rod to achieve the desired post-tension value which has been an average value of 750N to simulate a flexible pile and an average value of 1500N for simulating a relatively rigid model pile.

3.4.3. Monolithic Pile Preparation

The monolithic square model piles were produced from concrete mortar up to BS-EN 196-1 [77]. The mortar was made of Portland cement and dry sand having a 1:0.5:3 (cement, water, and sand) mixing ratio by weight. In order to get the suggested particle size distribution of the sand by BS-EN 196-1 for the production of mortars, the sand was sieved for each batch of mortar produced, and it was ensured that the sand used has a range of particle sizes as per to BS-EN 196-1 standard. The particle size distribution of the sand used for each batch is shown in Table 3.3.

The model piles have 34 cm length and 5 cm width and were cast in the molds having the same internal dimensions as the model piles dimensions. The molds, as shown in Figure 3.10, are made out of woods, and in order to facilitate the application of lateral and tensile loads on the pile, 12 cm threaded rods having 10 mm diameters were fixed on that side of the mold which was going to be used for applying loads and which constitutes the top of our model piles before casting the mortar.

Table 3.3. Particle size distribution of sand used to produce monolithic piles.

Sieve Size(mm)	Cumulative Sieve Residue (%)
2	0
1.7	2.2
1	28.2
0.5	64.3
0.15	92
0.075	100

Figure 3.10. Wooden mold for casting of monolithic model piles.

Figure 3.11. Demolded Monolithic pile.

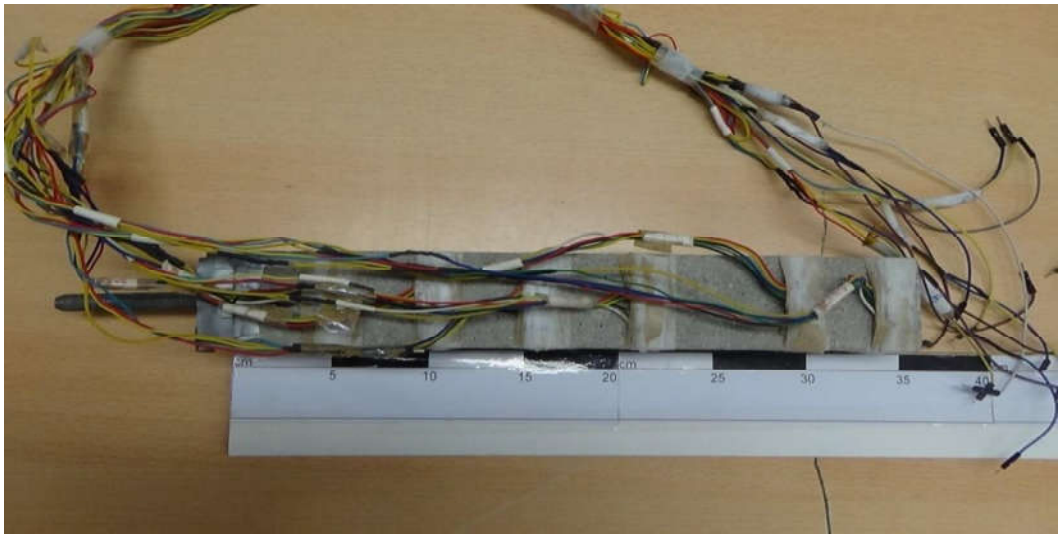

Figure 3.12. Instrumented monolithic pile with MPU9250 sensors.

The casted model piles, after demolding after 24 hours, were cured according to BS-EN 196-1 requirement for 28 days in water. The wooden mold and the unmolded monolithic pile are shown in Figure 3.10 and Figure 3.11 respectively.

Before conducting the lateral capacity tests on the monolithic model piles, three of the model piles were first used to find the flexural rigidity of the model piles under three-point bending test. The results of the tests are presented in chapter 4.

3.4.4. Model Piles Instrumentation

In order to observe and estimate the behavior of the MFJP model piles, 7 MPU 9250 sensors, produced by InvenSense Inc., were placed on the 1st, 3rd, 5th, 7th, 9th, 12th, 14th mortar blocks, as it is shown in Figure 3.7, to measure the rotation of the instrumented mortar blocks along the pile length. The instrumented monolithic pile is shown in Figure 3.12.

MPU 9250 sensors are 9 axis IMU, Inertial Measurement Unit, devices which mainly consist of a 3-axis magnetometer, a 3-axis gyroscope, a 3 axis accelerometer, and a digital motion processor, DMP, and are used for the position and orientation estimation of objects, especially in drone's technology. The gyroscope measures the angular velocity of the sensor in rad/sec and can measure angular velocities up to $\mp 2000\,^{\circ}/_{sec}$ range. The accelerometer measures the acceleration of the sensor in m/sec2 and can have a range of up to$\mp 16g$, and the magnetometers can have a full-scale range of $\mp 4800\mu T$ measuring magnetic field of the earth at a specified location [78].

MPU 9250 sensors are using 9 16-bit ADCs, Analog to Digital Converters, to digitalize the out of the gyroscope, magnetometer and accelerometer. The output of the gyroscope, magnetometer and accelerometer from an MPU9250 sensor can be read through an I^2C communication bus which uses a two-wire interface to provide data transfer between a microcontroller and the MPU9250 sensors [78].

In this study, an Arduino Mega 2560 microcontroller has been used to read the outputs of MPU9250 sensors. Since the Mega 2560 microcontroller only has one I^2C communication bus, it can only read the data from one MPU9250 sensor. Therefore, a TCA9548A multiplexer, which has 8 ports and can get the data from up to 16 sensors at the same time, was used to acquire the values from 7 MPU9250 sensors. Each port on the TCA9548A multiplexer can get data from two MPU9250 sensors based on the address of the MPU9250. The address of the MPU9250 sensors can be set to 0x68 or 0x69 by connecting the AD0 pin of the sensors to ground and voltage lines respectively. The devices used to obtain rotations are shown in Figure 3.13.

The acquisition of data from MPU9250 has been briefly described step by step below.

(i) The data from MPU9250 is transformed to TCA9548A multiplexer first.
(ii) Then it is passed to the Arduino Mega 2560 board.
(iii) Next, it is read by the Arduino software, IDE 1.8.13, or Integrated Development Environment by using the code provided by one of IDE library codes, Bolder Flight System MPU9250. The related codes are given in appendix C.
(iv) Finally, the data is saved with the help of an auxiliary application, known as PuTTY, in a comma-separated file format file.

The raw data obtained from MPU9250 sensors are not precise since the gyroscope, accelerometer, and magnetometers of MPU9250 are using MEMS (Micro Electrical Mechanical Systems) hardware for obtaining data, and MEMS hardware is affected adversely by many factors such as manufacturing imperfections, temperature, and the magnetic field of the earth. Therefore, the accelerometer, gyroscope, and magnetometer of the MPU9250 sensors need to be calibrated and filtered, and the raw data must be corrected against those calibrations. The calibration of the gyroscope, magnetometer, and accelerometer and are described in appendix B.

Even, the raw data from MPU9250 sensors are corrected and calibrated, they are noisy, especially the data from the magnetometer and accelerometer, and should be filtered in order to prevent the effect of noise on orientation estimation. Although the gyroscope data alone, which indicates the angular velocity of the sensors, can be used to find the orientation of the sensors, hence rotation of the piles, the gyroscope data tends to drift over time and gives unreliable values as time passes. Similarly, the data from the magnetometer and accelerometer can be used to estimate the orientation of the sensors with respect to gravity and the earth's magnetic field, but the values from the accelerometer and magnetometer are unreliable in the short term due to noise effects. Therefore, a comprehensive filter, AHRS (Attitude Heading Reference System), has been used to both filter the noise and combine the data from the gyroscope, accelerometer, and magnetometer for obtaining reliable orientation estimations. In other words, the AHRS filter combines the reliability of the magnetometer and accelerometer in long term with the gyroscope

reliability in short term along with filtering the data against noise to give a better prediction of sensors orientations [80].

For the application of the AHRS filter in this study, the ahrsfilter () function of the MATLAB Program has been used. This function gets the 3 axis accelerometer, 3 axis gyroscope and 3 axis magnetometer data in m/sec2, rad/sec, and μT respectively and return quaternion vectors which in turn can be converted to Euler Angles with the help of eulerd () function in MATLAB.

The Euler Angles are used to determine the orientation of the sensors in, Pitch (), Roll (), and Yaw (), angles which are calculated with respect to world frame NED (North, East, and Down). In other words, the difference between the initial Euler Angles at the beginning of the tests and the final Euler Angles, at the end of the tests, can provide the amount of rotation with respect to a specific axis.

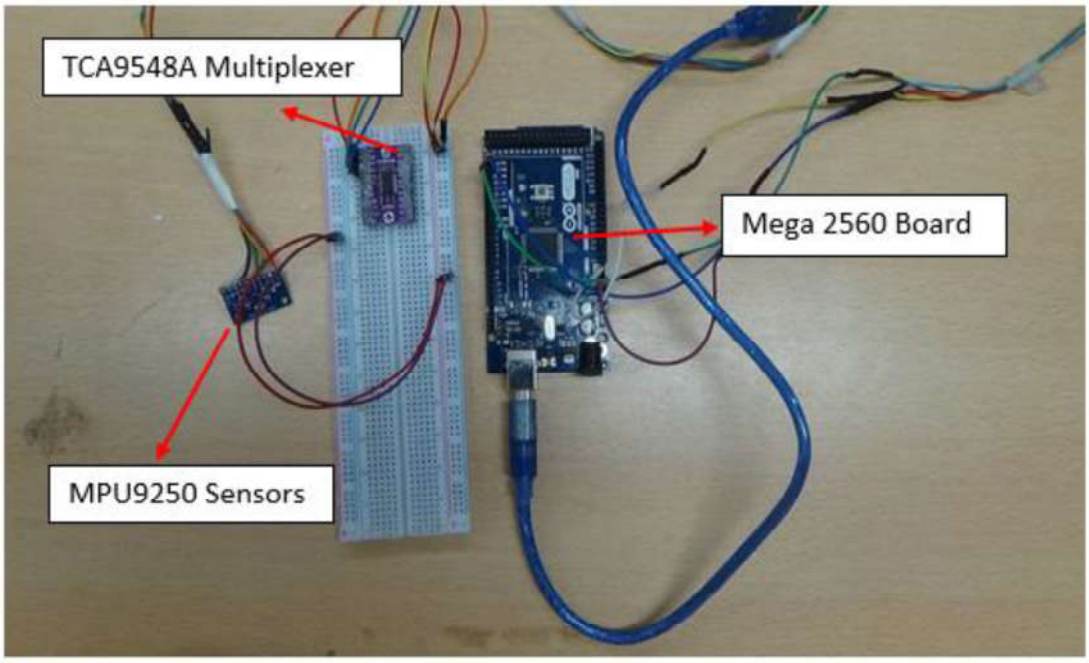

Figure 3.13. Devices used for measuring orientation.

The MPU9250 sensors in our case are fixed on the back of the pile, opposite to the direction of the lateral loading, in a way in which the x-axis of the sensors are heading toward down along the pile length, while the y-axis is perpendicular to the x-axis and is

representing horizontal axis as it is shown in Figure 3.7. Therefore, the rotation of the sensors around y-axis or pitch angle gives us the rotation of mortar blocks or pile around its horizontal axis.

3.5. General Experimental Procedure

The same basic experimental procedure in testing both the MFJP and Monolithic Concrete model piles were used. The following two subsections briefly outline the main steps for conducting the tests on model piles subjected to active and passive loadings respectively.

3.5.1. Experimental Procedure for Model Piles Subjected to Active Loading

The sequence of experimental procedure in the case of piles subjected to active lateral loading, and combined active lateral and tensile loading is summarized in the following steps:

(i) Model Pile Preparation.

(ii) The instrumented model pile was first assembled, in the case of MFJP model piles, according to the procedure outline in subsection 3.4.2. In the case of Monolithic model piles, this step is not required.

(iii) The load cell to measure lateral loading is fixed between the upper shear box and the step motor and the upper shear box is fixed in the middle of the lower fixed box.

(iv) The first 6 cm layer of sand is placed within the lower box. Then the pile is placed over this layer and it is fixed against the shear box wall through a plate, which can be fixed on both sides to the shear box wall by two bolts, at the head of the model pile.

(v) After fixing the model pile with the lower box, the remaining of the lower box is filled with sand in layers of 10 cm, 10 cm, 10 cm, and 4 cm respectively. It should be noted that the layers were compacted with a tamper to get either 20% relative density in the loose case or 50% relative density in the case of medium sand.

(vi) After filling the lower box, the head plate was discarded and the pile head was connected to the shear box through a steel wire, which transfers the load of the step motor through the shear box to the pile head. It is worthwhile to mention that this setup represents a cast-in-place free head model pile.

(vii) If the model piles were subjected to both lateral and tensile forces, before starting the later load, the pile was subjected to 75 percent of its tensile capacity, the tensile capacity according to the relative density used in the test, first by applying tensile force through the Pneumatic muscle and the tension frame described in section 3.2.3 (Loading Application System).

(viii) Finally, the linear actuator or step motor was initiated to apply lateral deformation on the pile head in case of active loading and lateral soil displacement in the case of passive loading with a rate of 1 mm/min until failure, i.e., until the load versus displacement curve becomes almost horizontal, while the lateral load, lateral displacement, and MPU9250 sensors readings were recorded by the TestLab Basic Sofware, and the Arduino respectively.

3.5.2. Experimental Procedure for Model Piles Subjected to Passive Loading

The procedure for model piles subjected to lateral soil movement is generally the same as the procedure for model piles subjected to active loading in terms of pile instrumentation, pile placement, sand preparation, and lateral loading setting. Except that, in the case of passive loading, only half of the depth of the lower box, only 20 cm out of 40 cm, is used and the upper box, which has a height of 20 cm, is filled with the sand completely. This way, the sliding length of the model piles is 20 cm and the embedded length of the model piles is 14 cm. In addition, in the case of passive loading, the pile head deflection is read with an LVDT set about two cm above the pile head with the help of a National Instrument and MATLAB.

4. TESTS RESULTS

4.1. Introduction

In this chapter, the results of the tests on multiple friction joint model piles (MFJP) and monolithic model piles have been investigated and presented. The model piles have been tested under both active and passive lateral loadings and combined active and passive lateral loadings along with axial tensile forces simultaneously to study the effect of tensile forces on the capacity and behavior of model piles under combined lateral and tensile forces.

To consider the effect of relative density, all tests on model piles have been conducted in loose sand with Dr=20% and medium sand with a Dr=50%. In addition, the effect of rigidity on behavior and capacity of model piles has been investigated as well by performing tests on a MFJP pile with a post-tension force of 750N, which represents a flexible pile, on a MFJP pile with a post-tension force of 1500N, which represents a nearly rigid pile, and on a monolithic pile, which represents a totally rigid pile in this study.

All the tests have been repeated three times in order to ensure accuracy and it was determined that the results have been with a standard deviation of 1.5. The flowchart in Figure 4.1 outlines the tests conducted on model piles.

4.2. Tensile Capacity and Flexural Rigidity of Model Piles

To be able to conduct combined lateral and tensile tests simultaneously on the model piles, first the tensile capacity of MFJP piles in loose and medium dense sand, and the tensile capacity of monolithic piles in medium soil only, since the combined lateral and tensile tests on MFJP pile are compared to that of monolithic pile just in medium soil, were determined. The tests are shown in appendix A.

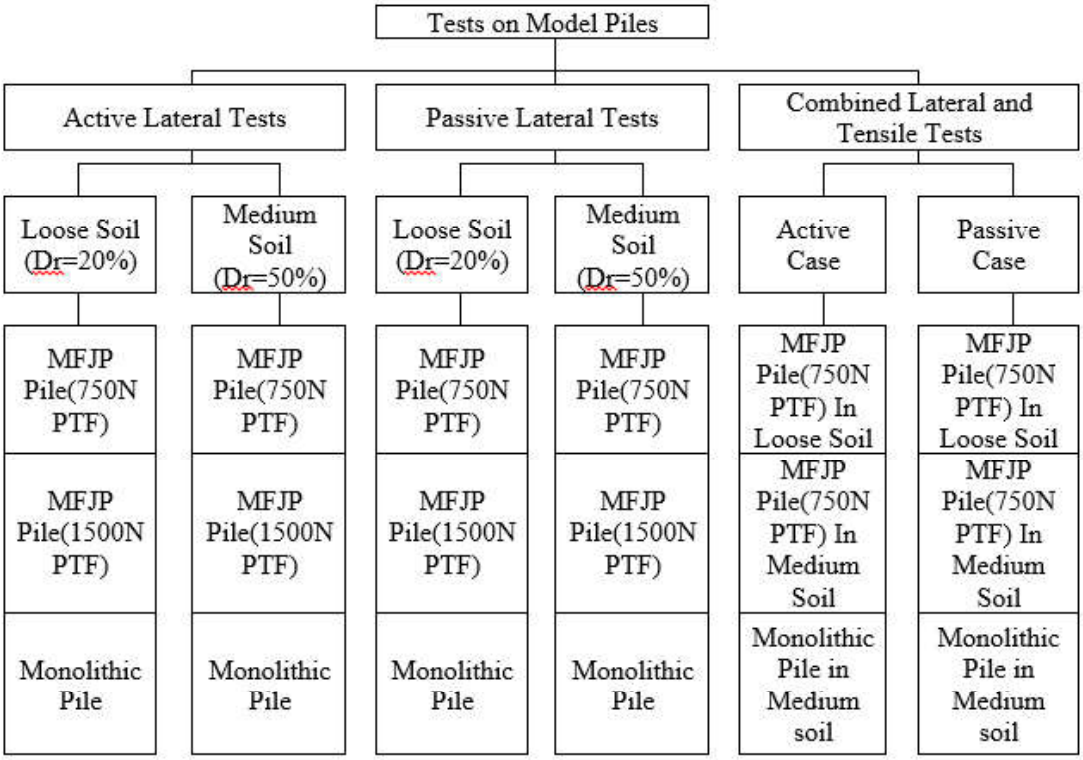

Figure 4.1. Flow chart of the conducted tests on model piles.

The tensile capacity of the MFJP pile is 392N and 235N in the case of loose sand and medium sand respectively while the tensile capacity of the monolithic pile in medium sand is about 323N. The marginal decrease in the tensile capacity in the monolithic concrete pile in medium soil is due to the smooth surface, hence small interface friction angle between the sand and pile surface, of the monolithic pile than the MFJP pile, as the MFJP pile surface is rough and it has rubber in between the concrete blocks as well.

To have an idea about the rigidity of model piles and to compare the rigidity of monolithic piles with that of MFJP piles, three-point bending moment tests were conducted on the three monolithic piles. The tests were continued until the cracks were evident on the surface of the monolithic piles. The result of the three-point bending moment on the monolithic pile is shown in Figure 4.2.

The flexural strength of the monolithic piles, having 34 cm length and 5 cm width, is about 7.7MPA and it happens at a strain of 0.0025. Comparing this with the flexural strength of the MFJP piles with 750N PTF (post-tension force) and 1500N PTF, as has been determined by past studies on the same type of MFJP pile in the geotechnical

laboratory of Boğaziçi university by Yahia [69] and Sengez [70] and are reported in Table 4.1, it can be asserted that the flexural strength of the monolithic pile is about 5 times of the MFJP pile with 1500N PTF and 11 times of MFJP pile with 750N PTF. This indicates that the monolithic pile is much more rigid than the MFJP piles with 750N PTF and 1500PTF while the MFJP pile with 1500N PTF is more rigid than the one with 750N. Similarly, the MFJP pile with 750N is much more flexible than the monolithic pile and relatively flexible than the MFJP pile with 1500N PTF. Therefore, by conducting the tests on each one of these model piles and comparing the results, it would allow the study of the effect of rigidity on the model pile's behavior and their capacity.

It is also worth mentioning that the strain at which the monolithic pile reaches its ultimate flexural strength is significantly lower than that of MFJP piles with 750N PTF and 1500N PTF which indicates that the structural failure in the monolithic pile is brittle and abrupt.

Table 4.1. Flexural strength of MFJP pile with 750N PTF and 1500PTF from past studies [69,70].

Post Tension Force(N)	**Ultimate Flexural Strength(MPA)**	**Strain at Flexural Strength**	**Source**
750	0.6	0.0025	Yahia[69]
1500	1.5	0.004	
750	0.8	0.004	Sengez[70]
1500	1.5	0.004	

4.3. Active Lateral Tests on MFJP and Monolithic Piles

The active lateral tests have been conducted on the MFJP piles and monolithic piles by applying a lateral displacement of 1 mm/min at the head of the model piles having 34 cm length and 5 cm width. The displacement at the head of the pile has been continued until the increase in the rate of lateral load, measured by a load cell assembled between the head of the pile and the step motor which applies displacement, compared to the head displacement is insignificant or until the lateral load vs pile head displacement was

observed to get a flat shape with a slope near to zero. In other words, the criteria for the ultimate lateral capacity in these test are the maximum load after which the lateral load vs pile head displacement curves gets relatively horizontal.

The active lateral tests have been conducted in loose sand and medium sand, and in the case of MFJP piles, the tests have been conducted on piles with 750N PTF and 1500N PTF to investigate the effect of rigidity.

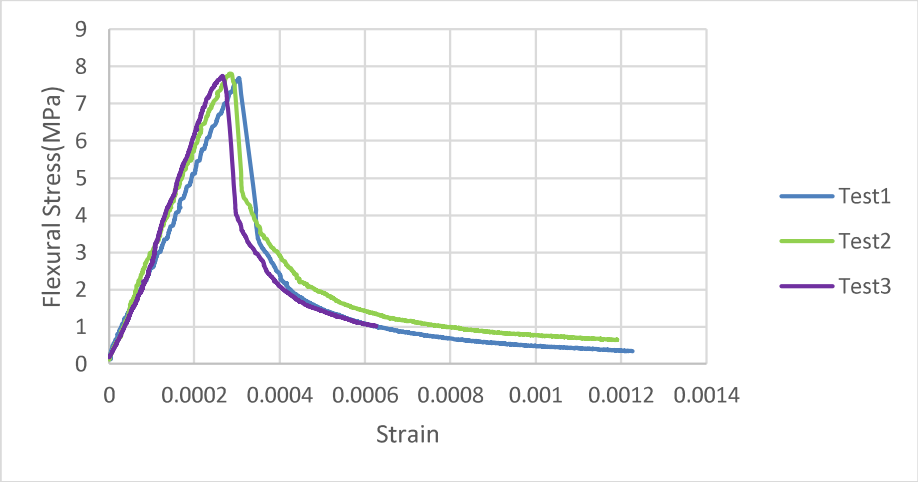

Figure 4.2. Three point bending moment tests results of monolithic pile.

4.3.1. Active Lateral Tests on MFJP and Monolithic Piles in Loose Sand (Dr=20%)

The results of the active lateral tests on MFJP and monolithic piles are shown in Figure 4.3, Figure 4.4, and Figure 4.5 for a MFJP pile with 750N PTF, a MFJP pile with 1500N PTF, and a monolithic pile respectively.

The lateral capacity of the MFJP pile with 750N PTF in loose sand is about 300N and it reaches a head displacement of about 48 mm or 1d (one pile diameter). The load-displacement curve behaves in a linear elastic manner up to a head displacement of 10 mm (0.2d) after which it begins to curve and show a non-elastic mode. As the post-tension increases from 750N to 1500N, the lateral capacity shows an increase of about 8% from 300N to 325N while the head displacement at which this capacity happens decreases to 40

mm. The linear behavior of the load-displacement curve in this test as well occurs up to a head displacement of 10 mm (0.2d) except that it is steeper than the test on 750N PTF.

The monolithic pile which indicates the most rigid pile among the model piles reaches a lateral capacity of 430N in loose sand, which indicates a 40% rise in capacity in comparison to the lateral capacity of the MFJP pile with 750N PTF. The head displacement at which the lateral capacity reaches for monolithic pile decreases significantly to 37 mm, this was about 48 mm for MFJP pile with 750N PTF, showing that as the pile gets more rigid, the lateral capacity mobilizes faster.

4.3.2. Active Lateral Tests on MFJP and Monolithic Piles in Medium Sand (D_r=50%)

The lateral load-displacement curves under active lateral loadings in medium sand show similar behavior as the ones in the loose case with a linear part following by a curved shape. The linear part of the load-displacement curves in the medium soil extends up to a pile head displacement of 10 mm (0.2d) as is the case in the loose soil save that the slope in the medium sand is steeper as it is expected.

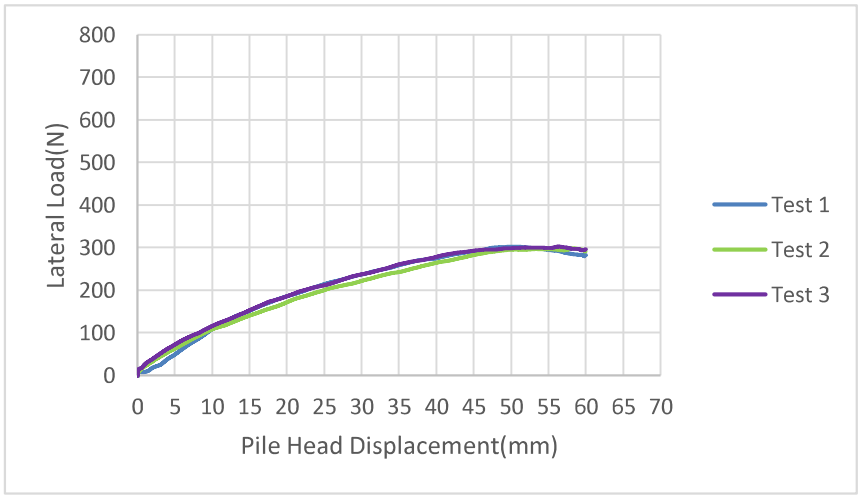

Figure 4.3. Active Lateral load test on a MFJP pile with 750N PTF in loose sand.

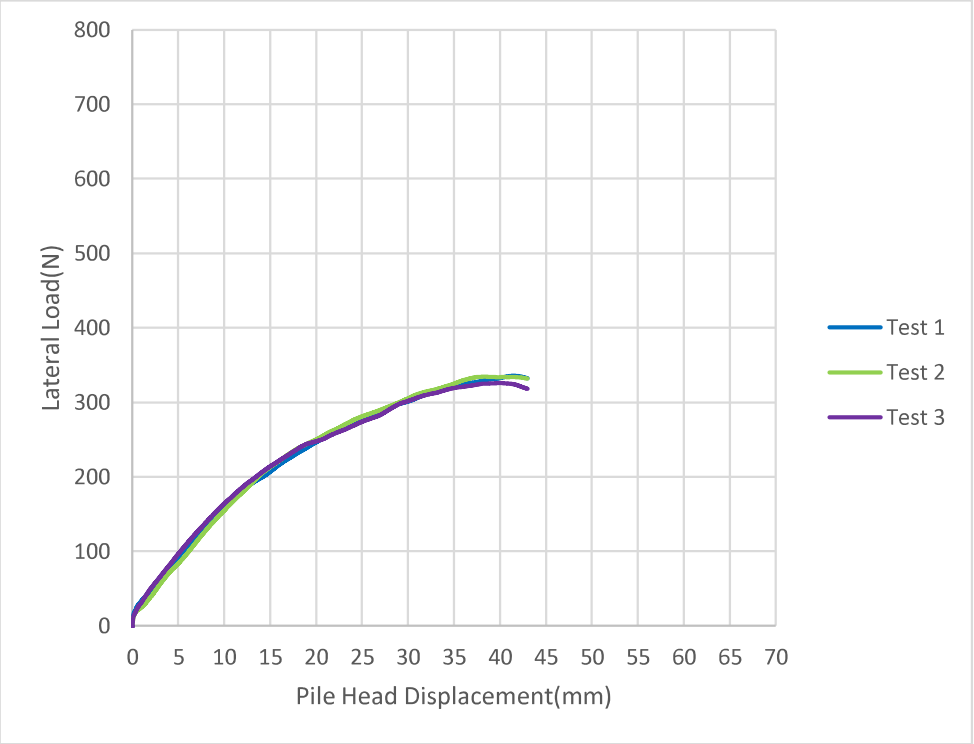

Figure 4.4. Active Lateral load test on a MFJP pile with 1500N PTF in loose sand.

The load-displacement curves for the MFJP pile with 750N PTF, MFJP pile with 1500N PTF, and monolithic pile are shown in Figure 4.6, Figure 4.7, and Figure 4.8 respectively. It is evident from these results that the lateral capacity has increased significantly from 300N, in the loose case, to 550N for medium sand for the MFJP pile with 750N PTF. Similarly, there is a noticeable increase in the lateral capacity of the MFJP pile with 1500N PTF, and monolithic pile in medium sand from 325N to 670N and from 430N to 670N respectively

The head displacement at which the ultimate lateral load is reached decreases as rigidity increases similar to that of the loose sand case with a marginal decrease of about 8% in case of the MFJP pile with 1500N PTF, and a sharp decrease of about 60% in case of monolithic pile compared to the more flexible pile of 750N PTF MFJP pile.

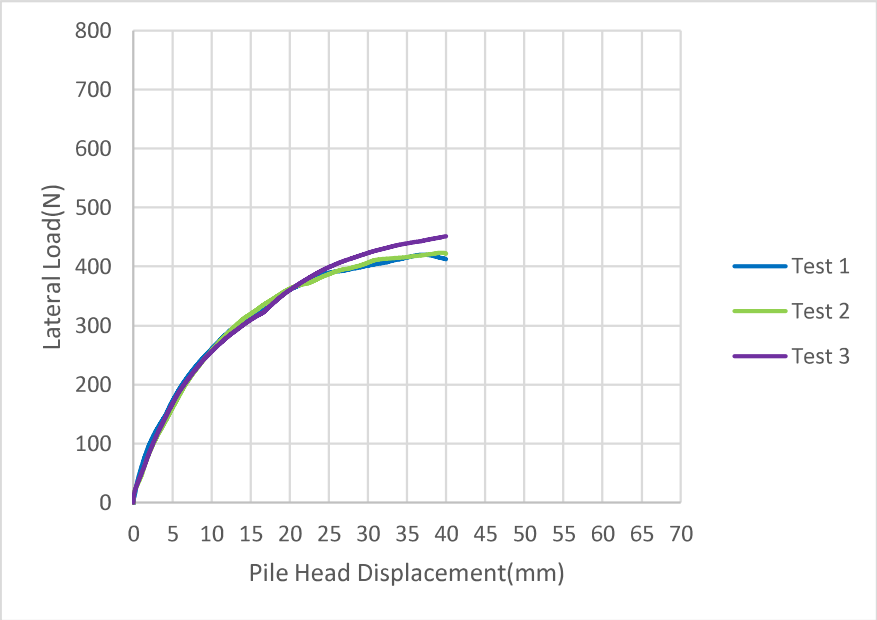

Figure 4.5. Active Lateral load test on monolithic pile in loose sand.

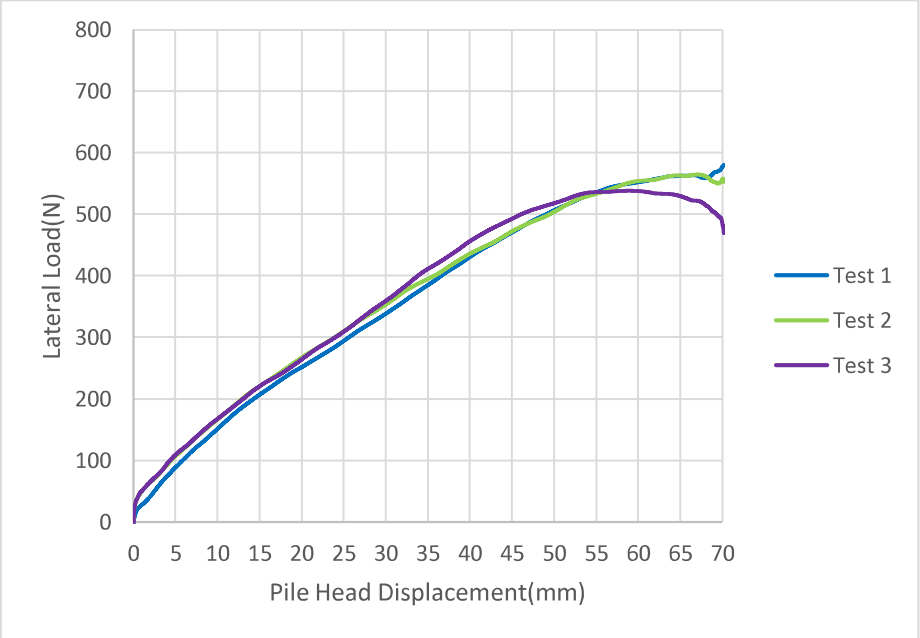

Figure 4.6. Active Lateral load test on a MFJP pile with 750N PTF in Medium sand.

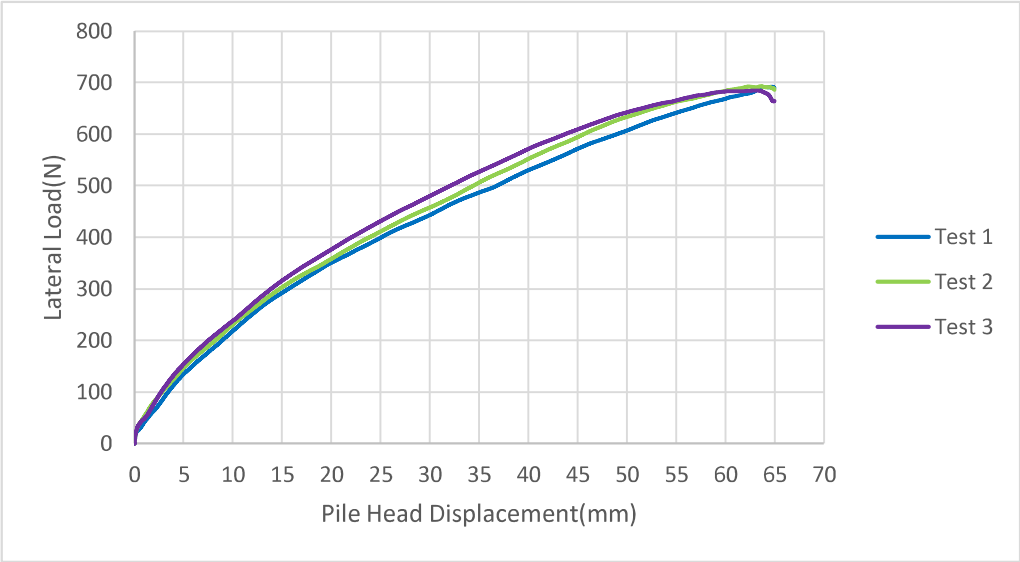

Figure 4.7. Active Lateral load test on a MFJP pile with 1500N PTF in Medium sand.

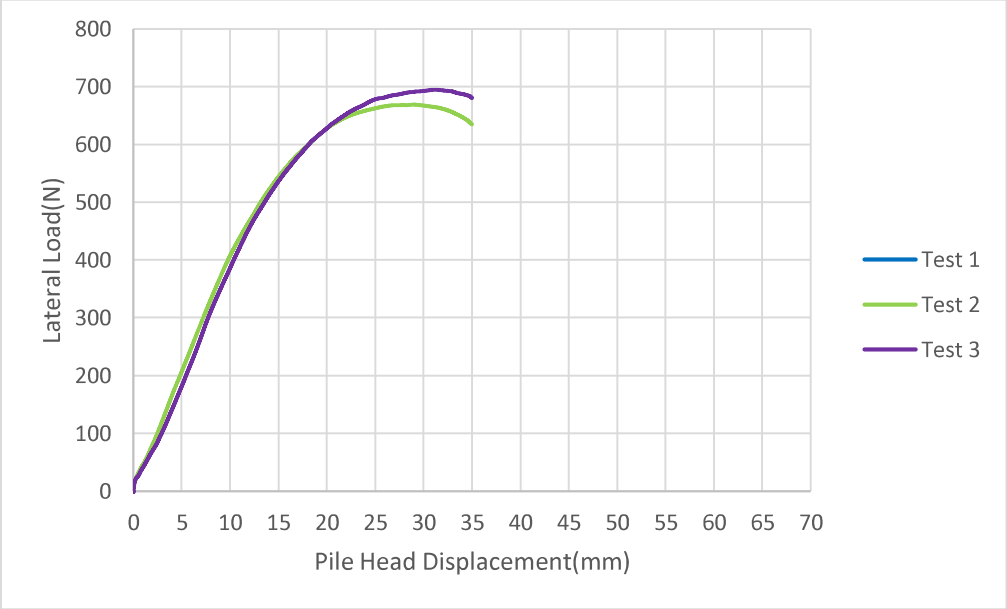

Figure 4.8. Active Lateral load test on monolithic pile in medium sand.

4.3.3. Combined Active Lateral and Tensile Tests on MFJP and Monolithic Piles

To investigate how the model piles behave under combine lateral and tensile forces, the MFJP piles with 750N were subjected to both lateral active loads and tensile forces simultaneously in loose and medium soil. The combined loading test was conducted on the

monolithic pile in medium sand as well to observe how rigidity affects the capacity and behavior of the pile subjected to active lateral loading and tensile forces at the same time.

The combined lateral and tensile tests were performed in a way that the pile head was displaced with a lateral rate of 1 mm/min while applying a constant tensile force equal to 75% (considering a factor of safety of 1.3) of the ultimate tensile capacity of the model piles. This factor of safety was applied in order to ensure that the pile should not fail immediately under the tensile forces as the aim of the combined tests was to study the effect of tensile forces on the lateral capacity of the model piles. The tensile capacity of the MFJP pile in loose and medium sand were about 392N and 235N respectively. Therefore, considering a factor of safety of 1.3, in the combined tests a tensile load of 294N and 176N were applied at the pile head during the lateral loadings until the pile failed laterally. Similarly, a load of 245N corresponding to 75% of the tensile capacity of the monolithic pile which was about 323N was applied at the pile head during the lateral loading in the case of monolithic piles.

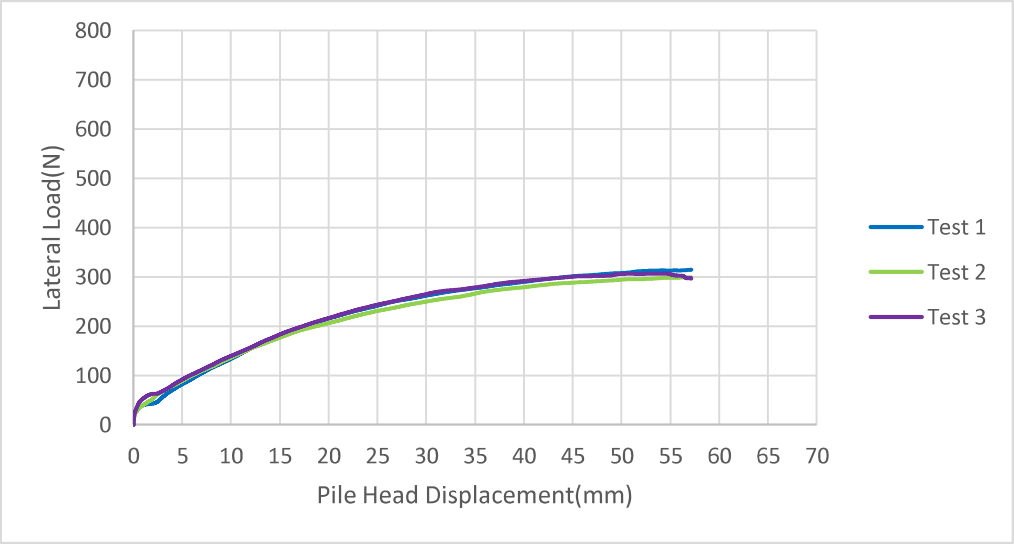

Figure 4.9. Combined active lateral load and tensile load test on MFJP pile in loose sand.

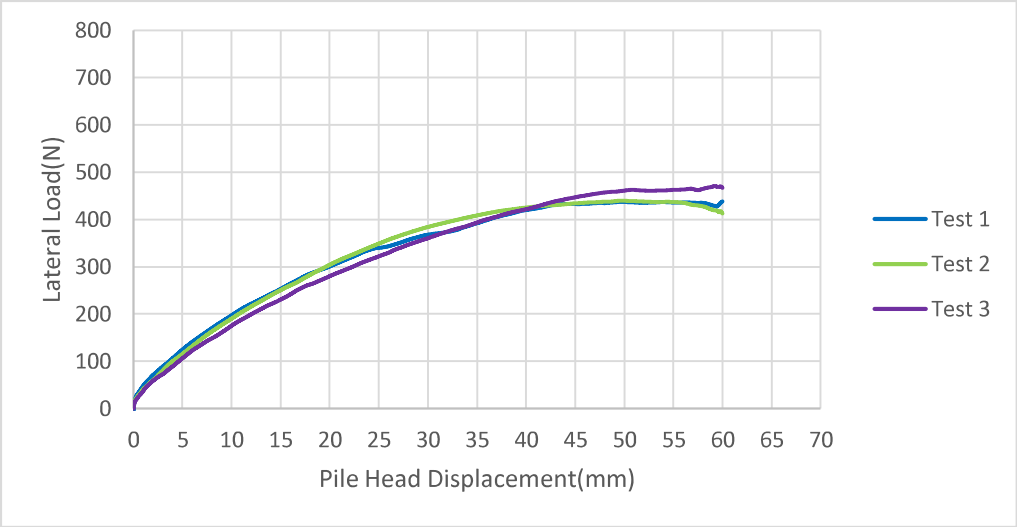

Figure 4.10. Combined active lateral load and tensile load test on MFJP pile in Medium sand.

The combined active lateral load and tensile load tests, as shown in Figure 4.9, Figure 4.10, and Figure 4.11, indicated that the lateral capacity of the MFJP piles doesn't show any change in loose sand compared to the corresponding capacity of the piles under only active lateral loadings. In contrast to the loose case, it can be asserted that there is a significant decrease in the lateral capacity of both MFJP and monolithic piles in medium sand while applying both lateral and tensile loads simultaneously. The lateral capacity of the MFJP pile falls from 550N to 440N (showing a decrease of 20%) and the lateral capacity of the monolithic pile diminishes to 600N from 670N.

The displacement at which the active lateral capacity reaches seems to not change noticeably in both loose and medium sand and in both MFJP and monolithic piles when comparing the results of the active lateral tests and combine lateral and tensile tests. In the same manner, the application of tensile forces does not affect the shape of the lateral load-displacement curves. They indicate the same trend of having a sharp slope up to 10 mm head displacement, which is about 0.2 of pile diameter and starts to flatten with a decrease in lateral load rates after 10 mm head displacement.

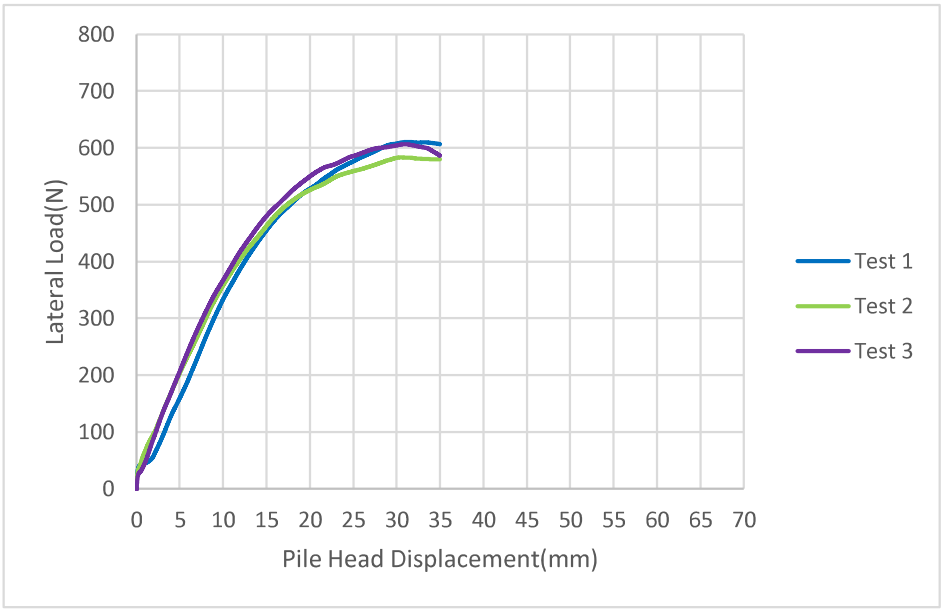

Figure 4.11. Combined active lateral and tensile loads test on monolithic pile in Medium sand.

4.4. Passive Lateral Tests on MFJP and Monolithic Piles

In the passive lateral tests, the square model piles having 34 cm length and 5 cm diameter were placed inside the large shear large displacement machine in a manner that the lower 14 cm length of the pile was embedded in the lower box or fixed box and the remaining upper length of the pile was in the upper or sliding box. In other words, the stable soil layer and sliding soil layer lengths were 20 cm and 14 cm respectively, and the pile sliding length to pile embedded length ratio was 0.4, or $\frac{L_s}{L_e} = 0.4$.

To find the passive lateral capacity of the model piles a rectangular horizontal soil displacement at a rate of 1 mm/min was applied by the upper sliding box on the sliding length of the piles first and the lateral load required to apply this horizontal soil movement was recorded by a load cell placed between the upper box and the step motor, which exert the horizontal movement, while the pile head displacement was recorded by the help of an LVDT. It should be notated that the application of the lateral soil movements was continued until the load-displacement curve become flat and showed a slope near zero.

Since the measured lateral load on the upper box represents the total resistance of both the pile resistance and the resistance of the sliding surface, between the upper sliding layer and the lower stable layer, free field tests were conducted in loose and medium sand, tests that were conducted on the soil only without the presence of the pile to determine the shear resistance of the soil-soil interface while sliding. Then the free-filed resistance or shear resistance due to soil alone was subtracted from the total resistance to find the resistance of the pile against lateral soil movement. Figure 4.12 shows the schematic of the model used in this study to find the lateral resistance of the model piles subjected to lateral soil movements.

The model indicates that the determination of the pile passive lateral capacity was a three-step procedure. In the first step, the total resistance, resistance from both the pile and the sliding surface, was found. The second step was to determine only the resistance due to sliding surface, and the final step was to get the pile lateral resistance to passive loading just by subtracting the shear resistance due to sliding surface of the soil sliding and stable layers from the total resistance.

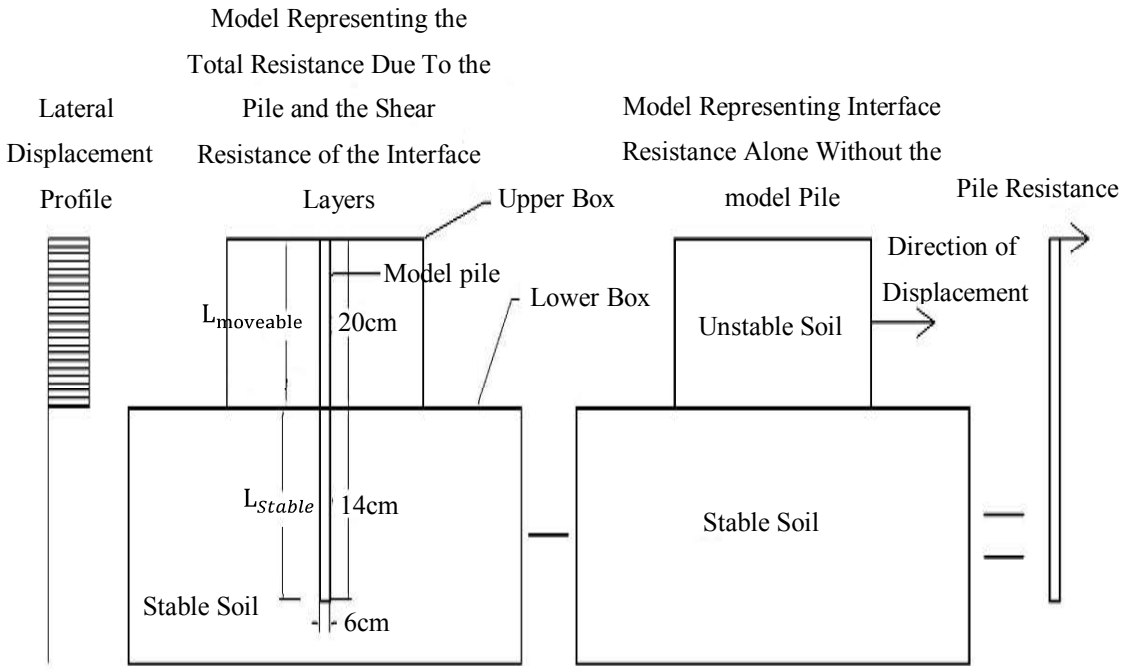

Figure 4.12. Schematic of the model used to determine the lateral resistance of the pile against lateral soil movements.

4.4.1. Passive Lateral Tests on MFJP and Monolithic Piles in Loose Sand (D_r=20%)

The passive lateral tests on the MFJP pile and monolithic pile in loose sand are presented in Figure 4.13 to Figure 4.18. Figure 4.13, Figure 15, and Figure 4.17 represent the plot of repeated three tests for total resistance that the pile and the soil, coming from shear resistance of the sliding surface, puts forward against the lateral soil movement versus pile head displacement. While Figure 4.14, Figure 4.16, and Figure 4.18, demonstrate the plots of average total resistance, sliding surface resistance or soil shear resistance, and the pile resistance alone against pile head displacement.

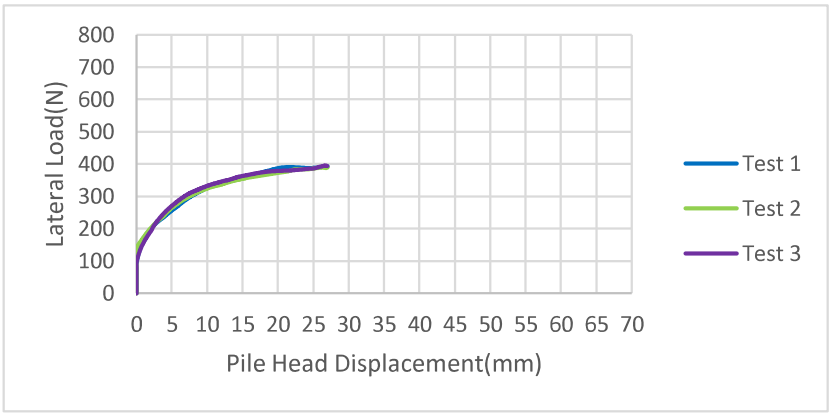

Figure 4.13. Total passive lateral resistance vs. pile head displacement for MFJP pile with 750N PTF in loose sand.

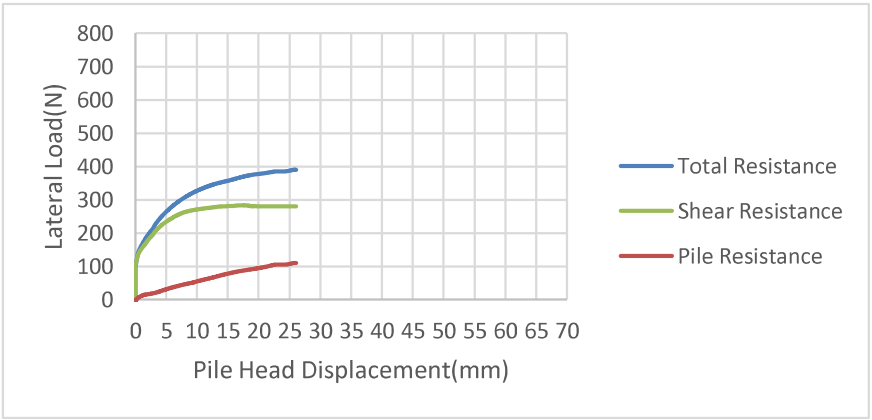

Figure 4.14. Average total resistance, pile resistance, and shear resistance vs pile head displacement for MFJP pile with 750N PTF in loose sand.

The results of the free field test on the soil only indicate that the resistance due to shear in the sliding surface between the moving layer and the stable layer is about 280N. The total resistance against lateral soil movement are 380N, 380N, and 415N for MFJP pile with 750N PTF, the MFJP pile with 1500N PTF, and monolithic pile respectively while the resistance due to the model piles alone is 100N, 100N, for MFJP piles with 750N PTF and 1500N PTF, and 135N for the monolithic piles.

The displacement at the head of the model piles at which the ultimate pile resistance reaches decrease as the rigidity increases similar to that of the active case with being 25 mm, 20 mm, and 15 mm for the MFJP pile with 750N PTF, MFJP pile with 1500N PTF and for the monolithic pile respectively.

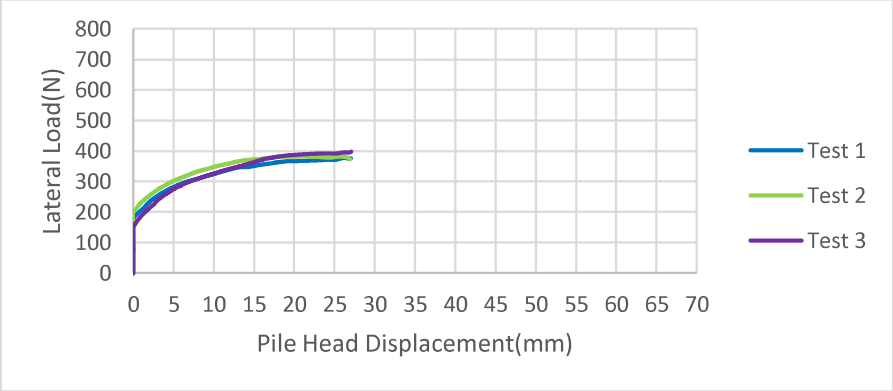

Figure 4.15. Total passive lateral resistance vs. pile head displacement for MFJP pile with 1500N PTF in loose sand.

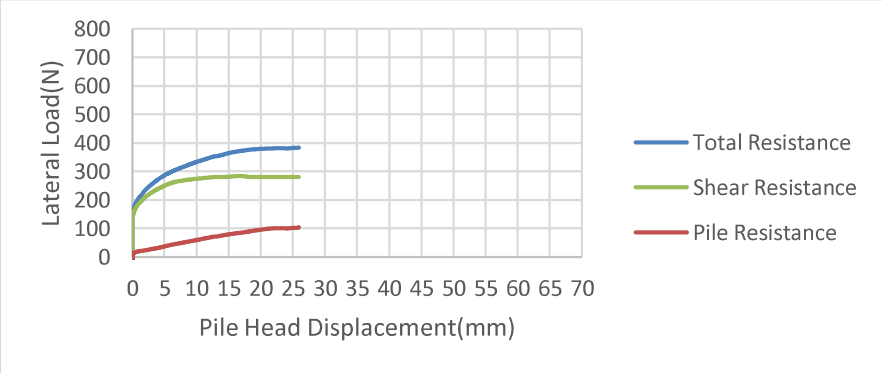

Figure 4.16. Average total resistance, pile resistance, and shear resistance vs pile head displacement for MFJP pile with 1500N PTF in loose sand.

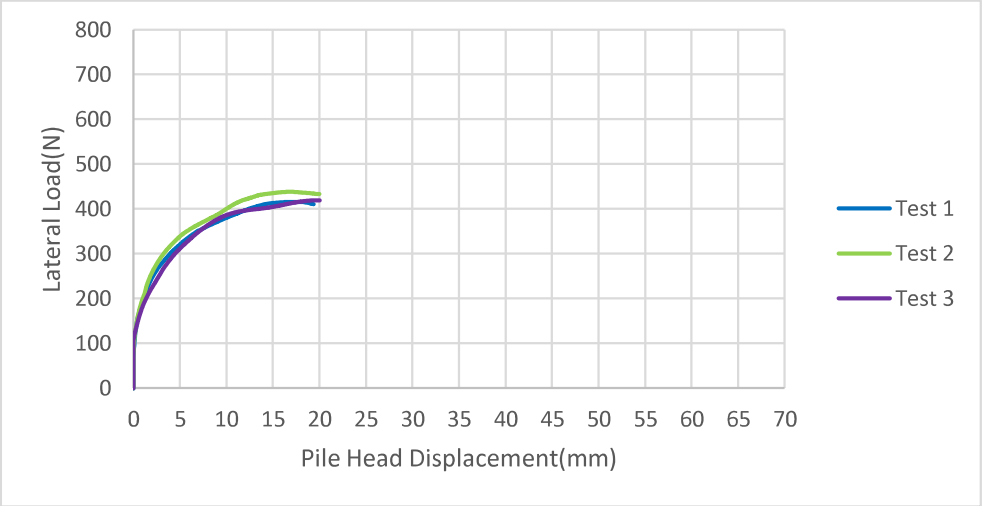

Figure 4.17. Total passive lateral resistance vs. pile head displacement for monolithic pile in loose sand.

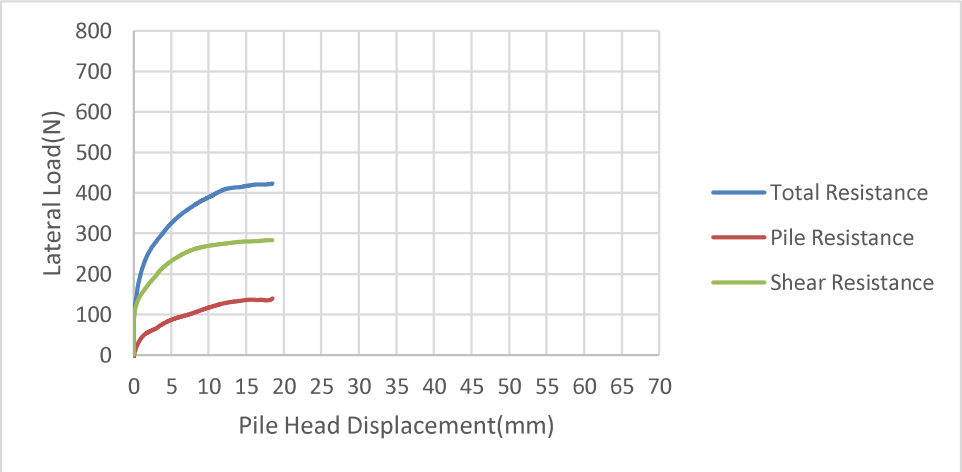

Figure 4.18. Average total resistance, pile resistance, and shear resistance vs pile head displacement for monolithic pile in loose sand.

4.4.2. Passive Lateral Tests on MFJP and Monolithic Piles in Medium Sand (D_r=50%)

The pile resistance against latera soil movement or passive loading in medium sand has increased significantly compared to that of loose sand as expected. In the medium soil, a significant increase can be seen in the lateral capacity of piles subjected to passive loading as the pile gets more rigid while the pile head displacement at which the ultimate lateral

resistance happens does not show a noticeable decrease though it is almost half of the pile head displacement at which ultimate pile resistance occur in loose sand. The results of the lateral passive tests on MFJP and monolithic model piles are shown in Figure 4.19 to Figure 4.24.

The model pile ultimate lateral resistance for a MFJP pile with 750N PTF, a MFJP pile with 1500N PTF, and a monolithic pile are 250N, 340N, and 380N in order while the pile head displacement at which the ultimate lateral resistance occurs are 10 mm, 9 mm, and 7 mm respectively for the above-mentioned model piles.

4.4.3. Combined Passive Lateral and Tensile Tests on MFJP and Monolithic Piles

While combined passive lateral load and tensile forces have been applied on the model piles, it was observed that the ultimate lateral pile resistance has fallen to almost half of the values corresponding to the case of only lateral soil movement, or passive lateral loading, for MFJP piles with 750N PTF from 100N and 250N to 50N and 125N in loose and medium sand respectively. This decrease in the case of the monolithic pile in medium sand is more severe in which the ultimate lateral pile resistance falls from 380N to 50N. The graphs related to these tests are shown in Figure 4.25, to Figure 4.30.

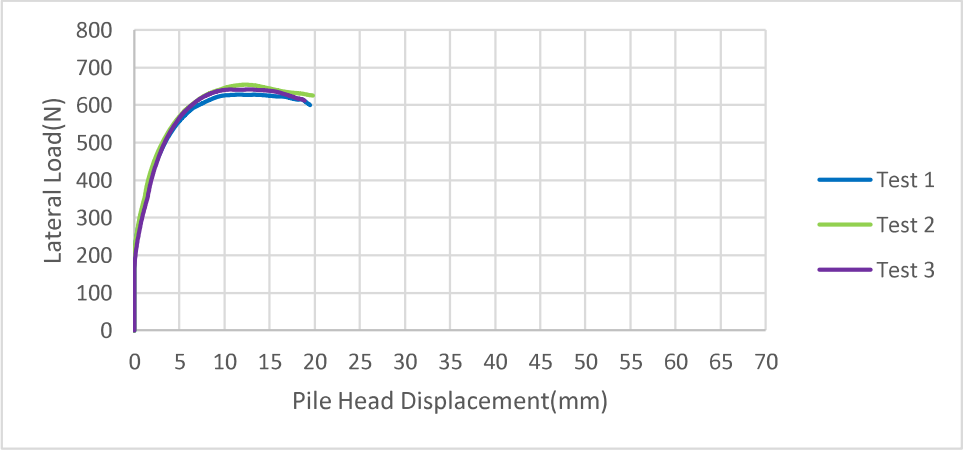

Figure 4.19. Total passive lateral resistance vs. pile head displacement for MFJP pile with 750N PTF in medium sand.

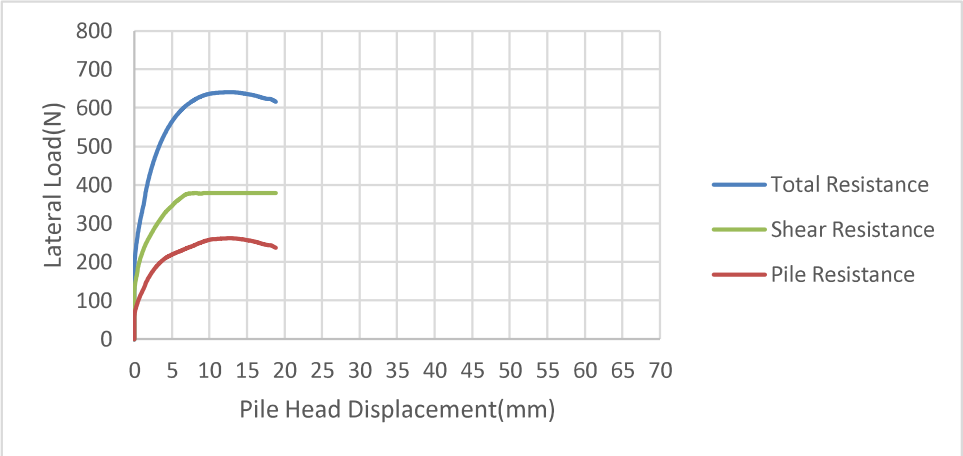

Figure 4.20. Average total resistance, pile resistance, and shear resistance vs pile head displacement for MFJP pile with 750N PTF in medium sand.

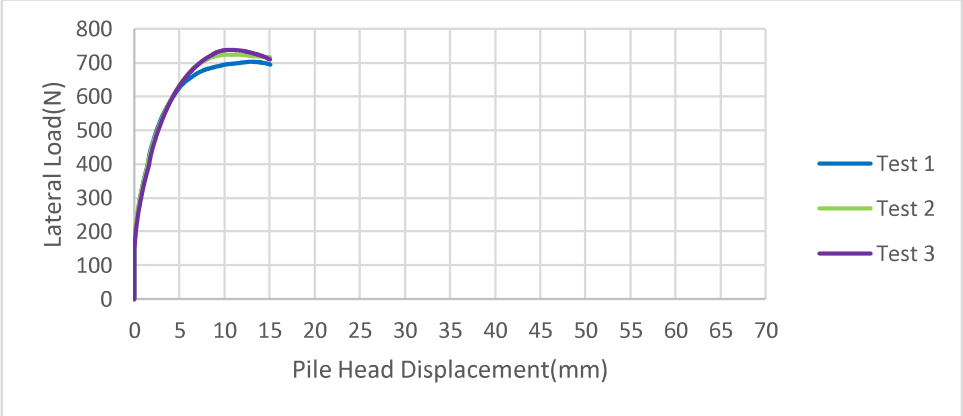

Figure 4.21. Total passive lateral resistance vs. pile head displacement for MFJP pile with 1500N PTF in medium sand.

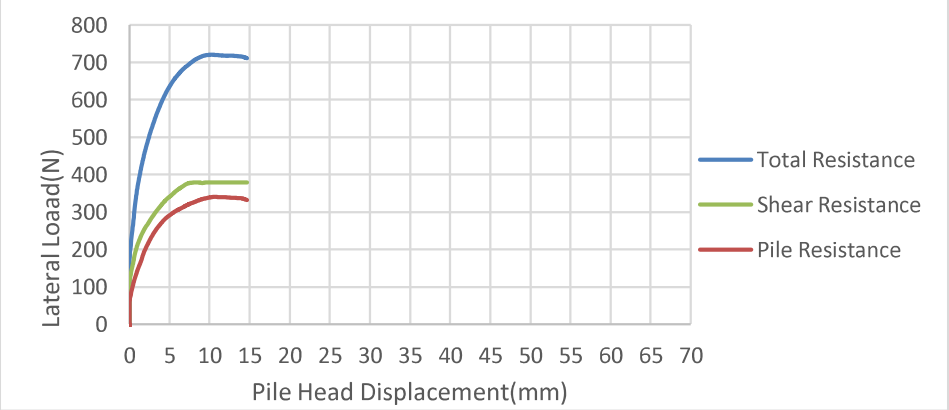

Figure 4.22. Average total resistance, pile resistance, and shear resistance vs pile head displacement for MFJP pile with 1500N PTF in medium

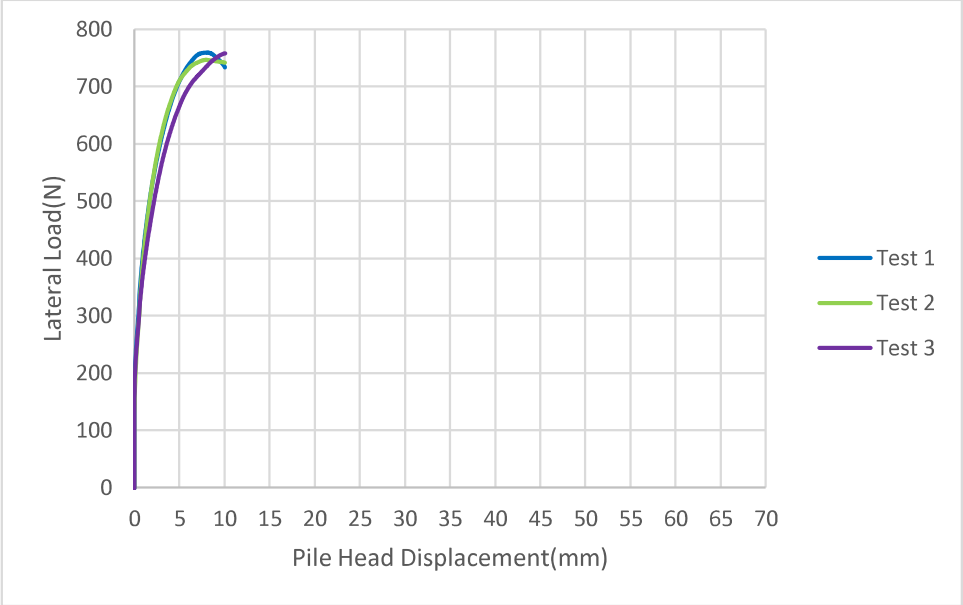

Figure 4.23. Total passive lateral resistance vs. pile head displacement for monolithic pile in medium sand.

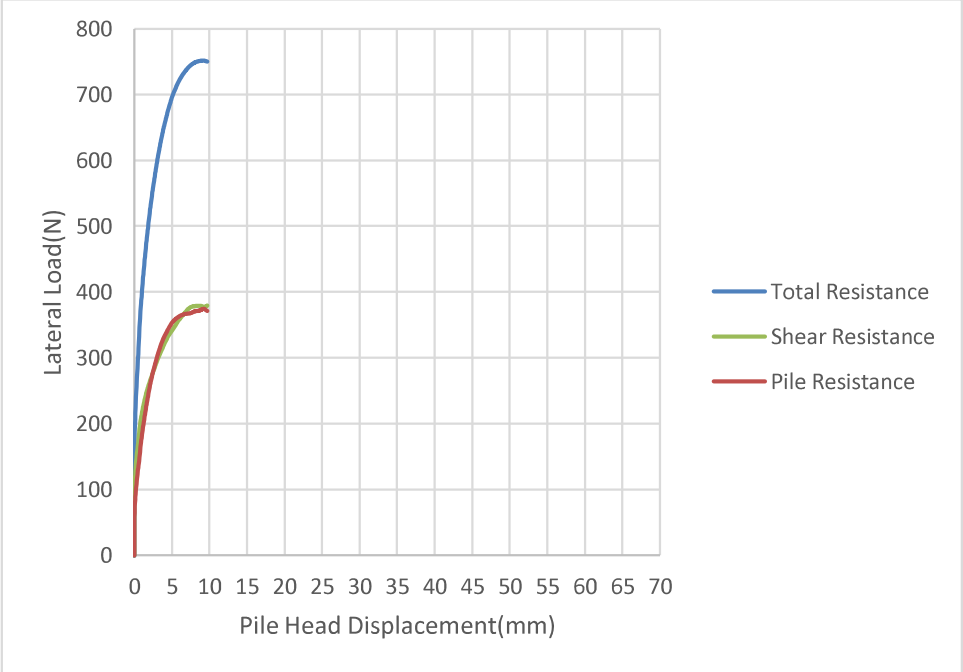

Figure 4.24. Average total resistance, pile resistance, and shear resistance vs pile head displacement for monolithic pile in medium sand.

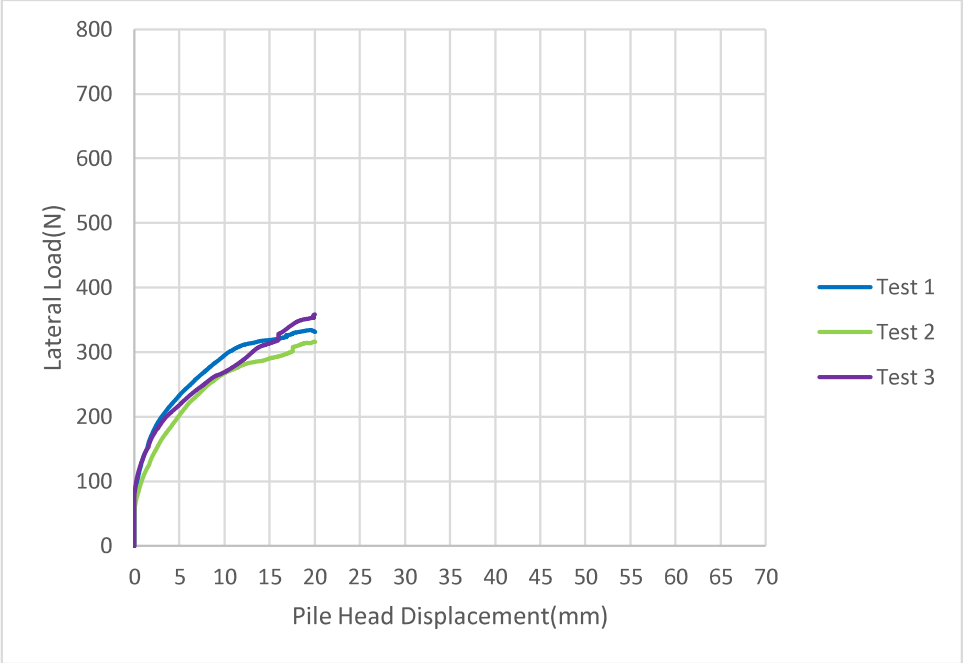

Figure 4.25. Total passive lateral resistance vs. pile head displacement for MFJP pile with 750N PTF subjected to combined loading in loose sand.

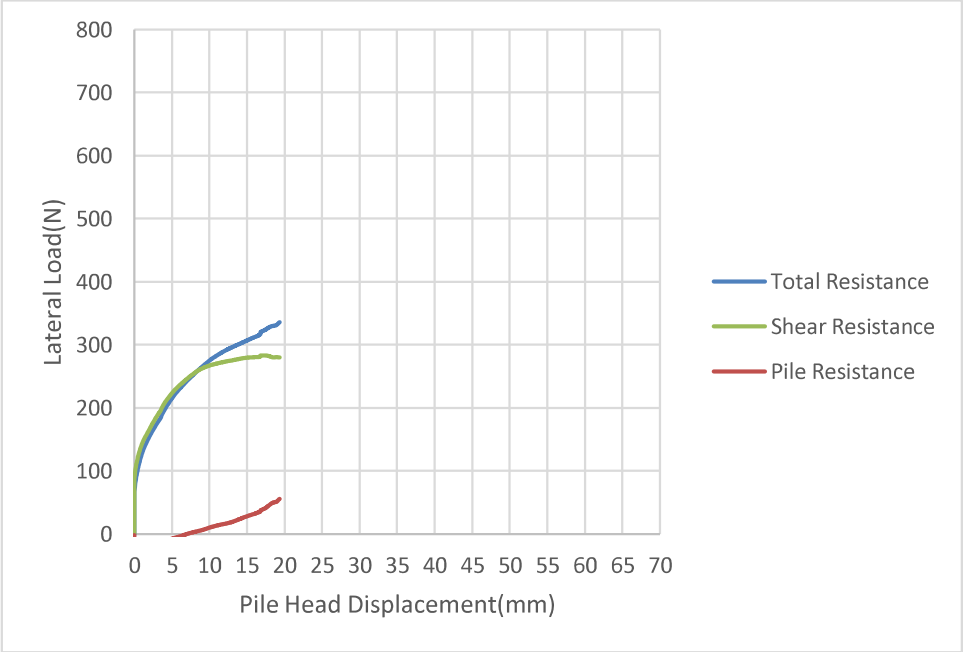

Figure 4.26. Average total resistance, pile resistance, and shear resistance vs pile head displacement for MFJP with 750N PTF pile subjected to combined loading in loose sand.

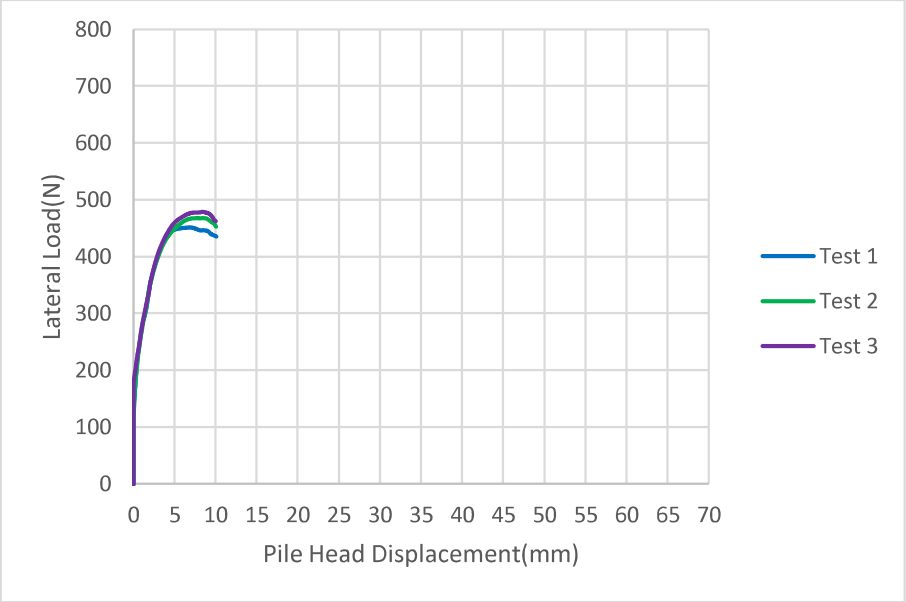

Figure 4.27. Total passive lateral resistance vs. pile head displacement for MFJP pile with 750N PTF subjected to combined loading in medium sand.

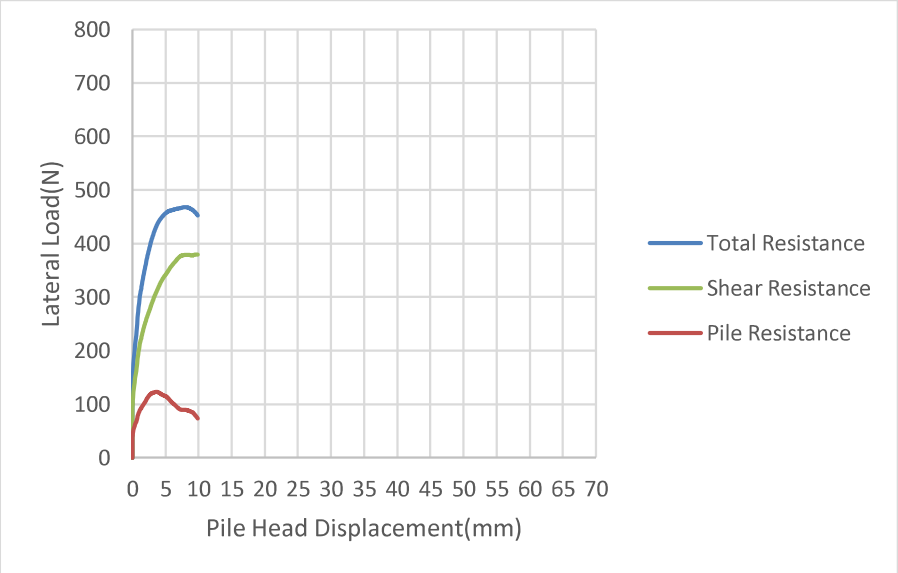

Figure 4.28. Average total resistance, pile resistance, and shear resistance vs pile head displacement for MFJP with 750N PTF pile subjected to combined loading in medium sand.

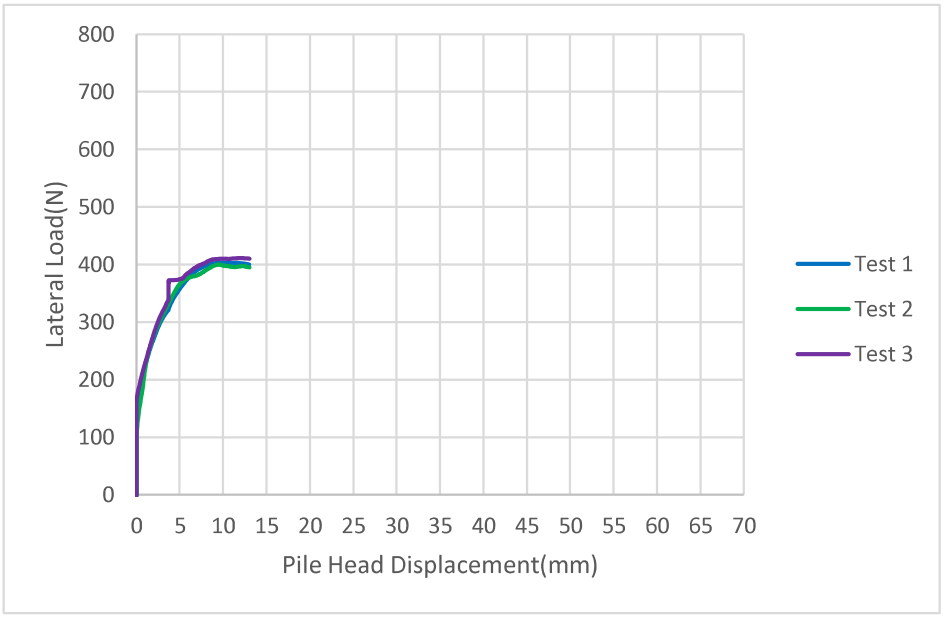

Figure 4.29. Total passive lateral resistance vs. pile head displacement for monolithic pile subjected to combined loading in medium sand.

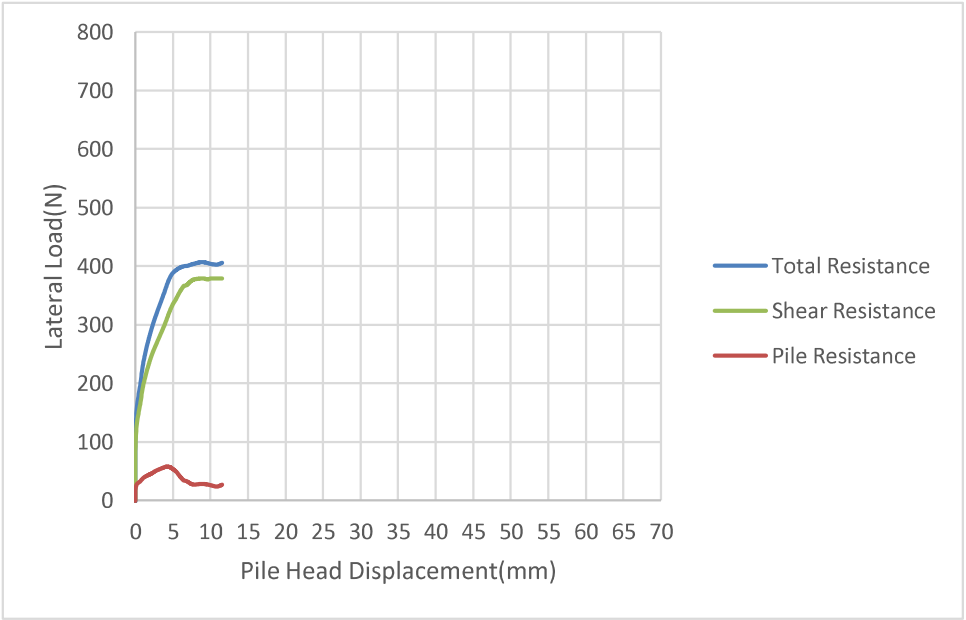

Figure 4.30. Average total resistance, pile resistance, and shear resistance vs pile head displacement for monolithic pile subjected to combined loading in medium sand.

4.5. Pile Rotation (From MPU9250 Sensor Analysis)

The rotations of the MFJP and monolithic piles along their length about the x, y, and z axes, the directions of the axis are shown in Figure 3.7 in chapter 3, have been calculated for all tests with the help of MPU9250 sensors and the related codes in MATLAB program. The rotations here indicate the amount of rotation that happened from the beginning of the test when the load is first applied until the end of the tests when the ultimate lateral capacity has been reached.

The average rotations of the three repeated tests in each case about x, y, and z axis are reported in the following tables, in Table 4.2 to Table 4.19. The rotation about the y axis shows the inclination of the model piles along their length. The rotations are calculated relative to the center of each sensor, and z in the following tables represent, the distance of the center of the sensors from the model piles head along the model piles length. It should be noted that among the x, y, and z axes, the rotations about the y-axis, i.e. the horizontal axis which is perpendicular to the longitudinal axis of the model piles, is of the main interest. The results of the rotations are discussed in detail in chapter 5.

Table 4.2. MFJP model pile, with 750N PTF, rotation about the x, y, and z axis subjected to active lateral loading in loose sand.

z(cm)	Block Number	Sensor Number	Rotations in Degree		
			x	y	z
1	1	4x68	17.85	31.38	4.10
5	3	3x68	18.80	18.65	5.61
10	5	3x69	16.11	2.03	8.92
15	7	5x68	8.71	5.06	4.79
20	10	5x69	4.40	1.23	0.69
28	12	6x68	2.51	9.02	8.71
33	14	6x69	1.87	4.40	1.28

Table 4.3. MFJP model pile, with 1500N PTF, rotation about the x, y, and z axis subjected to active lateral loading in loose sand.

z(cm)	Block Number	Sensor Number	Rotation in Degree		
			x	y	z
1	1	4x68	12.59	17.93	5.79
5	3	3x68	10.83	12.02	2.63
10	5	3x69	9.14	1.53	4.27
15	7	5x68	6.38	2.70	3.72
20	10	5x69	4.24	0.38	0.61
28	12	6x68	1.78	15.16	15.23
33	14	6x69	3.79	14.36	2.29

Table 4.4. Monolithic model pile rotation about the x, y, and z axis subjected to active lateral loading in loose sand.

z(cm)	Sensor Number	Rotation in Degree		
		x	y	z
1	4x68	9.92	10.09	7.26
5	3x68	8.98	8.05	5.75
10	3x69	7.15	4.64	0.36
15	5x68	7.12	8.48	0.74
20	5x69	7.01	5.44	1.14
28	6x68	33.11	8.27	7.85
33	6x69	9.88	27.60	5.73

Table 4.5. MFJP model pile, with 750N PTF, rotation about the x, y, and z axis subjected to active lateral loading in medium sand.

z(cm)	Block Number	Sensor Number	Rotations in Degree		
			x	y	z
1	1	4x68	23.25	47.09	5.27
5	3	3x68	23.59	23.26	5.74
10	5	3x69	16.56	9.37	6.21
15	7	5x68	9.24	7.95	6.99
20	10	5x69	3.64	2.23	0.91
28	12	6x68	15.63	11.69	11.44
33	14	6x69	8.11	0.57	7.68

Table 4.6. MFJP model pile, with 1500N PTF, rotation about the x, y, and z axis subjected to active lateral loading in medium sand.

z(cm)	Block Number	Sensor Number	Rotation in Degree		
			x	y	z
1	1	4x68	19.44	34.41	0.84
5	3	3x68	20.07	19.11	1.05
10	5	3x69	15.48	5.40	5.57
15	7	5x68	7.11	8.17	2.80
20	10	5x69	3.32	2.24	1.04
28	12	6x68	9.60	10.70	10.87
33	14	6x69	35.03	11.48	35.22

Table 4.7. Monolithic model pile rotation about the x, y, and z axis subjected to active lateral loading in medium sand.

z(cm)	Sensor Number	Rotation in Degree		
		x	y	z
1	4x68	7.14	8.68	4.87
5	3x68	6.76	6.42	4.14
10	3x69	5.46	2.44	0.40
15	5x68	5.56	4.93	0.45
20	5x69	5.56	2.53	0.31
28	6x68	28.36	4.59	5.59
33	6x69	7.53	28.42	4.46

Table 4.8. MFJP model pile, with 750N PTF, rotation about the x, y, and z axis subjected to combined active lateral loading and tensile forces in loose sand.

z(cm)	Block Number	Sensor Number	Rotation in Degree		
			x	y	z
1	1	4x68	15.73	18.24	7.29
5	3	3x68	14.84	13.81	6.38
10	5	3x69	10.90	6.00	2.01
15	7	5x68	8.26	8.65	2.52
20	10	5x69	7.30	6.96	2.22
28	12	6x68	22.72	8.13	6.66
33	14	6x69	40.77	3.17	39.49

Table 4.9. MFJP model pile, with 750N PTF, rotation about the x, y, and z axis subjected to combined active lateral loading and tensile forces in medium sand.

z(cm)	Block Number	Sensor Number	Rotation in Degree		
			x	y	z
1	1	4x68	18.71	22.07	6.77
5	3	3x68	17.81	16.03	1.70
10	5	3x69	13.82	5.60	3.24
15	7	5x68	7.64	8.41	2.01
20	10	5x69	3.99	3.04	0.86
28	12	6x68	5.71	5.91	4.68
33	14	6x69	37.31	2.94	39.19

Table 4.10. Monolithic model pile rotation about the x, y, and z axis subjected to combined active lateral loading and tensile forces in medium sand.

z(cm)	Sensor Number	Rotation in Degree		
		x	y	z
1	4x68	10.14	4.97	8.31
5	3x68	8.61	4.57	6.41
10	3x69	5.80	4.14	0.57
15	5x68	8.03	6.71	4.65
20	5x69	7.01	2.40	3.19
28	6x68	9.40	6.17	3.15
33	6x69	7.90	8.69	4.03

Table 4.11. MFJP model pile, with 750N PTF, rotation about the x, y, and z axis subjected to lateral soil movement, or passive loading, in loose sand.

z(cm)	Block Number	Sensor Number	Rotation in Degree		
			x	y	z
1	1	4x68	5.582	7.231	3.094
5	3	3x68	4.078	3.482	0.321
10	5	3x69	4.109	2.639	0.519
15	7	5x68	5.454	3.517	3.474
20	10	5x69	3.505	9.663	1.663
28	12	6x68	4.251	4.356	2.095
33	14	6x69	10.871	5.051	10.096

Table 4.12. MFJP model pile, with 1500N PTF, rotation about the x, y, and z axis subjected to lateral soil movement in loose sand.

z(cm)	Block Number	Sensor Number	Rotation in Degree		
			x	y	z
1	1	4x68	4.96	7.54	3.40
5	3	3x68	4.30	2.65	0.61
10	5	3x69	3.91	3.62	0.36
15	7	5x68	5.39	3.94	3.28
20	10	5x69	3.41	9.91	1.59
28	12	6x68	5.91	4.00	1.55
33	14	6x69	11.34	4.82	10.72

Table 4.13. Monolithic model pile rotation about the x, y, and z axis subjected to lateral soil movement in loose sand.

z(cm)	Sensor Number	Rotation in Degree		
		x	y	z
1	4x68	7.54	0.62	6.98
5	3x68	4.94	0.93	4.01
10	3x69	2.98	1.74	0.25
15	5x68	3.49	4.40	1.41
20	5x69	3.28	2.47	0.94
28	6x68	4.25	3.43	1.99
33	6x69	3.23	8.21	1.19

Table 4.14. MFJP model pile, with 750N PTF, rotation about the x, y, and z axis subjected to lateral soil movement in medium sand.

z(cm)	Block Number	Sensor Number	Rotation in Degree		
			x	y	z
1	1	4x68	4.69	4.52	3.93
5	3	3x68	2.98	2.07	0.87
10	5	3x69	2.65	2.17	0.18
15	7	5x68	3.29	2.31	1.44
20	10	5x69	2.48	6.32	1.30
28	12	6x68	3.73	2.80	0.98
33	14	6x69	5.65	1.88	4.92

Table 4.15. MFJP model pile, with 1500N PTF, rotation about the x, y, and z axis subjected to lateral soil movement in medium sand.

z(cm)	Block Number	Sensor Number	Rotation in Degree		
			x	y	z
1	1	4x68	2.92	4.09	2.34
5	3	3x68	2.31	3.87	1.16
10	5	3x69	2.02	1.37	0.23
15	7	5x68	2.46	1.97	1.04
20	10	5x69	2.01	3.59	0.41
28	12	6x68	1.77	2.28	1.10
33	14	6x69	3.52	1.92	2.68

Table 4.16. Monolithic model pile rotation about the x, y, and z axis subjected to lateral soil movement in medium sand.

z(cm)	Sensor Number	Rotation in Degree		
		x	y	z
1	4x68	2.32	2.13	1.92
5	3x68	1.58	0.74	0.92
10	3x69	1.25	0.86	0.51
15	5x68	1.56	1.42	0.46
20	5x69	1.47	0.90	0.21
28	6x68	3.92	1.62	1.49
33	6x69	1.46	3.51	0.43

Table 4.17. MFJP model pile, with 750N PTF, rotation about the x, y, and z axis subjected to combined lateral soil movement and tensile forces in loose sand.

z(cm)	Block Number	Sensor Number	Rotation in Degree		
			x	y	z
1	1	4x68	3.21	0.91	2.41
5	3	3x68	3.07	0.93	1.95
10	5	3x69	2.55	2.23	0.02
15	7	5x68	2.89	2.59	0.93
20	10	5x69	2.61	5.94	1.02
28	12	6x68	7.97	2.22	0.65
33	14	6x69	4.67	3.32	3.74

Table 4.18. MFJP model pile, with 750N PTF, rotation about the x, y, and z axis subjected to combined lateral soil movement and tensile forces in medium sand.

z(cm)	Block Number	Sensor Number	Rotation in Degree		
			x	y	z
1	1	4x68	1.46	3.10	0.72
5	3	3x68	1.14	1.12	0.63
10	5	3x69	1.18	1.04	0.13
15	7	5x68	1.51	1.75	0.64
20	10	5x69	1.55	2.67	0.53
28	12	6x68	3.99	1.51	0.51
33	14	6x69	3.47	3.34	2.99

Table 4.19. Monolithic model pile rotation about the x, y, and z axis subjected to combined lateral soil movement and tensile forces in medium sand.

z(cm)	Sensor Number	Rotation in Degree		
		x	y	z
1	4x68	2.81	0.68	2.10
5	3x68	3.04	0.89	2.42
10	3x69	1.85	1.16	0.29
15	5x68	2.05	3.09	0.56
20	5x69	1.84	3.02	0.72
28	6x68	0.65	1.80	0.57
33	6x69	2.00	1.77	0.16

5. DISCUSSION

5.1. Introduction

In this chapter the results of the tests on MFJP model piles, and monolithic piles subjected to lateral active loading, lateral soil movement, and combined lateral and tensile forces are discussed, analyzed, and compared. The chapter mainly explains and discuss the effect of pile flexibility, soil stiffness, loading type, and tensile forces on laterally loaded model piles in light of the experimental results on these model piles.

5.2. Effect of Pile Flexibility on Behavior and Lateral Capacity of Piles

The effect of flexibility has been investigated by comparing the results of the lateral tests on three different model piles with different flexibility. These model piles are a MFJP pile post-tensioned to 750N force, which represents a relatively flexible pile, a MFJP pile post-tensioned to 1500N, indicating a model pile with intermediate flexibility, and a monolithic concrete pile, representing a relatively rigid pile.

The energy absorption capacity of the model piles during the loading which is calculated from the area beneath the load-deflection curves, are shown in Table 5.1, Table 5.2, and Table 5.3. The MFJP piles have the capability to absorb higher energy both in the case of active lateral loading and passive lateral loading in medium sand compared to that of the monolithic pile, and hence have the capacity to carry loads under large displacements without structural failure. This is desirable since the MFJP model piles are constructed in trenches which needs good compaction after placing the MFJP pile inside the bore or trench, and the soil around the MFJP piles are medium or medium to dense soil.

In the same manner, the MFJP piles have to the capacity to absorb more energy and are able to undergo large displacements in medium soil while combined lateral and tensile forces are applied as well compared to that of monolithic piles. In contrast, in loose soil, the Monolithic piles and the MFJP piles does not show a significant difference in energy absorption.

Table 5.1. Model piles' energy absorption from load-displacement curve in active case.

	Energy Absorption (N.m)	
Pile Type	Loose Sand	Medium Sand
MFJP (750N PTF)	12.52	25.82
MFJP (1500N PTF)	9.95	29.45
Monolithic	12.82	17.31

Table 5.2. Model piles' energy absorption from load-displacement curve in passive case.

	Energy Absorption (N.m)	
Pile Type	Loose Sand	Medium Sand
MFJP (750N PTF)	1.69	4.28
MFJP (1500N PTF)	1.75	4.21
Monolithic	1.91	3.02

Table 5.3. Model piles' energy absorption from load-displacement curve in combined lateral loading case.

	Energy Absorption (N.m) In Medium Sand	
Pile Type	Combined Active and Lateral Loading Case	Combined Passive and Lateral Loading Case
MFJP (750N PTF)	19.69	9.67
Monolithic	15.176	1.35

The load-displacement curves related to active lateral loading tests on these three model piles in loose soil and medium soil, shown in Figure 5.1 and Figure 5.2 respectively, indicate that the pile head displacement at which the ultimate lateral capacity reaches decreases as the model piles get more rigid. Although the decrease in pile head displacement from the MFJP pile with 750N PTF to MFJP pile with 1500N PTF is not that severe with a fall of 8 mm and 5 mm in loose and medium sand, the head displacement diminishes significantly while comparing the flexible MFJP pile, having 750N, with the rigid monolithic pile, with a decrease of about 13 mm and 23 mm in loose and medium sand respectively.

The decrease in pile head displacement in rigid piles is a result of the different behaviors that the flexible and rigid piles put forward against lateral loading. In case of flexible pile, the soil pressure is distributed over a small length of the pile near the pile head which results in high pile head displacement under the same lateral load in comparison to rigid piles. In other words, the pile tends to rotate near to the pile head and only a small portion of the pile near the pile head carries the lateral load. While, in the rigid case, the pile rotates at a point near the pile base, and lateral loads are distributed along a large portion of the pile length resulting in a lower pile head displacement.

This has been indicated by the rotations of the model piles along their length from the longitudinal axes of the pile as well, as shown in Table 5.4, and Table 5.5. It is evident from these rotations that the flexible MFJP pile, having 750N PTF, shows significant rotations up to a length of 0.3L. At point 0.3L below pile head, there is no significant change in angle with respect to vertical axes and it denotes the inflection point after which the rotations are relatively small. In contrast, the MFJP pile having 1500N PTF and the monolithic pile seems to have their inflection point at a distance of 0.6L below the pile head and rotates significantly below this point. It should be noted that the rotations in Table 5.4 and 5.5 indicate the absolute values and the rotations below the inflection points are in the opposite direction of those above the inflection points.

The results also demonstrate that the ultimate capacity increases as the pile rigidity increases with an increase of 43% comparing the MFJP pile with 750N PTF and the monolithic pile in loose sand while there is a 27% increase for the same case in medium sand. This increase again could be the results of the fact that in rigid case a large portion of the pile length is pushed into the soil while in the flexible case a small portion of the pile length actively resists the lateral loading.

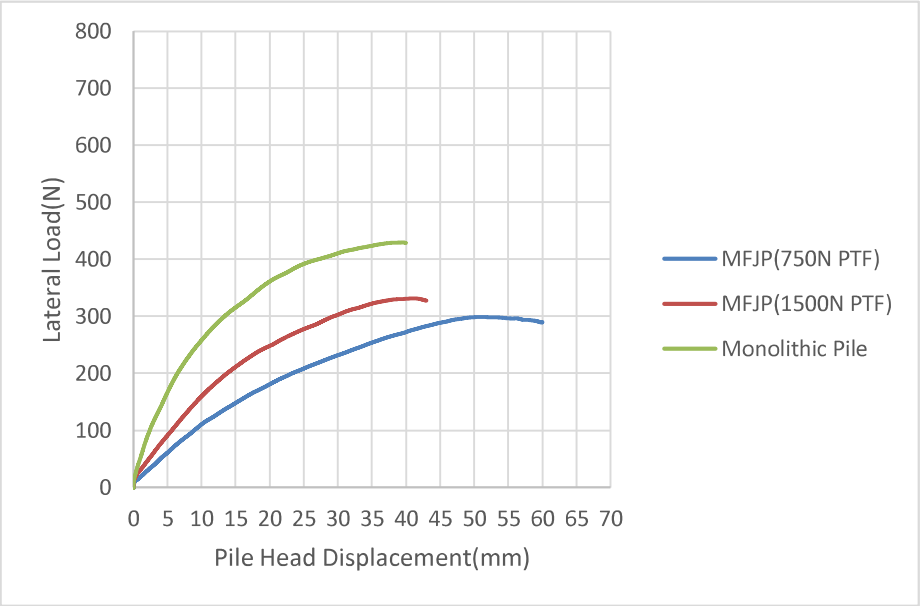

Figure 5.1. Active lateral loading vs. pile head displacement in loose sand.

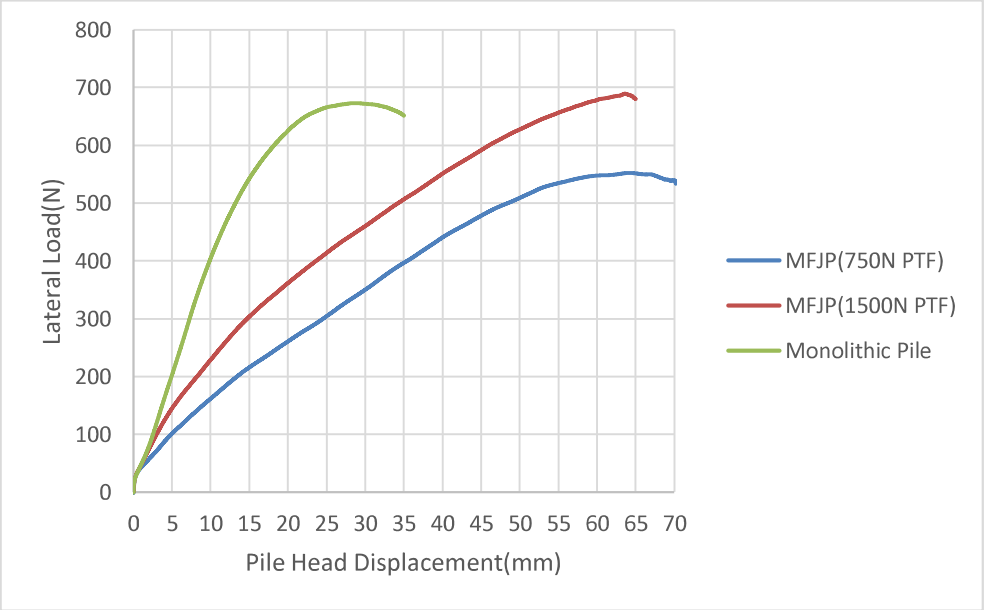

Figure 5.2. Active lateral loading vs. pile head displacement in medium sand.

Table 5.4. Pile rotations along its length about the horizontal axis in loose sand (Active).

z(cm)	Block Number	Sensor Number	Rotation in Degree about Horizontal Axis		
			MFJP Pile (750N PTF)	MFJP Pile (1500N PTF)	Monolithic Pile
1	1	4x68	31.38	17.93	10.09
5	3	3x68	18.65	12.02	8.05
10	5	3x69	2.03	1.53	4.64
15	7	5x68	5.06	2.7	8.48
20	10	5x69	1.23	0.38	5.44
28	12	6x68	9.02	15.16	8.27
33	14	6x69	4.4	14.36	27.6

Table 5.5. Pile rotations along its length about the horizontal in medium sand (Active).

z(cm)	Block Number	Sensor Number	Rotation in Degree about Horizontal Axis		
			MFJP Pile (750N PTF)	MFJP Pile (1500N PTF)	Monolithic Pile
1	1	4x68	47.09	34.41	8.68
5	3	3x68	23.26	19.11	6.42
10	5	3x69	9.37	5.4	2.44
15	7	5x68	7.95	8.17	4.93
20	10	5x69	2.23	2.24	2.53
28	12	6x68	11.69	10.7	4.59
33	14	6x69	0.57	11.48	28.42

The pile head displacement at which the ultimate lateral capacity reaches decreases as the pile gets more rigid while the piles are subjected to lateral soil movements, i.e. passive loading, similar to that of the active case as it is shown in Figure 5.3 and Figure 5.4. The pile lateral resistance increases as the rigidity increases as well, but the rotations along the pile length while passive loading is concern seem to not change significantly, as it is shown in Table 5.6 and Table 5.7. This indicates that the pile undergoes significant translational displacement, and rotates very less while lateral soil movement is applied, since only about 1/3L of the pile is embedded in the stable layer.

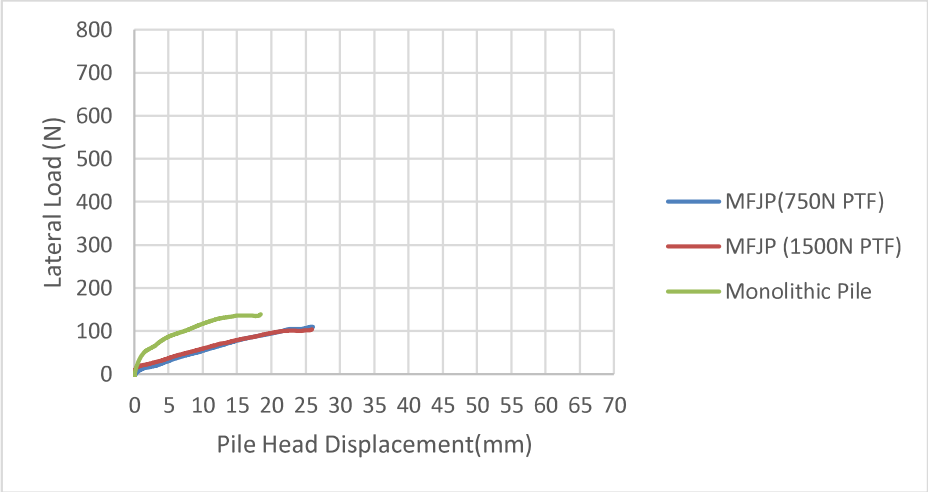

Figure 5.3. Passive lateral loading vs. pile head displacement in loose sand.

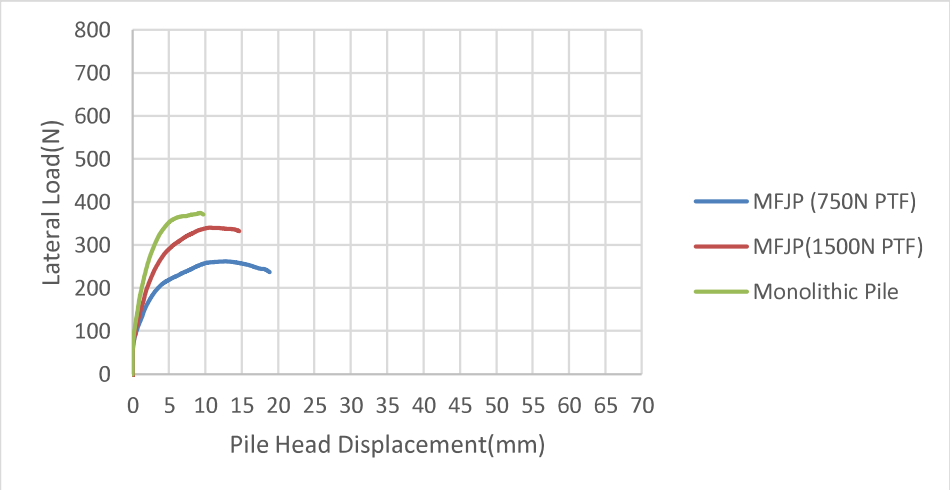

Figure 5.4. Passive lateral loading vs. pile head displacement in medium sand.

Table 5.6. Pile rotations along its length about the horizontal axis in loose sand (Passive).

z(cm)	Block Number	Sensor Number	Rotation in Degree about Horizontal Axis		
			MFJP Pile (750N PTF)	MFJP Pile (1500N PTF)	Monolithic Pile
1	1	4x68	7.231	7.54	0.62
5	3	3x68	3.482	2.65	0.93
10	5	3x69	2.639	3.62	1.74
15	7	5x68	3.517	3.94	4.4
20	10	5x69	9.663	9.91	2.47
28	12	6x68	4.356	4	3.43
33	14	6x69	5.051	4.82	8.21

Table 5.7. Pile rotations along its length about the horizontal axis in medium sand (Passive).

z(cm)	Block Number	Sensor Number	Rotation in Degree about Horizontal Axis		
			MFJP Pile (750N PTF)	MFJP Pile (1500N PTF)	Monolithic Pile
1	1	4x68	4.52	4.09	2.13
5	3	3x68	2.07	3.87	0.74
10	5	3x69	2.17	1.37	0.86
15	7	5x68	2.31	1.97	1.42
20	10	5x69	6.32	3.59	0.9
28	12	6x68	2.8	2.28	1.62
33	14	6x69	1.88	1.92	3.51

5.3. Effect of Soil Stiffness

As the relative density of the soil increases from D_r=20%, in loose sand, to D_r=50%, in medium sand, the ultimate lateral capacity of the pile increases in both cases while the pile is subjected to active lateral loading and passive lateral loading.

The active lateral capacity of the model piles in medium soil for the MFJP pile, having 750N PTF, and MFJP pile, having 1500N PTF, are almost double their lateral capacity in loose sand (Figure 5.5 and Figure 5.6). While, the active lateral capacity of the monolithic pile increases about 56% from 428N, in case of loose sand, to 670N, in medium sand as it is indicated in Figure 5.7.

The increase in pile resistance when passive loading is concerned is as prominent as it is in the case of active lateral loading also, as it is indicated in Figure 5.8, Figure 5.9 and Figure 5.10. The increase in lateral capacity of piles as soil relative density increases is, obviously, due to an increase in the shear strength and modulus of elasticity of the soil with the increase in relative density.

5.4. Effect of Tensile Force on the Lateral Capacity of Model Piles

The combined lateral and tensile forces on the MFJP and monolithic piles demonstrate that the lateral capacity of the model piles both in active and passive cases

decreases while the piles are subjected to a tensile force along with lateral loading, as it is shown in Figure 5.11 to Figure 5.14. The piles are subjected to 75% of their ultimate uplift capacity while laterally loaded. The decrease in lateral capacity is much more in the case of medium sand while compared to loose sand. The decrease in lateral capacity under combined loading is taught to be due to the decrease in the radial stresses around the pile while tensile forces are applied. This decrease in the radial stresses in the medium case seems to be more severe than the loose sand since the soil particles are more packed and more prone to loosening and disturbance.

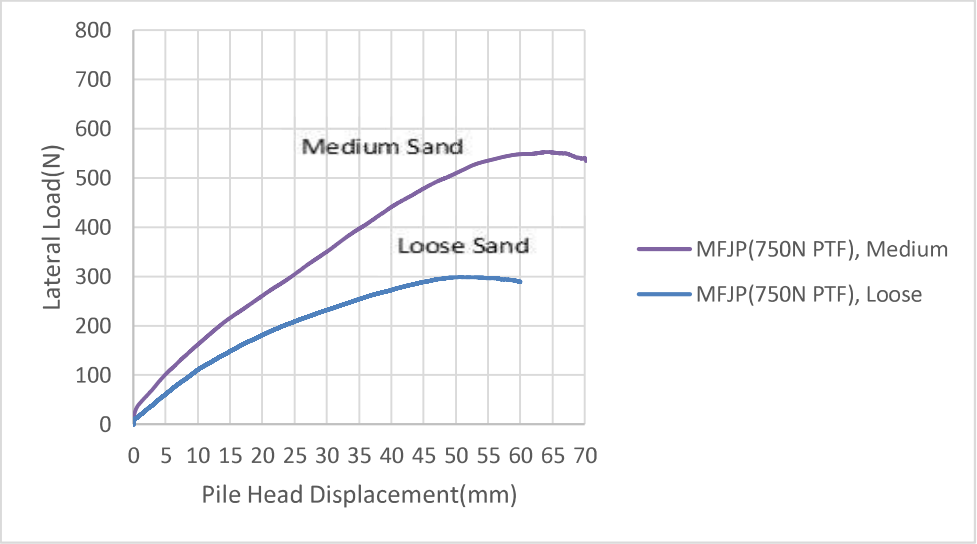

Figure 5.5. Lateral active tests on MFJP pile with 750N PTF in loose and medium sand.

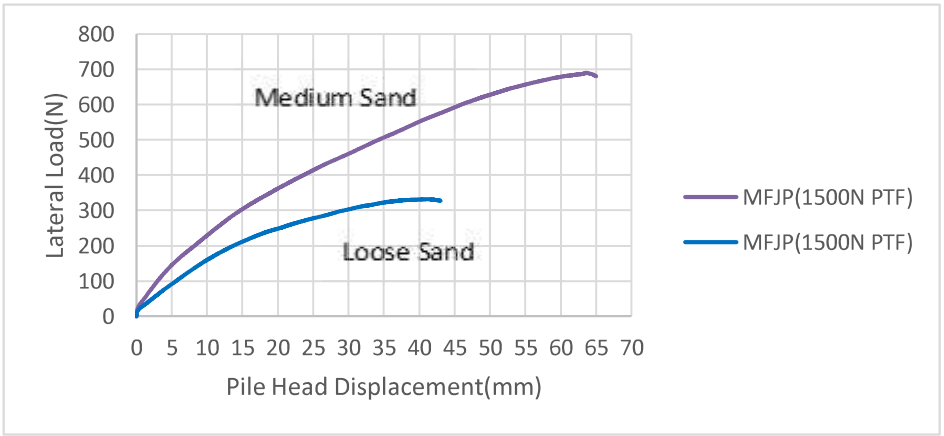

Figure 5.6. Lateral active tests on MFJP pile with 1500N PTF in loose and medium sand.

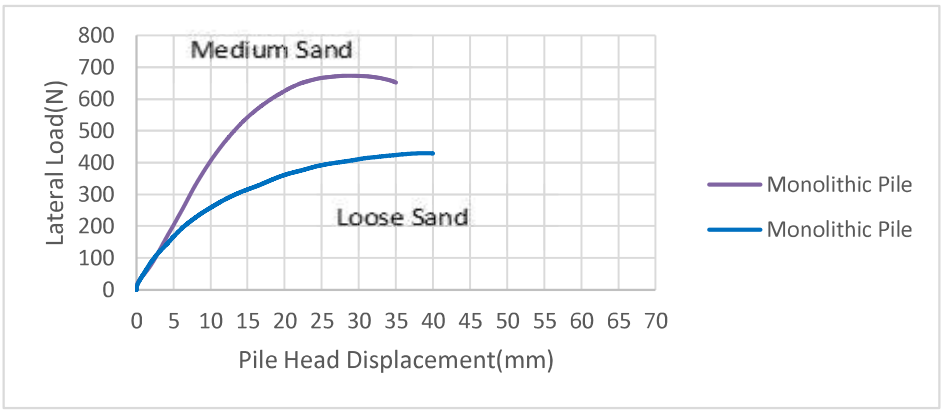

Figure 5.7. Lateral active tests on monolithic pile in loose and medium sand.

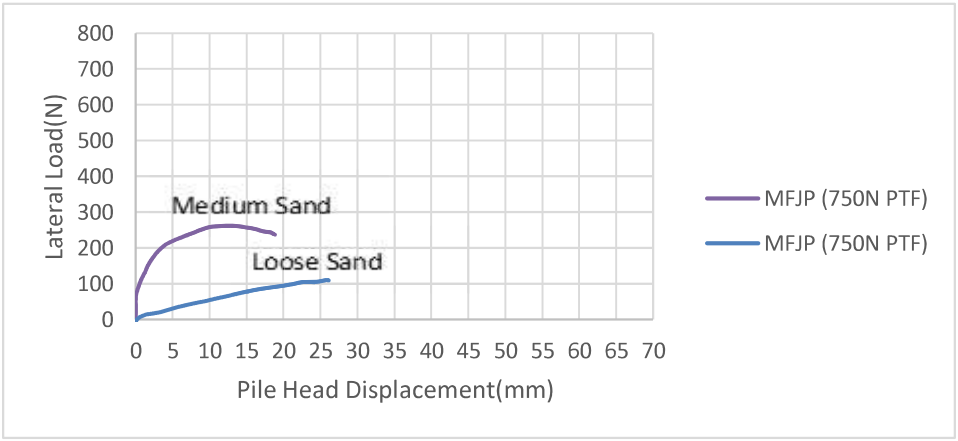

Figure 5.8. Lateral passive tests on MFJP pile with 750N PTF in loose and medium sand.

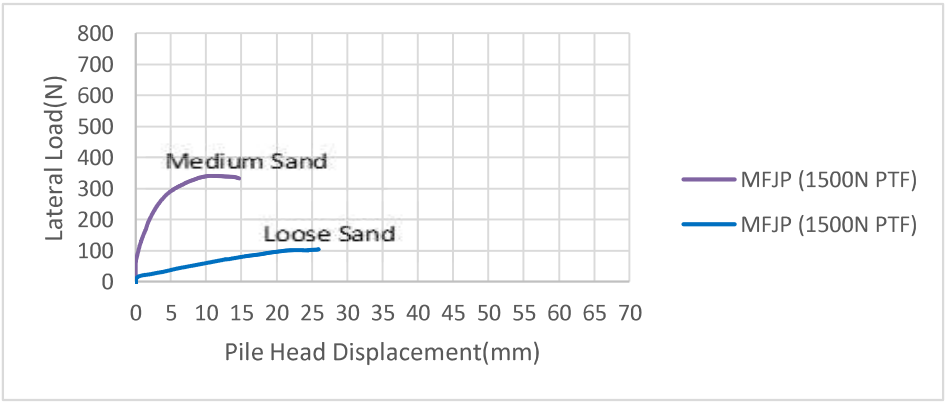

Figure 5.9. Lateral passive tests on MFJP pile with 1500N PTF in loose and medium sand.

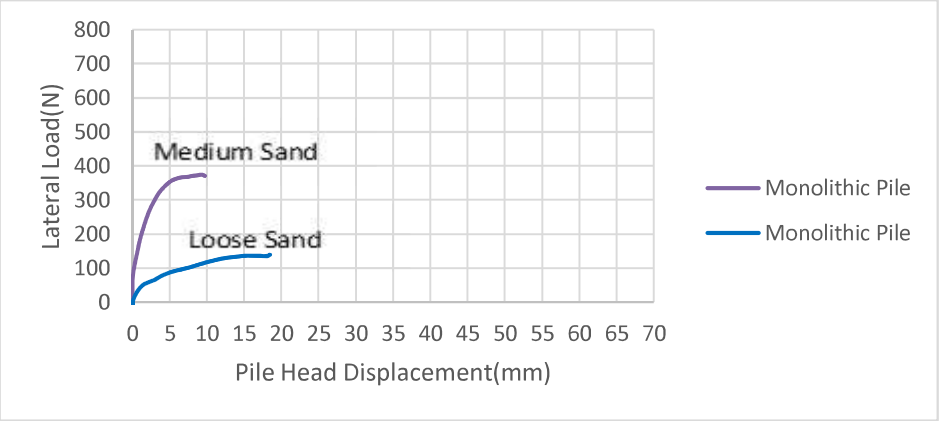

Figure 5.10. Lateral passive tests on monolithic pile in loose and medium sand.

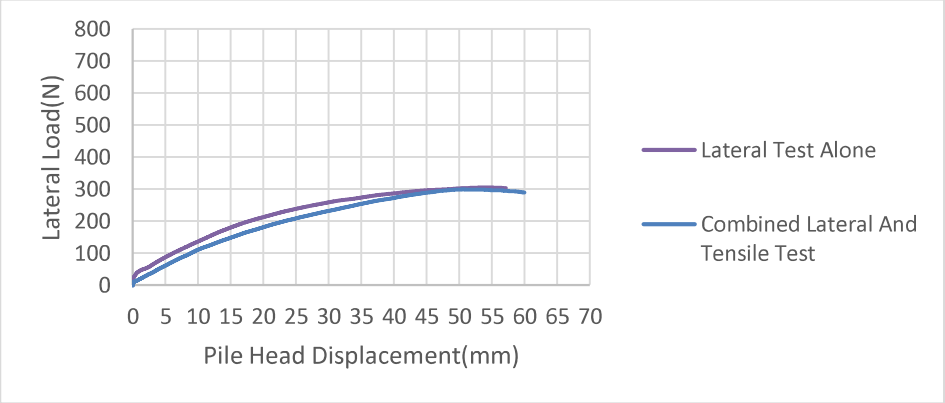

Figure 5.11. Combined active lateral and tensile loading test vs. active lateral test alone on a MFJP pile, having 750N PTF, in loose sand.

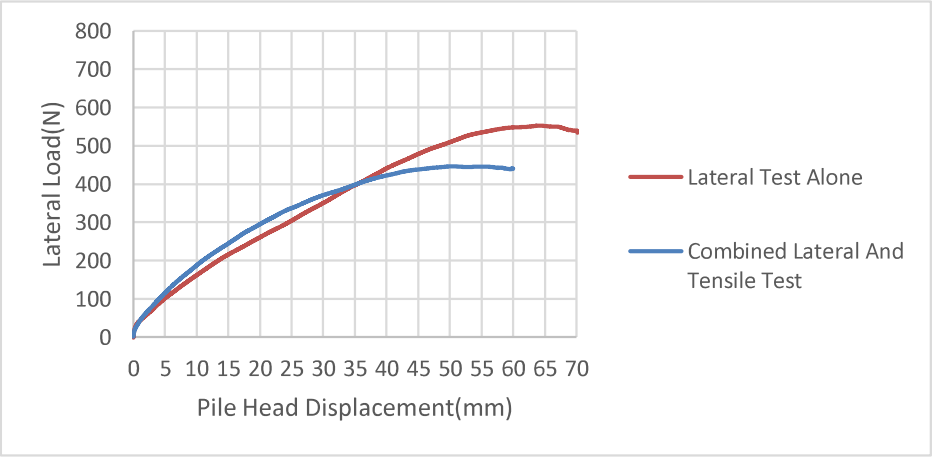

Figure 5.12. Combined active lateral and tensile loading test vs. active lateral test alone on a MFJP pile, having 750N PTF, in medium sand.

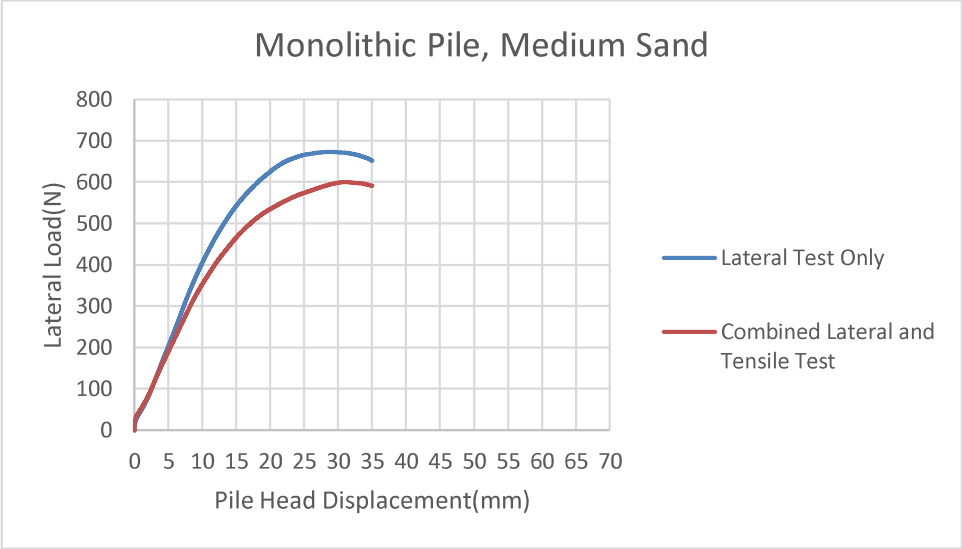

Figure 5.13. Combined active lateral and tensile loading test vs. active lateral test alone on monolithic pile in medium sand.

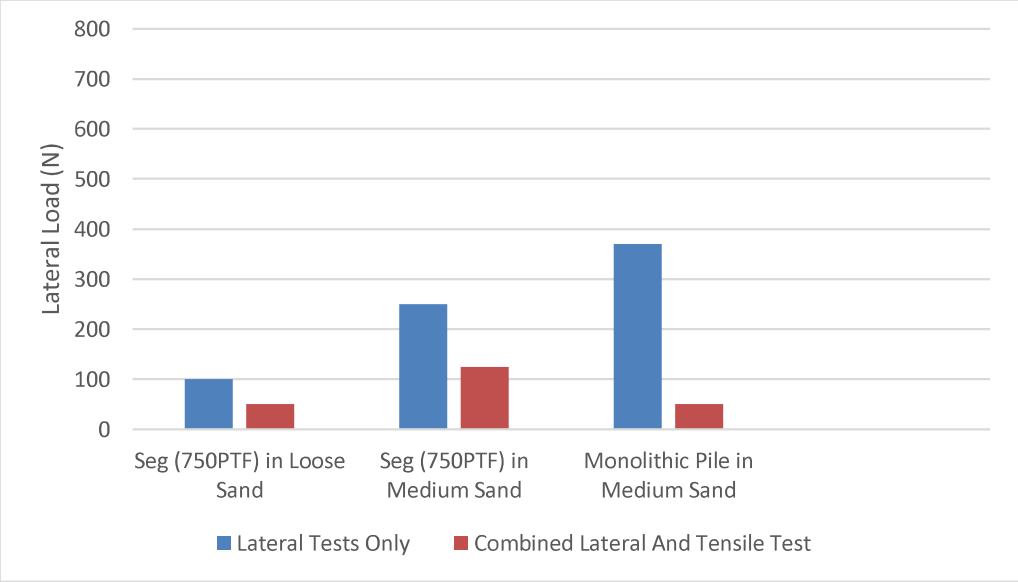

Figure 5.14. Combined passive lateral and tensile loading test vs. passive lateral test alone on monolithic pile in medium sand.

5.5. Effect of Loading Type on the Lateral Capacity of Model Piles

Since two types of loading, lateral active loading, and lateral passive loading, were applied on the model piles, we can determine how the type of loading has affected the

behavior and capacity of the model piles as well. The lateral capacity while the model piles are subjected to lateral soil movement, or passive loading, has decreased to almost one-third of the lateral capacities in case of active lateral loading as expected since the embedment length in the passive loading is much less, with 14 cm embedment, compare to that of the active lateral loading, in which the whole pile length of 34 cm resists against lateral loading. The below histogram in Figure 5.15 compare the results of the lateral capacity of the model piles subjected to active and passive loading.

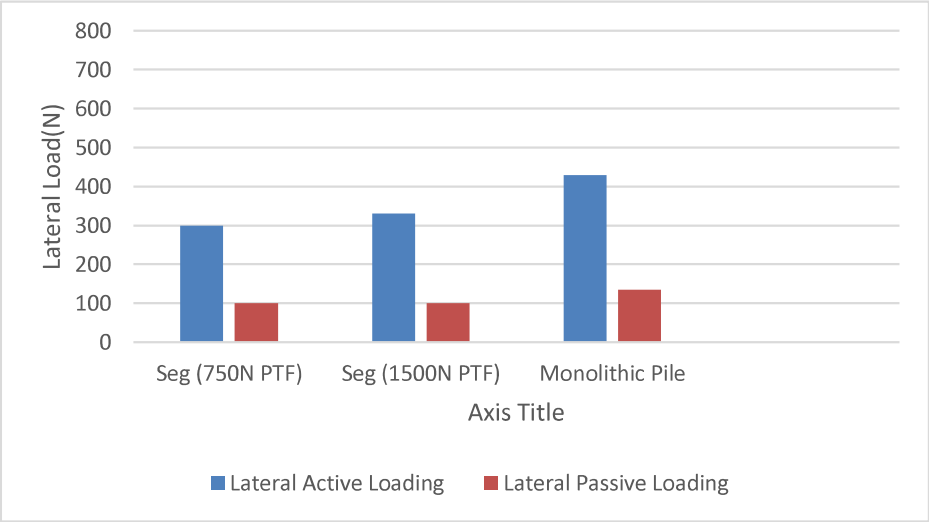

Figure 5.15. Loading type effect on lateral capacity of model piles in medium sand.

5.6. Post Tensioning Force on the central cable

The tension force on the cable, which is keeping the mortar blocks together, increases gradually when the multiple friction joint pile is subjected to active lateral loading and combined tensile and active lateral loadings. Both in the case of an MFJP post-tensioned to 750N force and in the case of an MFJP pile post-tensioned to 1500N, the post-tension force in the cable increases till a displacement equal to that of the displacement at which the ultimate lateral load happens (Figure 5.16). It can be asserted that until this ultimate displacement, which is the displacement at which soil failure happens, there is a resistance against the lateral pulling from the upper box wire, connected to the pile head for applying lateral displacement, hence, there is an increase in the post-tensioning force of the model

pile cable. After this displacement the posting tensioning force flats out and become constant.

The post-tensioning force of the MFJP piles in the cable, in the case of passive loading, and combined passive and tensile loading, remain the same and does not change as the head of the pile is not pulled laterally by a wire connection similar to that of active case (Figure5.17). The lateral displacement in this situation is applied to the pile through the horizontal soil displacements instead of a direct connection to the pile head.

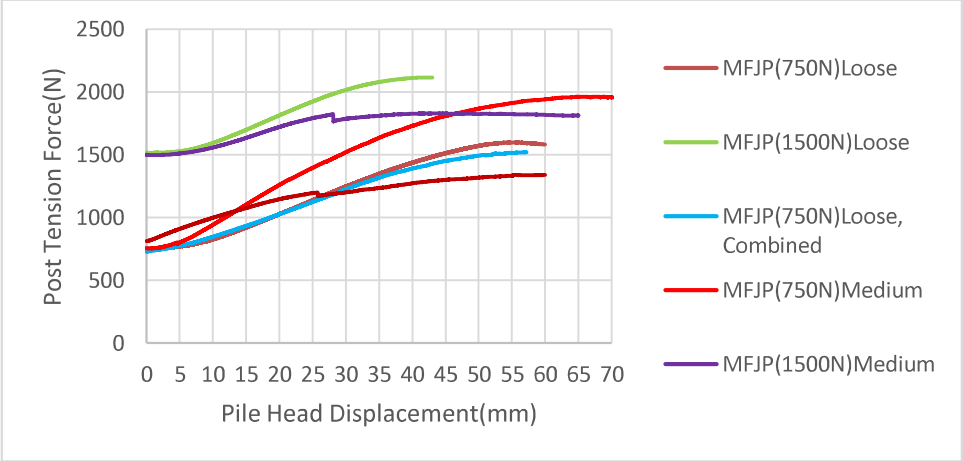

Figure 5.16. Post-tension force in the central cable of MFJP pile under active and combined active and tensile loadings.

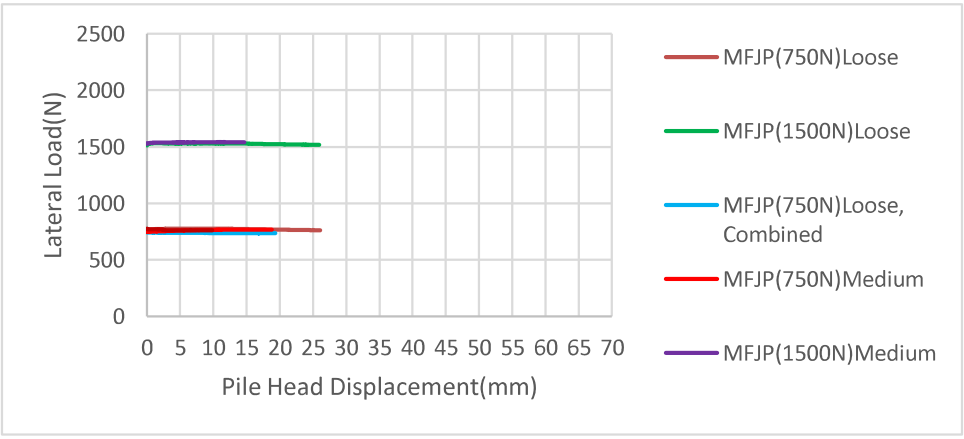

Figure 5.17. Post-tension force in the central cable of MFJP pile under passive and combined passive and tensile loadings.

6. CONCLUSION

The conclusions presented here are limited to the experimental setups, to the boundary conditions applied, and to the tests conducted on the multiple friction joint model piles (MFJP), and on the monolithic model piles. In addition, the tests on multiple friction joint piles post-tensioned to 1500N were not conducted under combined lateral and uplift loading due to the time limitations, and due to the ongoing pandemic.

Multiple friction joint tension piles subjected to large lateral displacements, and the effect of pile rigidity, soil stiffness, and type of loading on behavior and capacity of this type of piles were determined and evaluated. The lateral capacity and response of MFJP model piles were compared to that of a conventional rigid monolithic concrete model pile.

The MFJP model piles have the capacity to undergo large horizontal deformations in the order of one pile width without breakage under lateral loading and under combined lateral and tensile loadings.

The lateral capacity of the MFJP model pile, post-tensioned to 750N, and subjected to combined active lateral loading and tensile force in loose sand, is equal to that of the MFJP model pile subjected to active lateral loading alone. In contrast, the lateral capacity of both the MFJP model pile and the monolithic model pile demonstrate a fall of more than 10 percent in medium sand while subjected to combined active lateral loading and tensile force compared to that of the MFJP model pile and monolithic model pile subjected to active lateral loading alone. This fall is more predominant in the case of the MFJP model pile and monolithic model pile subjected to combined passive lateral loading and tensile force in medium sand with a fall of 50 and 86 percent respectively.

The MFJP model pile post-tensioned to 1500N force experiences a larger lateral capacity, both in active and passive cases, compared to that of the MFJP model pile post-tensioned to 750N force. This indicates that, as the pile rigidity increases, the lateral capacity increases as well. Although, the lateral capacity increases with an increase in pile rigidity, the lateral displacement at which the ultimate lateral capacity occurs decreases as

pile rigidity increases. The more flexible MFJP model pile, having 750N post-tensioned force, with the same geometry as that of the monolithic model pile can undergo larger deformation without breakage before reaching its ultimate capacity compared to that of monolithic model pile.

The soil stiffness is the dominant parameter affecting the lateral capacity of the MFJP and monolithic model piles compared to the effect of other parameters, i.e. pile rigidity, and tensile forces, on lateral capacity. The lateral capacity increases noticeably for both active and passive tests in medium sand compared to that of loose sand.

The post-tension force on the central cable, which is keeping the mortar blocks and the rubber sheets together, demonstrate an increase of 100% and more than 25% for the MFJP model pile post-tensioned to 750N and for the MFJP model pile post-tensioned to 1500N respectively under active lateral loadings. This increase in the post-tension force occurs up to a displacement equal to the ultimate lateral displacement or the displacement at which soil failure happens. After the ultimate lateral displacement, the increase in the post-tension force ceases and the post-tension force on the cable remains constant.

The response and capacity of model piles under combined static lateral and static uplift loading were investigated in the current study, but it would be a useful contribution to the piling engineering field to study the response and behavior of this type of model piles under combined cyclic lateral and cyclic uplift forces in future as the tension piles supporting offshore wind turbines, offshore platforms, and submerged floating tunnels are subjected to both cyclic lateral loading and cyclic uplift force due to wave loads in the field. Another possible future research could be the study of these model piles under combined lateral and inclined uplift forces to better simulate the battered piles. Moreover, the lateral tests and combined lateral and uplift loading tests were conducted on small-sized model piles in this study. It is recommended to perform these tests on actual large-sized piles in the field to better simulate the field conditions and capacity of piles subjected to lateral and combined lateral and uplift forces.

REFERENCES

1. Poulos, H. G. and E. H. Davis, *Pile Foundation Analysis and Design*, John Wiely & Sons, New York, 1980.

2. Fleming, K., A. Weltman, M. Randolph and K. Elson, *Piling Engineering*, 3rd edn. Wiley, New York, NY, USA, 2009.

3. Broms, B. B., "Lateral Resistance of Piles in Cohesion-less Soils" *Journal of the Soil Mechanics and Foundations Division*, ASCE, Vol. 90, SM2, pp. 123-156, 1964.

4. Reese, L. C., W. R. Cox and F. D. Koop, "Analysis of Laterally Loaded Piles in Sand", *6th Annual Offshore Technology Conference, Houston*, OTC 2080, Vol. 2, pp. 473-485, 1974.

5. Barton, Y. O., *Laterally Loaded Model Piles in Sand: Centrifuge Tests and Finite Element Analyses*, Ph.D. Thesis, University of Cambridge, 1982.

6. Reese, L. C., W. R. Cox and F. D. Koop, "Field testing and analysis of laterally loaded piles in stiff clay", *Proceeding of 7th Offshore Technology Conference*, Vol. 2, pp. 671-690, 1975.

7. Broms, B. B., "Lateral Resistance of Piles in Cohesion-less Soils", *Journal of the Soil Mechanics and Foundations Division*, ASCE, Vol. 90, SM2, pp. 123-156, 1964.

8. Matlock, H. S., "Correlations for Design of Laterally Loaded Piles in Soft Clay", *2nd Annual Offshore Technology Conf., Houston*, 1970.

9. Marsland, A. and M. F. Randolph, "Comparison of the Results from Pressuremeter Tests and Large In-Situ Plate Tests in London Clay, *Géotechnique*, Vol. 27, No. 2, pp. 217-243, 1977.

10. Murff, J. D. and J. M. Hamilton, "P-Ultimate for Undrained Analysis of Laterally Loaded Piles, *ASCE Journal of Geotechnical Engineering*, Vol. 119, No. 1, pp. 91-107, 1993.

11. Brinch Hansen, J., *the Ultimate Resistance of Rigid Piles against Transversal Forces*, Copenhagen: Geoteknisk Institute. Bull. No. 12, 1961.

12. Mei, G., Q. Chen and L. Song, "Model for Predicting Displacement-Dependent Lateral Earth Pressure", *Canadian Geotechnical Journal*, Vol. 46, No. 8, pp. 969-975, 2009.

13. Ito, T. and T. Matsui, "Methods to Estimate Lateral Force Acting on Stabilizing Piles", *Soils and Foundations*, Vol. 18, No. 4, pp. 43-59, 1975.

14. Chen, L. T. and H. G. Poulos, "Piles Subjected to Lateral Soil Movements", *Journal of Geotechnical and Geoenvironmental Engineering*, Vol. 123, No. 9, pp. 802-811, 1997.

15. Chaudhuri, D., *Pile Foundation Response to Lateral Ground Movement*, In Advances in Deep Foundations (GSP 132). Part of Geo-Frontiers 2005. Proceedings of the Sessions of the Geo Frontiers 2005 Congress, 2005.

16. Hassiotis, S. and J. L. Chameau, *Stabilization of Slopes Using Piles*, Rep. No. FHWAIIN/JHRP-84/8. Purdue University., West Lafayette, Indiana, 1984.

17. Ashour, M. and, H. Ardalan, "Analysis of Pile Stabilized Slopes Based on Soil-Pile Interaction", *Computers and Geotechnics*, Vol. 39, pp. 85-97, 2012.

18. Guo, W. D., "On Limiting Force Profile, Slip Depth and Response of Lateral Piles", *Computers and Geotechnics*, Vol. 33, No. 1, pp. 47-67, 2006.

19. Viggiani, C., "Ultimate Lateral Load on Piles Used to Stabilize Landslides", *In Proceedings of Xth ICSMFE, Stockholm*, Vol. 3, pp. 555-560, 1981.

20. Begemann H. K. S. and, E. H. De Leeuw, "Horizontal Earth Pressures on Foundation Piles as a Result of Nearby Soil Fills*", Proceedings of 5th European Conference on Soil Mechanics and Foundation Engineering, Madrid*, Vol. 1, pp. 3-9, 1972.

21. Won, J., K. You, S. Jeong, and S. Kim, "Coupled Effects in Stability Analysis of Pile-Slope System", *Computers and Geotechnics*, Vol. 32, No. 4, pp. 304-315, 2005.

22. Surjadinata, Hull, Carter and Poulos, "Combined finite- and boundary- element analysis of the effects of tunneling on single piles", *International Journal of Geotechnical Engineering*, Vol. 6, No. 5, pp. 374-377, 2006.

23. Ashour, M., G. Norris and P. Pilling, "Lateral Loading of a Pile in Layered Soil Using The Strain Wedge Model", *Journal of Geotechnical and Geoenvironmental Engineering*, ASCE 1998, Vol. 124, No. 4, pp. 303-15, 1998.

24. Mujah, Ahmad, Hazarika and Watanabe, "The Design Method of Slope Stabilizing Piles: a Review", *International Journal of Current Engineering and Technology*, Vol.3, No.2, 2013.

25. Reese, L. C. and, W. F. Van Impe, *Single Piles and Pile Groups under Lateral Loading*, A. A. Balkema, Rotterdam, Netherlands, 463, 2001.

26. Poulos, H. G. and L. T. Chen, "Pile Response Due to Excavation-Induced Lateral Soil Movement", *Journal of Geotechnical and Geoenvironmental Engineering*, Vol. 123, No. 2, pp. 94-99, 1997.

27. Vesic, A. S., "Bending of Beam Resting on Isotropic Elastic Solid", *Journal of Engineering Mechanics,* Division ASCE, Vol. 87, EM2, pp. 35-53, 1961.

28. Brinch Hansen, J., *The Ultimate Resistance of Rigid Piles Against Transversal Forces*, Copenhagen: Geoteknisk Institut. Bull. No. 12, 1961.

29. Wenz, K. P., *Über die Größe des Seitendrucks auf Pfählein bindigen Erdstoffen*, Universität Karlsruhe, Heft 12, 1963.

30. Francis, A. J., "Analysis of Pile Groups with Flexural Resistance", *Journal of Soil Mechanics and Foundation Division*, American Society of Civil Engineers, SM3, May, pp. 1-32, 1964.

31. Davisson, M. T., *Lateral Load Capacity of Piles*, Highway Research Record, No. 333, pp. 104-112, 1970.

32. Yoshida, I. and R. Yoshinaka, "A Method to Estimate Modulus of Horizontal Subgrade Reaction for a Pile", *Journal of Soils and Foundations*, Vol. 12, No. 3, September, pp. 1-17, 1972.

33. Smoltczyk H. U., *Seitendruck auf Pfahle. Inst, fur Grundbau u. Bodenmech*, Stuttgart, Kurs fur Erdbaumechanik, 1973.

34. De Beer, E. E., "The Effects of Horizontal Loads on Piles, Due to Surcharge of Seismic Effects", *Proceedings, Special Session 10, 9th International Conference, Soil Mechanics and Foundation Engineering, Tokyo*, 1977.

35. Chen, W. W. “Discussion: Laterally Loaded Piles: Program Documentation”, *Journal of Soil Mechanics and Foundation Division*, American Society of Civil Engineers, GT1, January, pp. 161-162, 1978.

36. Kourkoulis, R., F. Gelagoti, I. Anastasopoulos and G. Gazetas, “Hybrid Method for Analysis and Design of Slope Stabilizing Piles”, *Journal of Geotechnical and Geoenvironmental Engineering*, Vol. 138, No. 1, pp. 1-14, 2012.

37. Poulos, H. G., “Design of Reinforcing Piles to Increase Slope Stability”, *Canadian Geotechnical Journal*, Vol. 32, pp. 808-818, 1995.

38. Mindlin, R. D., “Force at a Point in the Interior of a Semi-Infinite Solid”, *Physics*, Vol. 7, No. 5, pp. 195-202, 1936.

39. Jeong, S., B. Kim, J. Won and J. Lee, “Uncoupled Analysis of Stabilizing Piles in Weathered Slopes”, *Computers and Geotechnics*, Vol. 30, No. 8, pp. 671-682, 2003.

40. Chen, L.T, H. G, Poulos and N. Loganathan, “Piles response caused by tunneling”, *Journal of Geotechnical and Geoenvironmental Engineering*, Vol. 125, No. 3, pp. 207-2015, 1999.

41. Mu, Haung and J. Fino, *Tunneling Effects on Lateral Behavior of Pile Rafts in Layered Soils*, Tunneling and Underground Space Technology 28, pp. 192-201, 2012.

42. Janalizadeh, and Zahmathesh, “Lateral Response of Pile Foundation in Liquefiable Soils”, *Journal of Rock Mechanics and Geotechnical Engineering,* 7, pp. 532-539, 2015.

43. Weaver, J., A. Ashford and, M. Rollins, "Response of 0.6m Cast-in-Steel-Shell Pile in Liquefied Soil under Lateral Loading", *Journal of Geotechnical and Geoenvironmental Engineering*, Vol. 13, No.1, pp. 94-102, 2005.

44. Matsui, T., W. P. Hong and T. Ito, "Earth Pressures on Piles in a Row Due to Lateral Soil Movement'', *Soils and Foundations*, Vol. 22, No. 2, pp. 71-81, 1982.

45. De Beer, E. E. and R. Carpentier, "Discussion on Methods to Estimate Lateral Force Acting on Stabilizing Pile by Ito, T. and Matsui, T.", *Soils and Foundations*, Vol. 17, No. 1, pp. 68-82, 1977.

46. Poulos, H. G., L. T. Chen and T. S. Hull, "Model Tests on Single Piles Subjected to Lateral Soil Movement", *Soils and Foundations*, Vol. 35, No. 4, pp. 85-92, 1995.

47. Qin, H. Y., and W. D. Gue, *Pile Responses Due to Lateral Soil Movement of Uniform and Triangular Profiles*, GeoFlorid: Advances in Analysis, Modeling & Design (GSP 199), ASCE, 2010.

48. Pan, J. L, A. T. C. Goh, K. S. Wong and C. I. Teh, "Ultimate Soil Pressures for Piles Subjected to Lateral Soil Movements", *Journal of Geotechnical and Geoenvironmental Engineering*, Vol. 128, No. 6, pp. 530-535, 2002.

49. Randolph, M. F. and G. T. Houlsby, ''The Limiting Pressure on a Circular Pile Loaded Laterally in Cohesive Soil'', *Geotechnique*, Vol. 34, No. 4, pp. 613-623, 1984.

50. Chen L. F., *The effect of lateral soil movements on pile foundation*, PhD thesis, Univ. of Sydney, Australia, 1994.

51. Ersoy, Ö. Ç. and S. Yıldırım, "Experimental Investigation of Piles Behavior Subjected to Lateral Soil Movement", *İMO Teknik Dergi*, writing 423, pp. 6867-6887, 2014.

52. Stewart, D. P., R. J. Jewell and, M. F. Randolph, "Centrifuge Modeling of Piled Bridge Abutments on Soft Ground", *Soils and Foundations*, Tokyo, Vol. 34, No. 1, pp. 41-51, 1994.

53. Leung, C. F., Y. K. Chow and, R. F. Shen, "Behavior of Pile Subject to Excavation Induced Soil Movement", *Journal of Geotechnical and Geoenvironmental Engineering*, Vol. 126, No. 11, pp. 947-2000, 2000.

54. Leung, C. F., J. K. Lim, R. F. Shen and, Y. K. Chow, "Behavior of Pile Groups Subject to Excavation-Induced Soil Movement", *Journal of Geotechnical and Geoenvironmental Engineering*, Vol. 129, No. 1, pp. 58-65, 2003.

55. Leung C. E., D. E. L. Ong and, Y. K. Chow, "Pile Behavior Due to Excavation-Induced Soil Movement in Clay II: Collapsed Wall", *Journal of Geotechnical and Geoenvironmental Engineering*, Vol. 132, No. 1, pp. 45-43, 2006.

56. Ong, D. E. L., C. E. Leung and, Y. K. Chow, *"Pile Behavior Due to Excavation-Induced Soil Movement in Clay I: Wall*', *Journal of Geotechnical and Geoenvironmental Engineering*, Vol. 132, No. 1, pp. 36-44, 2006.

57. Goh, A. T. C., K. S. Wong, C. I. Teh and D. Wen, "*Pile Response Adjacent to Braced Excavation*", *Journal of Geotechnical and Geoenvironmental Engineering*, Vol. 129, No. 4, pp. 383-386, 2003.

58. Lirer, S., *Landslide Stabilizing Piles: Experimental Evidences and Numerical Interpretation*, Engineering Goelogy 149-150, pp. 70-77, 2012.

59. Xiang, B., L. M. Zhang, L. R. Zhou, Y. Y. He and, L. Zhu, "Field Lateral Load Tests on Slope Stabilization Grouted Pipe Pile Groups", *Journal of Geotechnical and Geoenvironmental Eng*ineering, Vol. 141, No. 4, 2015.

60. Springman, S. M., *Lateral Loading on Piles Due to Simulated Embankment Construction*, PhD Thesis, University of Cambridge, 1989.

61. Stewart, D. P., *Lateral Loading of Piled Bridge Abutments Due to Embankment Construction*, PhD Thesis, University of Western Australia, 1992.

62. Bransby, M. F., *Piled Foundations Adjacent to Surcharge Loads*, PhD Thesis, University of Cambridge, 1995.

63. Chen, Y. C., *Numerical Analysis of Slope Stabilization Concept Using Piles*, PhD Thesis, University of Southern California, 2001.

64. Miao, L. F., A. T. C. Goh, K. S. Wong and C. I. Teh, "Three-Dimensional Finite element Analyses of Passive Pile Behavior", *International Journal for Numerical and Analytical Methods in Geomechanics*, Vol. 60, No. 7, pp. 599-613, 2006.

65. Leung, C. F., Y. K. Chow and, R. F. Shen, "Behavior of Pile Subject to Excavation Induced Soil Movement", *Journal of Geotechnical and Geoenvironmental Engineering*, Vol. 126, No. 11, pp. 947-2000, 2000.

66. Zhang, C., D. White and, M. Randolph, "Centrifuge Modeling of the Cyclic Lateral Response of a Rigid Pile in Soft Clay*"*, *Journal of Geotechnical and Geoenviromental Engineering*, ASCE, pp. 717-729, 2011.

67. Madhusudan, K. and R. Ayothiraman, "Experimental Studies on Behavior of Single Pile under Combined Uplift and Lateral Loading", *Journal of Geotechnical and Geoenvironmenttal Eng*ineering, Vol. 14, No. 17, 2015.

68. Baykal, G., *Ankraj Kablosu Germeli Eklemli Kazık Sistemi Geli_stirilmesi*, Tech. Rep., Boğaziçi Üniversitesi Blimsel Araştırma Projeleri, 2011.

69. Yahia, Y. I. O., *An Experimental Study On The Behavior Of Segmental Pile With Variable Flexural Rigidity (BAP-11A04D9),* Ph.D. Thesis, Bogazici University, 2014.

70. Sengez, M., *Lateral Capacity of Segmental Model Piles under Cyclic Loading (BAP 18A04P2),* Master's Thesis, Bogazici University, 2019.

71. Keklik, A., *An Experimental Study on the Behavior of Segmental Piles Subjected to Large Lateral Displacement*, Master's Thesis, Bogazici University, 2020.

72. Öztürk, B., *Stress & Displacement Measurement for Geotechnical Modeling Using Open Platform*, Master's Thesis, Bogazici University, 2020.

73. Baykal, G., "Large Displacement Constant Contact Area Geosynthetic-Soil Interface Direct Shear Test Device", *Proceedings of the 19th International Conference on Soil Mechanics and Geotechnical Engineering, Seoul, 2017.*

74. Baykal, G., *Development of Soil-Structure Interface Testing System Using Pneumatic Muscles*, BAP 5580 project, Boğaziçi University, İstanbul, 2015.

75. Festo Data and Property Sheet, Fluidic Muscle DMSP/MAS, 2008, https://www.festo.com/rep/en_corp/assets/pdf/info_501_en.pdf, accessed at 10 April 2021.

76. ASTM, *C270-19 Standard Specification for Mortar for Unit Masonry*, West Conshohocken, PA, 2019.

77. MPU-9250 Data Sheet, Product Specification Revision 1.1, 2015, https://3cfeqx1hf82y3xcoull08ihx-wpengine.netdna-ssl.com/wp-content/uploads/2015/02/PS-MPU-9250A-01-v1.1.pdf, accessed at 10 April 2021.

78. Treffers, C. and, L. Wietmarschen, *Position and Orientation Determination of a Probe with Use of the IMUMPU9250 and an ATmega328 Microcontroller,* Master's Thesis, TU Delft, 2016.

APPENDIX A: TENSILE TESTS ON MODEL PILES

To determine the tensile capacity of the model piles a series of tests were performed by applying tensile forces on the model piles head and measuring the model pile heads displacement with the help of an LVDT. The results of the tensile tests on monolithic and MFJP model piles are shown in Figure A.1, Figure A.2, and Figure A.3 respectively. As the rigidity doesn't have a significant effect on pile tensile capacity, the tensile tests on MFJP piles have been only conducted with piles-post tensioned with 750N force. Since the combined lateral and tensile tests for MFJP and monolithic piles were only compared in the case of medium sand, the tensile capacity test on the monolithic model piles was only performed on medium sand.

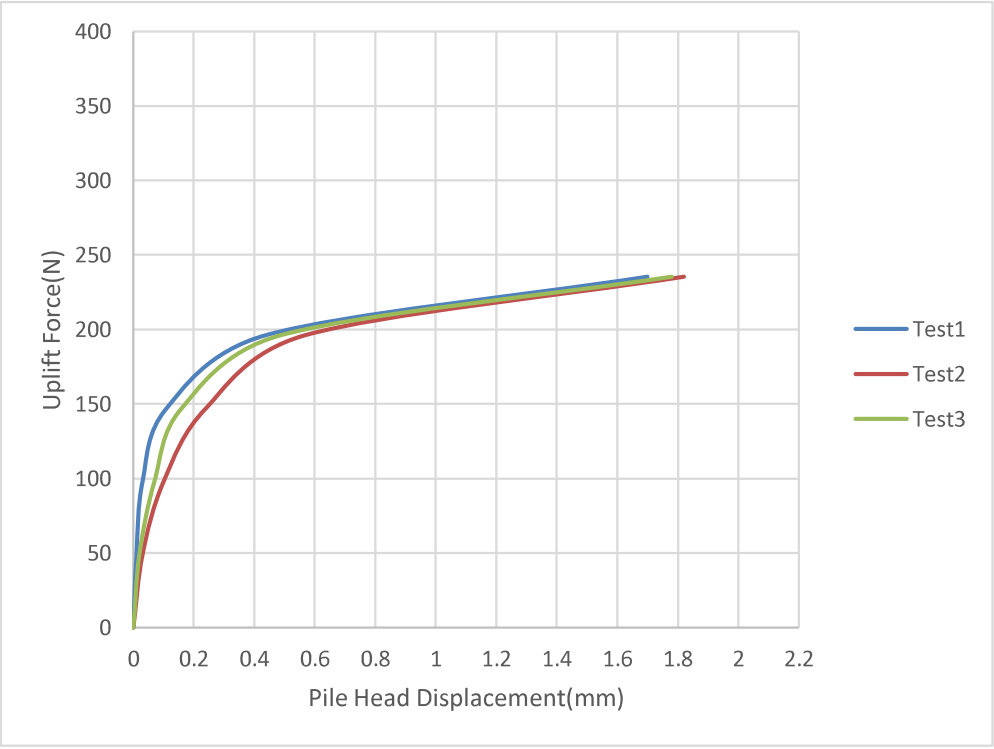

Figure A.1. Tensile capacity test on MFJP pile in loose sand.

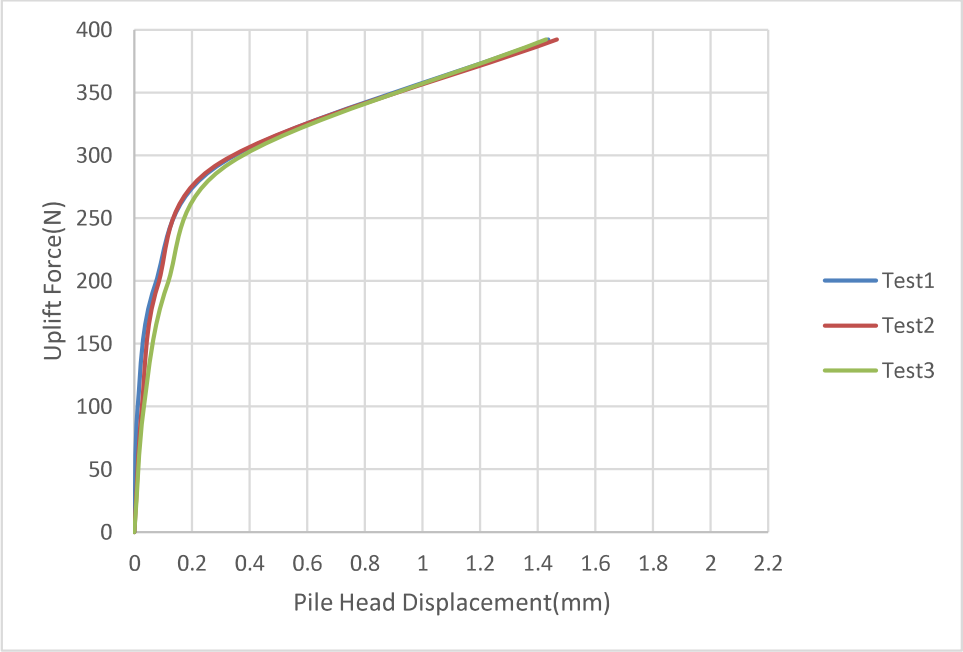

Figure A.2. Tensile capacity test on MFJP pile in medium sand.

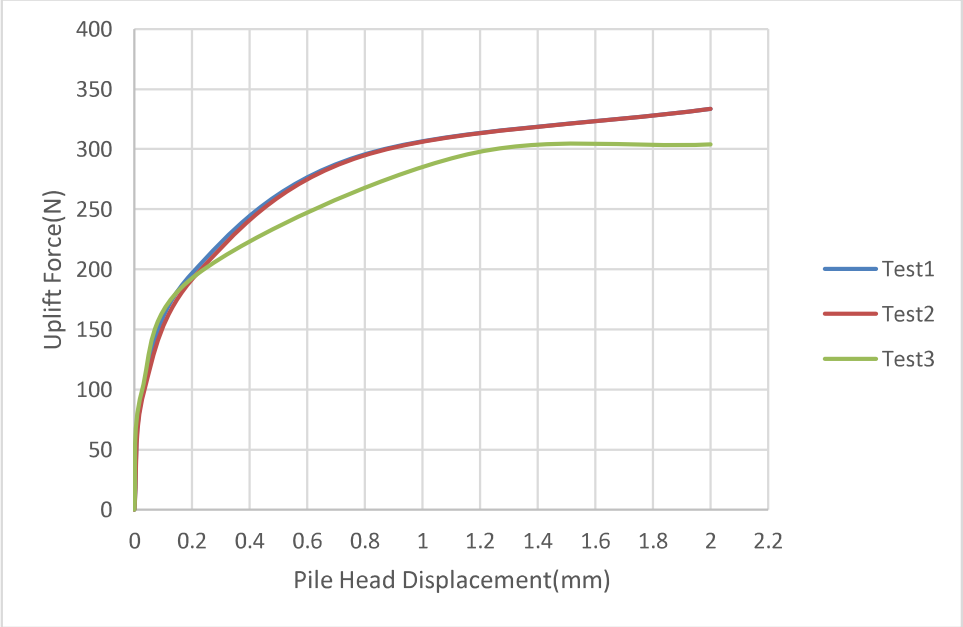

Figure A.3. Tensile capacity test on monolithic pile in medium sand.

APPENDIX B: MPU 9250 SENSORS CALIBRATIONS

The raw data from MPU9250 sensors are not accurate since the gyroscope, accelerometer, and magnetometers of MPU9250 are using MEMS (Micro Electrical Mechanical Systems) hardware for obtaining the data, and MEMS hardware is influenced adversely by many factors such as temperature, manufacturing imperfections, and the magnetic field of the earth. Therefore, the gyroscope, accelerometer, and magnetometer need to be calibrated, and the raw data must be corrected against those calibrations.

B.1. Gyroscope Calibration

The drifts in gyroscope readings are due to temperature and manufacturing imperfections. In order to find the gyroscope the MPU9250 sensor was locked in a place and readings were taken. The gyroscope ideally should measure zero angular velocity in x, y, and z directions as it is locked and does not move, But due to imperfections and change in temperature, it does not read zero velocities even it is locked in positon. Therefore, the averages of the angular velocities in these three directions are giving the offset or drift of the gyroscope and must be subtracted from the raw data obtained during the experiments. Figure B.1 shows the calibrated and uncalibrated data of the gyroscope of the sensor3x69.

B.2. Accelerometer Calibration

When locked in a flat surface, the accelerometer should read a value equal to the acceleration of the earth gravitational field, i.e. $9.81\frac{\mathrm{m}}{\mathrm{s}^2}$, in its downward axis and zero on the other two axes, but there is always some drifts from these ideal values and the accelerometer reading should be subtracted from these drifts in x, y, and z axes. In order to calibrate the accelerometers, the in-built recommended code from Arduino by Hideakitai for MPU9250 was used. The code is designed in a way that it takes raw data from positioning or rotating the MPU9250 sensors on a flat surface in a manner that each axis x, y, and z happens to be in the positive and negative direction of the gravitational acceleration field once. After placing the sensors in all six directions, the code returns the

drift and scale factors for the sensor. The calibrated data are obtained by subtracting the drifts from raw data and multiplying them by the scale factor. Figure B.2 shows the calibrated and uncalibrated data of the accelerometer of an MPU9250.

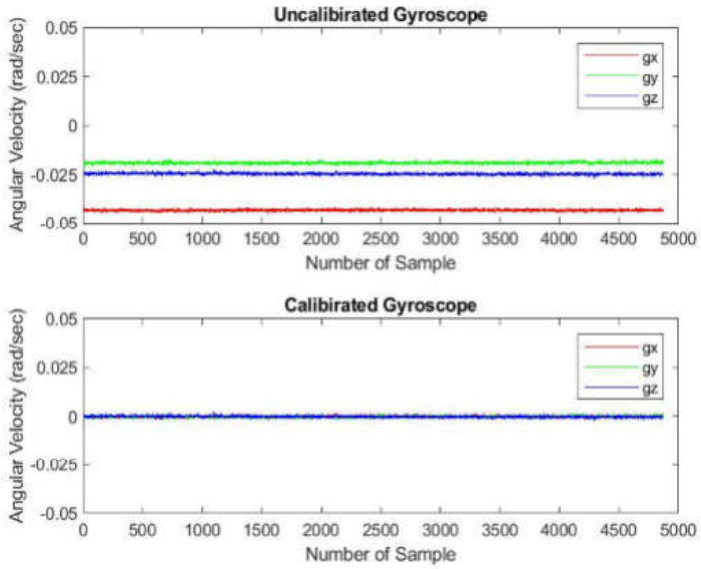

Figure B.1. Gyroscope raw and calibrated data for sensor 3x69.

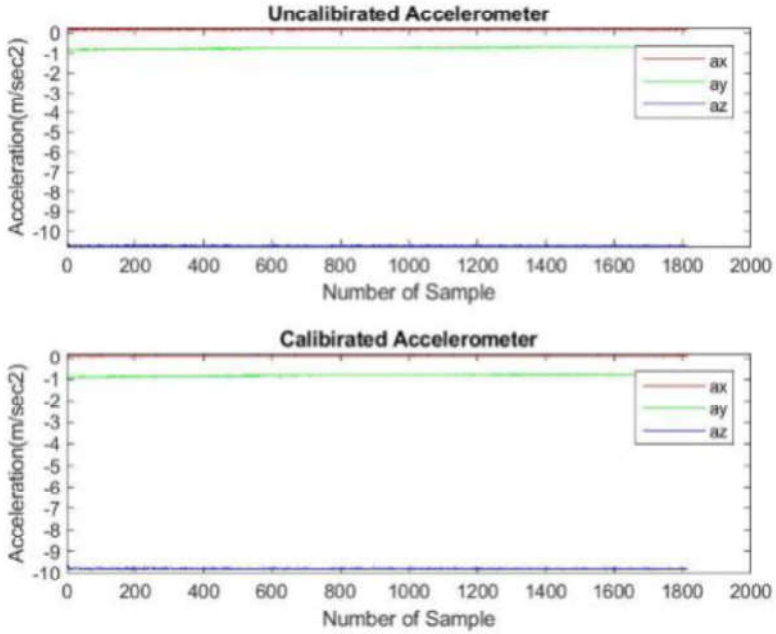

Figure B.2. Accelerometer raw and calibrated data.

B.3. Magnetometer Calibration

The magnetometer of the MPU9250 sensors are measuring the magnetic field of the earth in three directions x, y, and z. similar to the gyroscope and accelerometer. Since most electrical devices have magnetic components that interact with the magnetic field of the earth, similar to the gyroscope and accelerometer, there are some disturbances in the raw data of magnetometer as well. The disturbances in magnetometer data are generally divided into two parts of hard iron effect and soft iron effect. The hard iron effect is due to the magnetized component of the MPU9250 itself while the soft iron effect is due to current induced on the un-magnetized component of the sensor due to the ferromagnetic materials around the sensor. An ideal magnetometer values in x, y, and z directions should make a perfect sphere around the origin, but the hard iron effect diverges its position with respect to the origin and the soft iron effect distorts its spherical shape.

The calibration of the magnetometers of the MPU9250 sensors were done again by the Arduino Library code, built for the calibration of MPU9250 sensors' magnetometer, in which the sensor is rotated in figure 8 while the code is running until it gets enough data to detect the hard and soft iron effects after which it returns an offset and scale factor for the sensor. Subtracting the offset from magnetometer raw data and multiplying it by the scale factor gives the calibrated magnetometer values. Figure B.3 shows the calibrated and uncalibrated magnetometer data of sensor3x69 in XY, XZ, and YZ planes.

Note that how the uncalibrated magnetometer data are drifted away from the origin (0, 0) in these graphs, while the calibrated magnetometer data are making nearly a circle around the origin, which is expected from the data of an undisturbed magnetometer or a unaffected magnetometer from hard iron and soft iron effects due to the magnetism of the electric components near it.

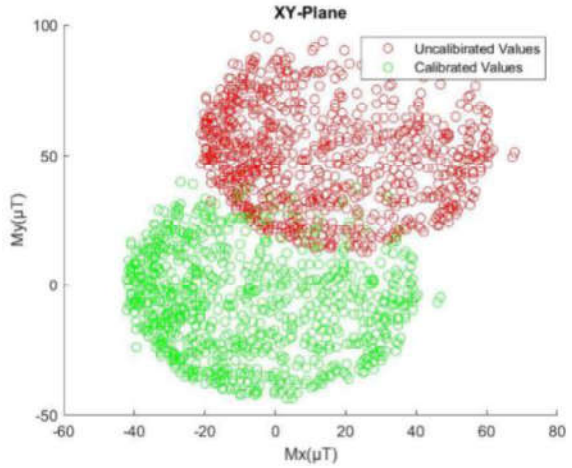

(a)

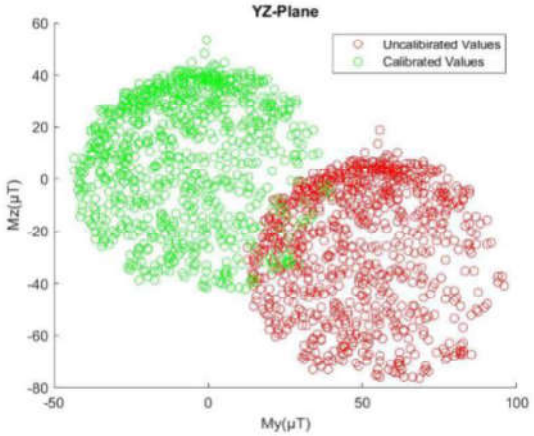

(b)

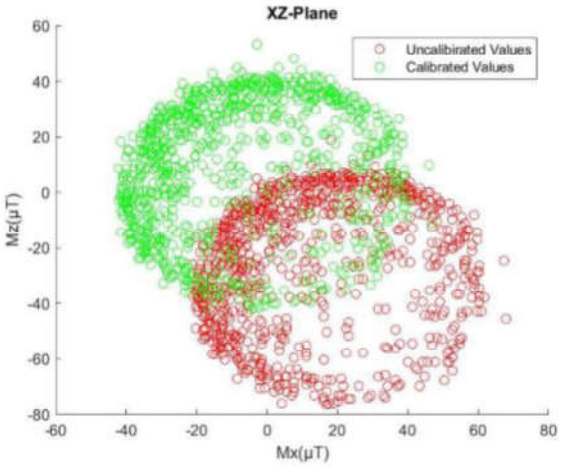

(c)

Figure B.3. Raw and calibrated data of sensor3x69 in (a) XY, (b) XZ, and (c) YZ planes.

APPENDIX C: ARDUINO AND MATLAB CODES USED TO CALCULATE EULAR ANGLES AND LVDT DISPLACEMENTS

C.1. Arduino Code for Reading the MPU9250 Sensors' Data

```
#include <Arduino.h>
#include <Esplora.h>
#include "MPU9250.h"
#include "TCA9548A.h"
TCA9548A I2CMux;
MPU9250 IMU68(Wire,0x68);
MPU9250 IMU69(Wire,0x69);
int status68;
int status69;
int portNumber;
unsigned long myTime;
void setup() {
Serial.begin(115200);
while(!Serial) {}
I2CMux.begin(Wire);
for (portNumber = 4; portNumber < 7; portNumber++) {
I2CMux.closeAll();
I2CMux.openChannel(portNumber);
Serial.print("\nChannel ");
Serial.print(portNumber);
Serial.print("\n");
status68 = IMU68.begin();
if (status68 < 0) {
Serial.println("IMU68: NO CONNECTION");
} else {
Serial.println("IMU68: OK");
IMU68.setAccelRange(MPU9250::ACCEL_RANGE_8G);
```

```
IMU68.setGyroRange(MPU9250::GYRO_RANGE_500DPS);
IMU68.setDlpfBandwidth(MPU9250::DLPF_BANDWIDTH_20HZ);
IMU68.setSrd(19);
}
status69 = IMU69.begin();
if (status69 < 0) {
Serial.println("IMU69: NO CONNECTION");
} else {
Serial.println("IMU69: OK");
IMU69.setAccelRange(MPU9250::ACCEL_RANGE_8G);
IMU69.setGyroRange(MPU9250::GYRO_RANGE_500DPS);
IMU69.setDlpfBandwidth(MPU9250::DLPF_BANDWIDTH_20HZ);
IMU69.setSrd(19);
}
if (portNumber == 3) {
IMU68.setAccelCalX(0.110384,1.001144);
IMU68.setAccelCalY(0.110384,1.003558);
IMU68.setAccelCalZ(0.278201,0.985362);
IMU69.setAccelCalX(0.089108,0.998424);
IMU69.setAccelCalY(0.089108,1.004287);
IMU69.setAccelCalZ(-0.768233,0.986029);
}
else if (portNumber == 4) {
IMU68.setAccelCalX(0.076116,0.999617);
IMU68.setAccelCalY(0.076116,0.999561);
IMU68.setAccelCalZ(-0.243755,0.987193);
}
else if (portNumber == 5) {
IMU68.setAccelCalX(0.038561,1.001427);
IMU68.setAccelCalY(0.038561,1.000543);
IMU68.setAccelCalZ(0.000000,1.000000);
IMU69.setAccelCalX(0.088453,0.998944);
IMU69.setAccelCalY(0.088453,1.003792);
```

```
IMU69.setAccelCalZ(0.806701,0.991872);
}
else if (portNumber == 6) {
IMU68.setAccelCalX(0.241024,0.997491);
IMU68.setAccelCalY(0.241024,0.998858);
IMU68.setAccelCalZ(0.792590,0.981792);
IMU69.setAccelCalX(0.182268,0.998319);
IMU69.setAccelCalY(0.182268,1.004492);
IMU69.setAccelCalZ(0.290850,0.988126);
}
I2CMux.closeChannel(portNumber);
}
}
void loop() {
for (portNumber = 3; portNumber < 7; portNumber++) {
I2CMux.openChannel(portNumber);
if (portNumber==4){
Serial.print(portNumber);
Serial.print(",");
Serial.print(millis());
Serial.print(",");
Serial.print("68,");
IMU68.readSensor();
Serial.print(IMU68.getAccelX_mss(),6);
Serial.print(",");
Serial.print(IMU68.getAccelY_mss(),6);
Serial.print(",");
Serial.print(IMU68.getAccelZ_mss(),6);
Serial.print(",");
Serial.print(IMU68.getGyroX_rads(),6);
Serial.print(",");
Serial.print(IMU68.getGyroY_rads(),6);
Serial.print(",");
```

```
Serial.print(IMU68.getGyroZ_rads(),6);
Serial.print(",");
Serial.print(IMU68.getMagX_uT(),6);
Serial.print(",");
Serial.print(IMU68.getMagY_uT(),6);
Serial.print(",");
Serial.println(IMU68.getMagZ_uT(),6);
}
else if (portNumber==3 || portNumber==5 || portNumber==6){
Serial.print(portNumber);
Serial.print(",");
Serial.print(millis());
Serial.print(",");
Serial.print("68,");
IMU68.readSensor();
Serial.print(IMU68.getAccelX_mss(),6);
Serial.print(",");
Serial.print(IMU68.getAccelY_mss(),6);
Serial.print(",");
Serial.print(IMU68.getAccelZ_mss(),6);
Serial.print(",");
Serial.print(IMU68.getGyroX_rads(),6);
Serial.print(",");
Serial.print(IMU68.getGyroY_rads(),6);
Serial.print(",");
Serial.print(IMU68.getGyroZ_rads(),6);
Serial.print(",");
Serial.print(IMU68.getMagX_uT(),6);
Serial.print(",");
Serial.print(IMU68.getMagY_uT(),6);
Serial.print(",");
Serial.print(IMU68.getMagZ_uT(),6);
Serial.print(",");
```

```
Serial.print("69,");
Serial.print(millis());
Serial.print(",");
IMU69.readSensor();
Serial.print(IMU69.getAccelX_mss(),6);
Serial.print(",");
Serial.print(IMU69.getAccelY_mss(),6);
Serial.print(",");
Serial.print(IMU69.getAccelZ_mss(),6);
Serial.print(",");
Serial.print(IMU69.getGyroX_rads(),6);
Serial.print(",");
Serial.print(IMU69.getGyroY_rads(),6);
Serial.print(",");
Serial.print(IMU69.getGyroZ_rads(),6);
Serial.print(",");
Serial.print(IMU69.getMagX_uT(),6);
Serial.print(",");
Serial.print(IMU69.getMagY_uT(),6);
Serial.print(",");
Serial.print(IMU69.getMagZ_uT(),6);
Serial.print("\n");
}
I2CMux.closeChannel(portNumber);
delay(200);
}
}
```

C.2. MATLAB Code for Reading LVDT Outputs

```
dq = daq("ni");
dq.Rate = 100;
ch = addinput(dq,"cDAQ1Mod1", "ai0","Bridge");
```

```
ch.BridgeMode = 'Full';
ch.NominalBridgeResistance = 351.0;
ch.ADCTimingMode = 'HighResolution';
n=1;V0=-0.000011187;V100=-0.0025;L=100;
store=cell(1,1);
fprintf('starting the test');
while (1)
start(dq);
Time=datestr(now,'HH:MM:SS');
scandata = read(dq,seconds(1), "OutputFormat", "Matrix");
Vi=mean(scandata);
store{n,1}=Time;
store{n,4}=Vi;
store{n,5}=((Vi-V0)*100)/(V100-V0);
fprintf('Distance: [%.2f]mm\n\n',store{n,5})
n=n+1;
stop(dq);
end
```